Chapter 2

Transcriptomic characterization of a forebrain-specific OGT cKO

Portions of this chapter are adapted from the published work:

Wang, AC, **Jensen EH**, Rexach JE, Vinters HV, and Hsieh-Wilson LC. "Loss of *O*-GlcNAc glycosylation in forebrain excitatory neurons induces neurodegeneration." *PNAS*. **2016**, *113*(52):15120-15125. doi: 10.1073/pnas.1606899113. Research article.

2.1 Abstract

O-GlcNAc glycosylation is a dynamic, inducible post-translational modification (PTM) found on proteins associated with neurodegenerative diseases such as α-synuclein, amyloid precursor protein, and tau. Deletion of the *O*-GlcNAc transferase (*Ogt*) gene responsible for the modification causes early postnatal lethality in mice, complicating efforts to study *O*-GlcNAc glycosylation in mature neuronal function and dysfunction. Here, we report that forebrain-specific loss of OGT in adult mice leads to progressive neurodegeneration, including neuronal death, neuroinflammation, hyperphosphorylated tau, amyloidogenic Aβ-peptides, and memory deficits. In the OGT cKO hippocampus, we show the upregulation of neuroinflammatory genes and downregulation of cholesterol and lipid biosynthetic genes supporting a critical role of OGT in the regulation of lipid metabolism. Additionally, a gene network analysis (WGCNA) revealed that the OGT cKO mice showed perturbations in cell cycle, which were verified using immunohistochemistry (IHC). Another WGCNA comparing the OGT cKO with other FTDP and AD mouse models showed striking transcriptional similarities between the OGT cKO and neurofibrillary tangle (NFT)-forming FTDP/AD mouse models with increased correlation with a neuroinflammatory gene network and decreased correlation with a synaptic gene network. In contrast, amyloid plaque-forming AD mouse models showed no correlation with the synaptic gene network, suggesting that NFT formation specifically compromises synaptic transcription. These studies indicate that *O*-GlcNAcylation regulates pathways critical for the maintenance of neuronal health and suggest that dysfunctional *O*-GlcNAc signaling may be an important contributor to

neurodegenerative diseases.

2.2 General approach to generation of an OGT cKO mouse and validation

Previous studies have demonstrated that knocking out OGT in mice is embryonic lethal, and selectively knocking out neuronal OGT leads to motor dysfunction, brain development abnormalities, and eventual death.[1,2] This established OGT as a critical enzyme especially during development and in particular, neuronal development. In addition, *in situ* hybridization studies have shown that OGT and OGA are expressed at their highest levels in the hippocampus.[3] These previous studies encouraged our lab to cross a floxed OGT (OGTfl) mouse with mice with Cre downstream of a calcium/calmodulin kinase IIα (CaMKIIα) promoter (CaMKIIα-Cre, obtained from the Kennedy lab).[4] Wherever Cre integrase is expressed, it will selectively excise DNA segments that are flanked by LoxP sites, so that that excised DNA sequence is no longer transcribed.[5] The expression pattern for CaMKIIα in the murine brain is restricted primarily to the adult forebrain where it is expressed at high levels in the hippocampus and cortical neurons and at moderate levels in the caudate-putamen. Crucially, CaMKIIα is not expressed until after embryogenesis when its expression increases an order of magnitude from P1 to P21 and continues to gradually increase up to P90.[6] This design allows normal neural development to resume before *O*-GlcNAc modification is depleted in the adult. In this way, it mirrors the time course of the pathogenicity of adult-onset neurodegenerative disorders, which manifest well after neural development and considerable neural degeneration.[7] As OGT is an X-linked gene, only about half of males born from a CaMKIIα-Cre male x OGTfl female cross were forebrain-specific OGT knock-outs (fbOGT cKO).[2] The CaMKIIα-Cre transgene is expressed between postnatal

day 14-21 in excitatory neurons in the postnatal forebrain, including the cortex, hippocampus, caudate nucleus, thalamus, and hypothalamus.[8] Beginning at 1 month of age, the mice showed progressive depletion of *O*-GlcNAcylation in the hippocampus and cortex, but not in the cerebellum.

2.3 Overview of the phenotypes of the OGT cKO mouse: morphological and behavioral features

Andrew Wang, a former graduate student in the lab, characterized the OGT cKO mouse morphologically and behaviorally and showed the following OGT cKO features. Due to the embryonic and perinatal lethality phenotypes observed in total and neuronal-specific knockout, we sought to generate a knockout that would allow for normal neuronal development. Toward that end, the OGT cKO mouse was generated by crossing floxed *OGT* (OGTfl) mice with CaMKIIα-Cre transgenic mice.[2,8] By 6 months, few neurons were *O*-GlcNAc negative due to the loss of neurons lacking OGT and *O*-GlcNAc. Starting at 7 weeks of age, the OGT cKO began to show significant reductions in weight and brain size when compared to their wildtype littermates, which advanced to significant morphological changes in the cortex and hippocampus at 6 months of age (Figure 2.1A). At 2 months of age, progressive neuronal loss was observed in the hippocampus and cortex escalating to an 83% and 60% decrease in neuronal density in the dentate gyrus (DG) and CA1 respectively at 6 months of age (NeuN staining). In addition, the majority of DG region neurons and ~10% of cortical neurons displayed apoptotic neurodegeneration using Tdt dUTP Nick-Labeling (TUNEL) and Fluoro-Jade C (FJC) staining while their WT littermates displayed no TUNEL- or FJC-positive neurons (Figure 2.1B).

At 2 months of age, the OGT cKO mouse displayed significant increases in gliosis and neuroinflammation as measured by immunohistochemical (IHC) staining with the astrocyte marker, glial fibrillary acidic protein (GFAP), and the microglial marker, ionized calcium-binding adaptor molecule (Iba-1) (Figure 2.1B). Furthermore, the OGT cKO demonstrated increases in aberrantly and hyperphosphorylated tau and protein aggregation in the hippocampus (Thioflavine S staining) at both 2 and 6 months of age (Figure 2.1C). The ratio of the amyloidogenic 42-mer Aβ-peptide to the 40-mer Aβ-peptide increased 2.5-fold when compared to their wildtype littermates. These OGT cKO morphological changes are accompanied by long-term memory (LTM) impairments in amygdala-dependent cued and hippocampus-dependent contextual fear conditioning experiments at 4 months of age. Finally, Jessica Rexach, a former graduate student in the lab, showed that OGT protein levels were decreased by 1.6-fold in the brains of AD patients with the most severe memory decline (Braak VI) ($P < 0.0005$).

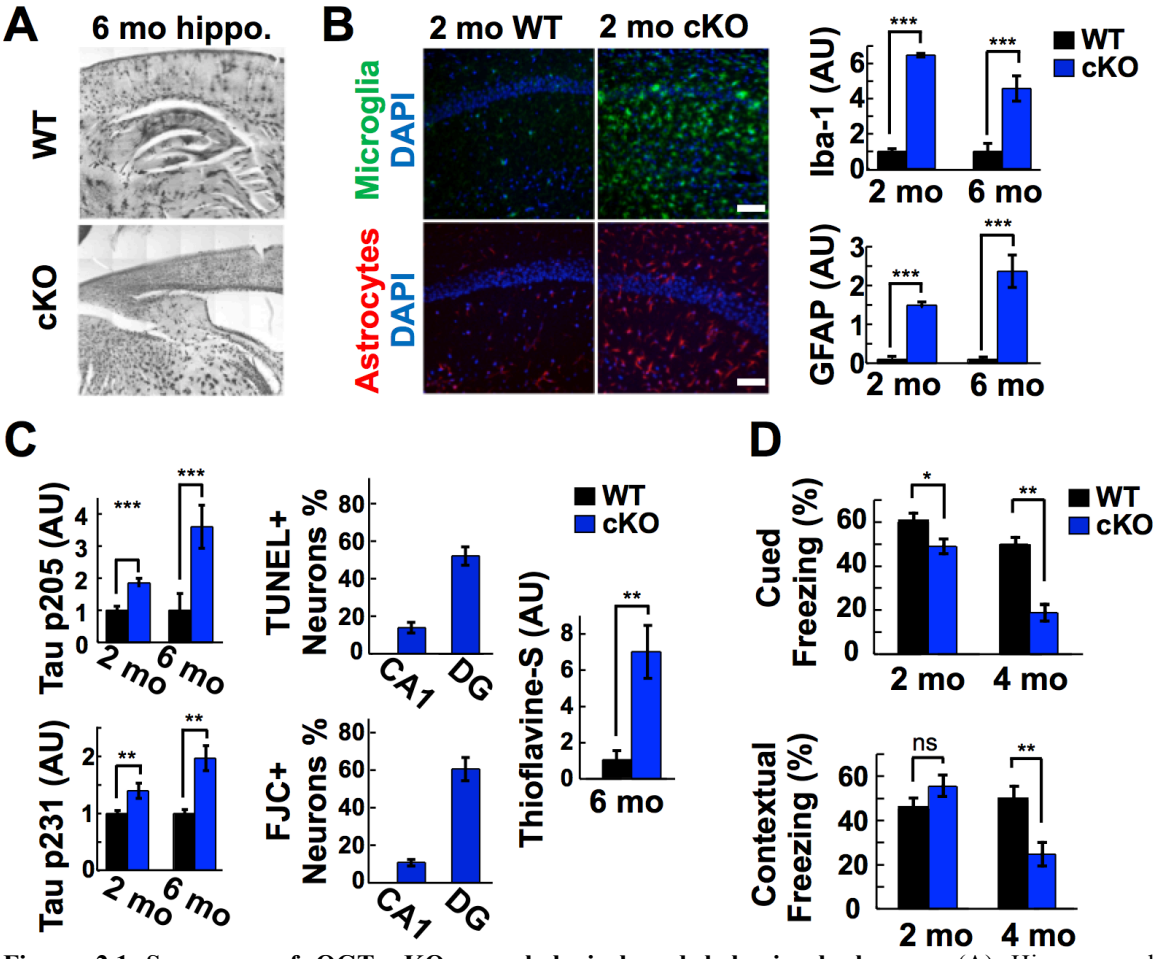

Figure 2.1 Summary of OGT cKO morphological and behavioral changes. (A) Hippocampal shrinkage, a decrease in the number of neurons, and disruption of the hippocampal neuronal network are revealed by golgi stains of the hippocampi of the WT and OGT cKO mice at 6 months of age. (B) Elevated expression of the neuroinflammatory markers Iba-1 (green) and GFAP (red) in the CA1 hippocampus of 2-month-old OGT cKO compared to WT mice. Total pixel intensity (green or red) from each field of view was quantified, and mean ± SEM is shown. $n = 3$. Scale bar = 50 µm. (C) Pathological phosphorylation of tau (pThr-205, pThr-231) increased in DG neurons of 2-month and 6-month-old OGT cKO mice based on IHC. Fluoro-Jade C and TUNEL staining identified degenerating and apoptotic neurons respectively in the DG and CA1 regions of the hippocampus of OGT cKO mice at 2 months of age. Thioflavine S-positive aggregates accumulated in 6-month-old OGT cKO mice. (D) Deficits in cued fear conditioning were observed at 2 months in OGT cKO mice. Deficits in both cued and contextual learning and memory were observed at 4 months. $n = 12$ per group. $^{*}P < 0.05$, $^{**}P < 0.005$, $^{***}P < 0.0005$. Figure from Andrew Wang.

2.4 Few differentially-expressed genes in OGT cKO hippocampi at 3 weeks

To identify global transcriptional changes associated with the behavioral and histological phenotypes, we performed gene expression microarray analyses. At 3 weeks of age, only 10 differentially-expressed (DE) genes were identified in the hippocampus of

OGT cKO mice compared to WT mice, consistent with the minimal extent of OGT ablation and neuronal loss shown by histology (Table 2.1). Complement component 1, q subcomponent, C chain (*C1qc*) and lectin, galactoside-binding, soluble, 3 binding protein (*Lgals3bp*) are immune-response related genes that are upregulated in the OGT cKO mice (1.3-fold and 1.6-fold respectively). A 3.0-fold upregulation of the SLX4 structure-specific endonuclease subunit homolog (*Slx4*), a Holliday junction resolvase critical for homology-directed repair (HDR) in response to DNA interstrand crosslinking, replication, and telomeric extension.[9-11] This increase in SLX4 expression could be priming cells for genotoxic stress response or replication. The upregulation of *C1qc*, *Lgals3bp*, and potentially *Slx4* indicate incipient immune response in the 3-week OGT cKO.

Several genes that are involved in neuronal activity and growth are also DE at 3 weeks in the OGT cKO. Upregulated in OGT cKO (1.5-fold), abhydrolase domain containing 11 (ABHD11, *Abhd11*) is an α/β serine lipid hydrolase that is currently poorly characterized.[12,13] One study implicated ABHD11 in axonal pathfinding and astroglial organization in the forebrain during zebrafish embryogenesis.[14] Furthermore, Abhd11os, a long non-coding RNA (lncRNA), binds to the 3'UTR region of ABHD11 mRNA and upregulates ABHD11 expression has been shown to be neuroprotective in Huntington's disease suggesting that ABHD11 may play a role in HD.[15] Cadherin 6 (*Cdh6*), a protein critical for axonal guidance, is downregulated in the OGT cKO (-1.6-fold), suggesting that there may be impairments in axonal targeting in the OGT cKO mouse.[16] Proline-rich transmembrane protein 1 (SynDIG4, *Prrt1*) associates with extrasynaptic glutamate α-

amino-3-hydroxy-5-methyl-4-isoxazolepropionic acid (AMPA) receptors, but its function is not yet known.[17,18]

Finally, a metabolic and an mRNA turnover regulator are also upregulated in the OGT cKO at 3 weeks. The gene 6-phosphofructo-2-kinase/fructose-2,6-biphosphatase 3 (PFKFB3, *Pfkfb3*) is upregulated 1.8-fold in the OGT cKO mice. PFKFB3 is a master regulator of glycolysis through its production of 2,6-biphosphate, a major allosteric agonist of 6-phosphofructokinase-1 (PFK1), the enzyme that catalyzes the rate-limiting step of glycolysis.[19] Under excitotoxic conditions, PFKFB3 is stabilized and shunts neurons to glycolysis exacerbating oxidative stress and leading to neurodegeneration.[19,20] Poly(A) binding protein, cytoplasmic 6 (*Pabpc6*), upregulated 1.6-fold in the OGT cKO, is required for mRNA translation initiation and mRNA degradation.[21] Finally, both *1810062O18Rik* and *4930597O21Rik* are RNA transcribed from the antisense strand of DNA, indicating that these are likely to be involved in RNA interference, but the actual functions or targets of these transcripts is currently unknown.[22] In summary, at 3 weeks of age, the OGT cKO shows the upregulation of a few immune response genes and the differential expression of neuronal activity, metabolism, and mRNA processing genes.

Table 2.1 Differentially-expressed genes in the OGT cKO at 3 weeks.

Genes	Description	FC	*P*-values
Pfkfb3	6-phosphofructo-2-kinase/fructose-2,6-biphosphatase 3	1.8	$1.4x10^{-19}$
Prrt1	proline-rich transmembrane protein 1	1.6	$1.8x10^{-11}$
Cdh6	cadherin 6	-1.6	$5.8x10^{-9}$
Pabpc6	poly(A) binding protein, cytoplasmic 6	1.6	$1.0x10^{-7}$
Lgals3bp	lectin, galactoside-binding, soluble, 3 binding protein	1.6	$4.9x10^{-7}$
Abhd11	abhydrolase domain containing 11	1.5	$1.9x10^{-5}$

Slx4	SLX4 structure-specific endonuclease subunit homolog (*S. cerevisiae*)	3.0	$2.6x10^{-5}$
C1qc	complement component 1, q subcomponent, C chain	1.3	$2.6x10^{-4}$
1810062O18Rik	RIKEN cDNA 1810062O18 gene	1.3	$5.7x10^{-4}$
4930597O21rik	RIKEN cDNA 4930597O21 gene	-1.4	$5.7x10^{-4}$

Table 2.1 Listed above are the differentially-expressed genes in the OGT cKO mice compared to their WT littermates at 3 weeks of age. FC = fold-change where negative values denote decreases. Reported *P*-values are Bonferroni corrected (*P*-values < 0.001).

2.5 Upregulation of immune response and AD-related genes in the OGT cKO mouse at 2 months

At 2 months of age, we observed a dramatic upregulation of hundreds of genes in the hippocampus of OGT cKO mice (Appendix I). Among the most highly upregulated were glial proliferation and immune response genes such as glial fibrillary acidic protein (*Gfap*, 6.0-fold), complement component 1q (*C1qb*, 4.0-fold), and complement component 3 (*C3*, 2.1-fold) (Appendix I). In addition, both *Lgals3bp* (5.0-fold in 2 month) and *C1qc* (3.5-fold in 2 month) were upregulated in OGT cKO hippocampi at both 3 weeks and 2 months of age. Increased expression of these and other representative genes was confirmed independently by qRT-PCR (Table 2.2). Notably, many of the same genes are upregulated in established AD mouse models that express familial Alzheimer's disease (FAD) mutations in presenilin 1 (*Psen1*), presenilin 2 (*Psen2*), and/or amyloid precursor protein (*App*) that lead to early onset AD (Table 2.2, Figure 2.2).[23,24] In addition, we validated these upregulated genes using qPCR as well. Importantly, these AD mouse models show similar levels of neuroinflammatory gene expression at 12-18 months of age while our mice are only 2 months of age.

Table 2.2 Upregulated genes in the OGT cKO at 2 months and in AD mouse models

		OGT cKO/WT Microarray		*OGT* cKO/WT qRT-PCR	AD Mouse Model Microarray[1]			AD Mouse Model qRT-PCR[2]	
Genes	**Description**	**FC**	***P*-values[3]**	**FC[4]**	**A**	**B**	**C**	**B**	**SEM**
Gfap	glial fibrillary acidic protein	6.0	$1.0x10^{-37}$	12	1.3	6.3	7.3	4.83	0.64
C1qb	complement component 1 q subcomponent beta polypeptide	4.0	$1.0x10^{-37}$	6.8	1.6	2.5	2.8	2.00	0.16
Tyrobp	TYRO protein tyrosine kinase binding protein	4.0	$1.0x10^{-37}$	6.1	2.0	3.6	4.8	2.54	0.06
Cd14	CD14 antigen	3.9	$1.0x10^{-37}$	5.4	1.4	1.8	2.3	-	-
C1qc	complement component 1, q subcomponent, C chain	3.5	$1.0x10^{-37}$	6.2	2.0	3.6	4.8	-	-
Gusb	glucuronidase beta	2.7	$1.0x10^{-37}$	3.6	1.4	2.3	2.4	-	-
B2m	beta-2 microglobulin	2.1	$1.8x10^{-29}$	4.4	-	-	-	2.03	0.09
C3	complement component 3	2.1	$2.6x10^{-21}$	8.1	-	-	-	-	-
Vim	vimentin	1.9	$5.2x10^{-4}$	3.1	-	-	-	1.81	0.14
Man2b1	mannosidase 2, alpha B1	1.7	$6.4x10^{-34}$	2.3	1.3	1.9	2.1	1.62	0.07

[1] Fold-expression changes of regulated genes in (A) 18-month old $APP^{NLh/NLh}/PS\text{-}1^{P264L/P264L}$ mice[24]; (B) 12-month-old Tg2576/$PS\text{-}1^{P264L/+}$ mice[24]; and (C) 12-month old Tg2576/$PS\text{-}1^{P264L/P264L}$ mice[24];

[2] Fold-expression changes of regulated genes in the 17-18-month old Tg2576/$PS\text{-}1^{P264L/P264L}$ mice[23]; SEM = standard error of the mean

[3] Microarray *P*-values were Bonferroni-corrected; FC = fold-change

[4] qRT-PCR *P*-values were calculated using a two-tailed Student's *t*-test (*P*-values < 0.05) ; FC = fold-change

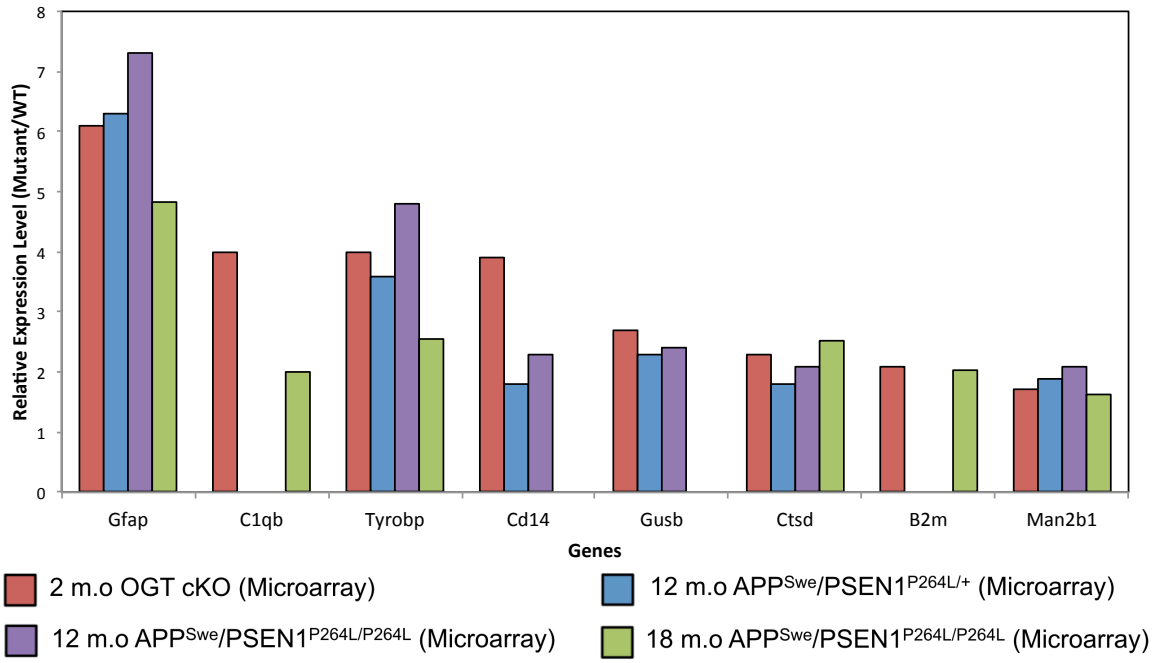

Figure 2.2 Barplot of upregulated genes in OGT cKO and AD mouse models. Here are the expression levels of representative upregulated genes from Table 2.2 (only microarray levels) in the 2 month old (m.o.) OGT cKO, 12 m.o. $APP^{Swe}/PSEN1^{P264L/+}$, 12 m.o. $APP^{Swe}/PSEN1^{P264L}$, and 18 m.o. $APP^{Swe}/PSEN1^{P264L}$. These upregulated genes are all involved in immune response.

Interestingly, there is also upregulation of genes that have been shown to affect the susceptibility for late-onset AD in humans, including the microglial genes: triggering receptor expressed on myeloid cells 2, *Trem2* (6.0-fold increase); inositol polyphosphate-5-phosphatase D, *Inpp5d* (2.3-fold); and phospholipase C, γ2, *Plcg2* (1.5-fold).[25-28] Using the Database for Annotation, Visualization, and Integrated Discovery (DAVID) bioinformatics tool, we found the top 3 GO categories were immunity (FDR < $2.0x10^{-33}$), immune system process (FDR < $1.4x10^{-29}$), and innate immunity (FDR<$1.6x10^{-27}$) (Table 2.3). The upregulation of microglial and immune response genes indicates substantial neuroinflammation in the OGT cKO at 2 months of age, confirming the IHC data and revealing elevated GFAP and Iba-1 staining at this age.

Table 2.3 DAVID GO annotation of OGT cKO/WT upregulated genes at 2 months

GO term	#	Gene names	FE
Immunity	73	*Zc3hav1, Ly86, Tirap, Tlr2, Tlr3, Ly9, C1qc, Tlr7, Btk, B2m, Isg20, C1ra, Tmem173, Myd88, Oasl2, Oasl1, Mx2, Pik3cg, Gbp5, Bst2, Inppl1, Herc6, H2-Dmb1, Serping1, Cd84, C1qa, C1qb, Cd86, Lat2, Lrmp, H2-Aa, Eif2ak2, Tnfaip8l2, C3, Csf1, Ifitm3, Gsdmd, Unc93b1, Ifi30, Oas2, Cd74, Naip6, Tap2, Tap1, Naip5, Iigp1, Inpp5d, Dhx58, Csf1r, Havcr2, Tlr12, Irgm1, Cfb, Hck, Tlr13, Axl, Myo1g, Samhd1, H2-Ab1, Trim25, Fcgr1, Psmb8, Lgals9, Psmb9, Ddx58, Ifit2, Trim56, Ifit1, Irf5, Irf7, H2-Eb1, Clec7a, Cd14*	6.3
Immune system process	72	*Zc3hav1, Ly86, Tirap, Tlr2, Tlr3, Ly9, C1qc, Tlr7, Btk, B2m, Isg20, C1ra, Tmem173, Myd88, Oasl2, Oasl1, Mx2, Pik3cg, Gbp5, Bst2, Inppl1, Herc6, H2-Dmb1, Serping1, Cd84, C1qa, C1qb, Cd86, Lat2, Lrmp, H2-Aa, Eif2ak2, Tnfaip8l2, C3, Csf1, Ifitm3, Gsdmd, Unc93b1, Ifi30, Oas2, Cd74, Naip6, Tap2, Tap1, Naip5, Iigp1, Inpp5d, Dhx58, Csf1r, Havcr2, Tlr12, Irgm1, Cfb, Hck, Tlr13, Axl, Myo1g, Samhd1, H2-Ab1, Trim25, Fcgr1, Psmb8, Lgals9, Psmb9, Ddx58, Ifit2, Trim56, Ifit1, Irf5, Irf7, H2-Eb1, Cd14*	5.6
Innate immunity	53	*Zc3hav1, Ly86, Tlr2, Tirap, Tlr3, Ly9, C1qc, Tlr7, Isg20, Btk, C1ra, Tmem173, Myd88, Oasl2, Oasl1, Mx2, Bst2, Herc6, Serping1, C1qa, Cd84, C1qb, Eif2ak2, Tnfaip8l2, C3, Csf1, Ifitm3, Gsdmd, Unc93b1, Oas2, Naip6, Naip5, Iigp1, Dhx58, Csf1r, Tlr12, Havcr2, Irgm1, Cfb, Hck, Tlr13, Axl, Samhd1, Trim25, Fcgr1, Ddx58, Trim56, Ifit2, Ifit1, Irf5, Irf7, Clec7a, Cd14*	7.7
Glycoprotein	225	*Kcne1l, Scpep1, A2m, Adora3, Ltbp3, Atp1b2, Osmr, Fgfrl1, Ptgs1, Aqp4, Cd52, Cd53, Megf10, Cd48, C1ra, Cd44, Apod, Serpine2, Grin2c, Ch25h, Ggta1, F11r, Ptprf, Pdpn, F9, Serping1, Sirpa, C1qa, Sstr5, C1qb, Cd37, Npc2, Ccr5, Serpinf1, Hepacam, Pmp22, Wfdc3, Il1r2, Il1r1, Mfng, Ifi30, Fcgrt, Oas2, Cd72, Cd74, Slc11a1, Lgals3bp, Slc29a3, Cd68, Lamb2, Fgl2, Gcnt1, Spp1, St6gal1, Slamf9, Cfb, Gusb, Tgfbr2, Rhbdf1, Sepn1, Col16a1, Cd63, Fcgr1, Fcgr3, Notch1, Clec7a, Tmem119, Gpr84, Gpr160, Mpeg1, Ly86, Il4i1, Ly9, Cd151, Ednrb, Tnfrsf11a, Scrg1, P4ha3, Angpt1, Sepp1,*	2.1

		Il13ra1, Lag3, Icam1, Gpr37l1, Bgn, Adam17, Fmod, C3, Csf1, Gpr65, Cxcl9, Tpcn1, Nagpa, Lect1, Ly6e, Il10ra, Thbs1, Thbs4, Pla2g15, Axl, H2-Ab1, P2ry13, Fcgr2b, Gria2, Abcc3, Slc15a3, Cd14, Slc44a2, Tspan4, Lgmn, Tlr2, Tlr3, Cspg5, Tlr7, Tapbp, Slc7a7, Olfml3, St3gal4, Csf3r, Lgi4, Asph, Il1a, Bst2, Plxnb2, H2-Dmb1, Hcst, Pnpla7, Gns, Cst7, Prcp, Reln, C3ar1, Ccl2, Abca9, Unc93b1, Lrig1, Itgb5, Itgb2, Abca1, Trf, Itgam, Timp1, Angptl6, P2ry6, Itgax, Ttyh2, P2ry1, Entpd4, Mfap3l, Entpd2, Csf1r, Havcr2, Tlr12, Mrc2, Tlr13, Tst, Lamp2, Gpr34, Itga6, Slc7a3, Cd274, H2-Eb1, Slc13a3, Scara3, Mertk, Igdcc4, Gm2a, Lrrc8a, Hexa, Hexb, Bcan, Cxadr, Sdc4, Sdc3, Glb1, Slc1a4, Ccrl2, Tor3a, Slc1a3, Hpse, Csf2rb, Itih3, Man2b1, Csf2ra, Slc43a3, Taar3, Lair1, Ctsz, Spint1, Ctss, Dnase2a, Cd84, Cd83, Ctsl, Serpina3n, Cd86, Grn, H2-Aa, Ctsd, Ctsb, Trem2, Pros1, Ctsh, Vim, Cd24a, Scarf2, Vcam1, Tnfrsf1a, Cd9, Tnfrsf1b, Glycam1, Smoc1, Gpnmb, Fgfbp1, Selplg, Gba, Tmc6, Ptprc, Hpn, Sun2, Sparc, Il6ra, Rgs20, Liph, Slc14a1	
Membrane	339	*Kcne1l, S100a6, Aif1, Atp1b2, Osmr, Ptgs1, Fgfrl1, Aqp4, Cd52, Cd53, Itsn1, Megf10, Rnf213, Btk, B2m, Cd48, Hmha1, Bak1, Cd44, Serpine2, Grin2c, Wnk4, Ch25h, Oasl1, Rapgef3, Ggta1, Pik3cg, Sgpl1, F11r, Gbp6, Gbp5, Ptprf, Pdpn, Ncf1, Ncf4, Pld4, Ptbp1, Ifi47, Gem, Lpcat2, Sirpa, Sstr5, Cd37, Aaas, Hepacam, Ccr5, Parp14, Cx3cr1, Tmem184b, Rab13, Pmp22, Eif2ak2, Il1r2, Mfng, Il1r1, Rtp4, Gnai2, Gsdmd, Fcgrt, Oas2, Cd72, Kcnj2, Sfxn5, Cd74, Slc11a1, Cd68, Slc29a3, Lgals3bp, Rac2, Cklf, Fcer1g, Gcnt1, Tyrobp, Blnk, St6gal1, Slamf9, Gusb, Rhbdf1, Tgfbr2, Nckap1l, Sepn1, Cd63, Fcgr1, Fcgr3, Atp13a4, Notch1, Gngt2, Rgs1, Parp9, Tmem119, Gpr84, Gfap, Slc20a1, Gpr160, Mpeg1, Fermt3, Kcnj10, Ly9, Cd151, Hvcn1, Ednrb, Tnfrsf11a, Pik3ap1, Fam129b, Il13ra1, Lag3, Icam1, Fmnl3, Inppl1, Clic1, Flnc, Arrdc3, Fcrls, Gpr37l1, Ripk1, Adam17, Lrmp, Susd3, Hsd3b7, Csf1, Gpr65, Hk2, Mfsd1, Apbb1ip, Tpcn1, Sft2d2, Glipr2, Nagpa, Lpxn, Lect1, Igtp, Dapp1, Ly6e, Klc1, Plin4, Il10ra, Rasa4, Irgm1, Pla2g15, Tbxas1, Irgm2, Plek, Baiap2l2, Rrbp1, Axl, Cyp4f14, Elavl1, H2-Ab1, Cyp4V3, Atp1a2, Gjb6, Capn2, Appl2, Itpr2, P2ry13, Rab31, Fcgr2b, Gria2, Plscr2, Abcc3, Cmtm7, Cmtm3, Slc15a3, Cd14, Tmem176b, Cmtm6, Tmem176a, Tspo, Gna15, Slc44a2, Tspan4, Tlr2, Tirap, Tlr3, Cspg5, Tlr7, Iqgap1, Slc7a7, Vcl, Tapbp, St3gal4, Csf3r, Asph, Scamp2, Myo6, Bst2, Plxnb2, Tor1aip1, H2-Dmb1, Pde4d, Psd2, Hcst, Pnpla7, Igsf6, Lat2, Plce1, Gbp3, Spata13, Gbp2, Mvp, Fxyd1, C3ar1, Gal3st4, Cav1, Abca9, Mcl1, Snx5, Ifitm3, Stk10, Phka1, Unc93b1, Itgb5, Lrig1, Itgb2, Abca1, Trf, Itgam, P2ry6, Dock1, Laptm5, Itgax, Ttyh2, Rasal3, P2ry1, Iigp1, Mfap3l, Entpd2, Csf1r, Hist1h4h, Arhgdib, Havcr2, Srebf1, Tlr12, Tlr13, Mrc2, Myo1g, Dock8, Reep3, Ddx58, Myo10, Lamp2, Gpr34, Slc7a3, Itga6, Ifi27l2a, H2-Eb1, Cd274, Plcg2, Slc13a3, Scara3, Mertk, Rhoj, Igdcc4, Tln1, Lrrc8a, Hexa, Hexb, Cxadr, Sdc4, Rhou, Syngr2, Sdc3, Ccrl2, Slc1a4, Cdc42, Tmem173, Slc1a3, Plekhb1, Hpse, Hmox1, Necap2, Csf2rb, Rhoc, Msn, Yap1, Csf2ra, Rhog, Ahnak, Slc43a3, Taar3, Lair1, Noxo1, Ms4a6c, Ms4a6d, Adipor2, Ctss, Slc9a3r1, Slc7a11, Vasp, Cd84, Stom, Cd83, Cd86, H2-Aa, Trem2, Cyth4, Cd24a, Scarf2, Vcam1, Cd9, Tnfrsf1a, Tnfrsf1b, Glycam1, Sh3glb1, Map3k1, Tap2, Shisa5, Tap1, Plcd4, Pik3r5, Inpp5d, Slc25a45, Appbp2, Gpnmb, Fgfbp1, Selplg, Inpp5a, Gba, Slc39a1, Snx20, Ehd4, Guca1a, Ptprc, Tmc6, Hpn, Gnao1, H2-M3, Hck, Sun2, Anxa5, Anxa3, Anxa2, Il6ra, Cyba, Rgs20, Itpripl2, Liph, Bmpr1b, Slc14a1*	1.5
Disulfide bond	183	*A2m, Adora3, Ltbp3, Atp1b2, Osmr, Lgmn, Fgfrl1, Ptgs1, Tirap, Tlr2, Tlr3, Cspg5, Megf10, C1qc, Tapbp, Cxcl10, Slc7a7, B2m, Cd48, C1ra, Olfml3, Isg15, Cd44, Apod, St3gal4, Csf3r, Asph, F11r, Bst2, Ptprf, Plxnb2, F9, H2-Dmb1, Serping1, Tcn2, Sirpa, Hcst, Igsf6, C1qa, Sstr5, C1qb, Npc2, Ccr5,*	2.0

		Hepacam, Cst7, Cx3cr1, Prcp, Reln, Wfdc3, Il1r2, C3ar1, Il1r1, Mfng, Ccl3, Ccl2, Gsdmd, Lrig1, Ifi30, Chchd2, Itgb5, Itgb2, Fcgrt, Abca1, Cd72, Ccl5, Ccl4, Trf, Itgam, Cd74, Timp1, Ccl6, Angptl6, Cd68, Lgals3bp, P2ry6, Lamb2, Itgax, P2ry1, Fcer1g, Fgl2, Entpd4, Mfap3l, Entpd2, Gcnt1, Csf1r, Tyrobp, Havcr2, St6gal1, Cfb, Slamf9, Tgfbr2, Mrc2, Fcgr1, Fcgr3, Notch1, Lamp2, Gpr34, Itga6, H2-Eb1, Cd274, Clec7a, Mertk, Igdcc4, Gm2a, Hexa, Ly86, Hexb, Bcan, Il4i1, Ly9, Cxadr, Ccrl2, Ednrb, Tnfrsf11a, Ang, Csf2rb, Angpt1, Man2b1, Il13ra1, Lag3, Taar3, Icam1, Lair1, Ctsz, Spint1, Ctss, Clic1, Fcrls, Gpr37l1, Dnase2a, Slc7a11, Cd84, Ctsl, Cd83, Cd86, Bgn, Grn, Ctsd, H2-Aa, Adam17, Ctsb, Susd3, Trem2, Ctsh, Pros1, Fmod, Cxcl5, C3, Csf1, Ndp, Endou, Cxcl9, Gpr65, Scarf2, Vcam1, Cd9, Tnfrsf1a, Nagpa, Tnfrsf1b, Lect1, Ly6e, Il10ra, Smoc1, Thbs1, Selplg, Fgfbp1, Thbs4, Gba, Hpn, Pla2g15, H2-M3, Axl, H2-Ab1, Sparc, Il6ra, P2ry13, Ccl12, Fcgr2b, Gria2, Liph, Bmpr1b, Cd14, Igfbp5	
Extracellular exosome	174	*S100a4, Scpep1, S100a6, Tspo, A2m, Slc44a2, Ltbp3, Lgmn, Ptgs1, Cd53, Aldh1l2, C1qc, Iqgap1, Vcl, B2m, Cd48, C1ra, Cd44, Apod, St3gal4, Rapgef3, Ddah1, F11r, Gbp6, Myo6, Scamp2, Bst2, Ptprf, Plxnb2, Ptbp1, F9, Serping1, Tcn2, Sirpa, Gltp, C1qa, Gns, Arpc1b, C1qb, Lat2, Renbp, Cd37, Npc2, Serpinf1, Prcp, Rab13, Vsig4, Mvp, Gal3st4, Naglu, Gnai2, Stk10, Ifitm3, Apoc1, Itgb5, Itgb2, Tagln2, Trf, Itgam, Cd74, Timp1, Angptl6, Lgals3bp, Lamb2, Rac2, Rasal3, Fgl2, Entpd2, Hist1h4h, Arhgdib, Spp1, Havcr2, Ptpn6, St6gal1, S100a16, Cfb, Lgals1, Gusb, Ephx2, Myo1g, Fcgr4, S100a10, Nckap1l, Cd63, Psmb8, S100a13, Psmb9, Fcgr3, Tst, Lamp2, H2-Eb1, Plcg2, Cd274, Slc13a3, Rhoj, Tln1, Gm2a, Hexa, Fermt3, Hexb, Sdc4, Syngr2, Glb1, Slc1a4, Tor3a, Cdc42, Ang, Acot11, Tubb6, Rhoc, Angpt1, Msn, Sepp1, Fam129b, Itih3, Cdk5rap2, Man2b1, Rhog, Ahnak, Lair1, Icam1, Ctsz, Padi2, Spint1, Clic1, Slc9a3r1, Was, Vasp, Dnase2a, Stom, Cd84, Mtmr11, Ctsl, Serpina3n, Cd86, Bgn, Grn, Ctsd, Ctsb, Ctsh, Pros1, Carhsp1, C3, Csf1, Vim, Vcam1, Aldh1a1, Glipr2, Sft2d2, Cd9, Sh3glb1, Shisa5, Thbs1, Inpp5a, Thbs4, Ehd4, Gba, Bcas1, Ptprc, Tmc6, Hpn, Pla2g15, Axl, Cotl1, Capn2, Anxa5, Appl2, Anxa4, Anxa3, Anxa2, Capg, Hpgd, Cmtm6, Cd14*	2.1
Cell surface	72	*Tln1, Lrrc8a, Tlr2, Tlr3, Cspg5, Ly9, Cd53, Sdc4, Cxadr, Sdc3, Slc1a4, Tnfrsf11a, Slc1a3, Cd44, Msn, Il1a, Icam1, Bst2, Plxnb2, Ctss, Slc7a11, Hcst, Cd86, Bgn, Ccr5, Adam17, Ctsb, Siglech, Cav1, Il1r1, Ifitm3, Ndp, Itgb5, Itgb2, Abca1, Cd24a, Itgam, Cd74, Trf, Vcam1, Slc11a1, Cd9, Tnfrsf1a, Itgax, P2ry1, Fcer1g, Pcsk6, Thbs1, Fgfbp1, Entpd2, Csf1r, Tyrobp, Havcr2, Ptprc, Hpn, Lgals1, Mrc2, Tgfbr2, Axl, Fcgr4, H2-Ab1, Sparc, Cd63, Anxa4, Anxa2, Il6ra, Notch1, Itga6, Fcgr2b, Gria2, Cd274, Cd14*	3.6
Phospho-protein	325	*S100a6, Adora3, Aif1, Pdlim4, Aqp4, Amotl1, Itsn1, Rnf213, Btk, Hmha1, C1ra, Fli1, Myd88, Cd44, Grin2c, Wnk4, Rapgef3, Ccna2, Ddah1, Pik3cg, Sgpl1, F11r, Ptprf, Suclg2, Ncf1, Ncf4, Ptbp1, F9, Gem, Sirpa, Aaas, Hepacam, Serpinf1, Ccr5, Parp12, Parp14, Cx3cr1, Tmem184b, Rab13, Eif2ak2, Il1r1, Gsdmd, Fcgrt, Cd72, Tagln2, Cd74, Tal1, Slc29a3, Lamb2, Fcer1g, Tyrobp, Blnk, Spp1, St6gal1, Ikzf1, Ptpn18, Lgals1, Rhbdf1, Tgfbr2, Fcgr1, S100a13, Tnni2, Notch1, Parp9, Tmod3, Clec7a, Tmem119, Sash3, Gpr84, Gfap, Zcchc24, Slc20a1, Fermt3, Fastk, Kcnj10, Ttc28, Ly9, Nfkb2, Hvcn1, Cdt1, Ednrb, Tnfrsf11a, Pbxip1, Tubb6, Epsti1, Pik3ap1, Sepp1, Fam129b, Zfp36, Batf3, Srpk3, Fmnl3, Hist1h1c, Inppl1, Clic1, Flnc, Was, Gpr37l1, Dok1, Ripk1, Adam17, Lrmp, Map3k14, Phyhd1, Triobp, Carhsp1, Nmi, C3, Klc4, Mfsd1, Apbb1ip, Zfp36l1, Sft2d2, Plekhg2, Lpxn, Dapp1, Klc1, Plin4, Bcl3, Fyb, Bcas1, Irgm1, Plek, Baiap2l2, Rrbp1, Hcls1, Zfp703, Axl, Elavl1, Trim25, Atp1a2, Samd4, Itpr2, Stat2, Rab31, Fcgr2b, Gria2,*	1.5

		Rps6ka1, Plscr2, Capg, Rassf2, Abcc3, Sh3rf2, Slc15a3, Tmem176b, Cmtm6, Tmem176a, Slc44a2, Prc1, Zc3hav1, Tirap, Tlr3, Cspg5, Aldh1l2, Iqgap1, Slc7a7, Kank2, Vcl, Trim47, Eif4ebp1, Aspg, Rbms2, Asph, Dap, Il1a, Scamp2, Myo6, Socs3, Plxnb2, Dtx3l, Rela, Tor1aip1, Mlxipl, Pde4d, Psd2, Foxn3, Ddit3, Hcst, Pnpla7, Gns, Tns3, Arpc1b, Lat2, Renbp, Plce1, Hspb6, Timeless, Nfe2l2, Spata13, Mvp, Fxyd1, C3ar1, Cav1, Mcl1, Snx5, Ifitm3, Stk10, Phka1, Unc93b1, Rabgap1l, Itgb5, Itgb2, Abca1, Trf, Timp1, Spc25, Dock1, Laptm5, Gmip, Ttyh2, Rasal3, Mfap3l, Runx1, Csf1r, Hist1h4h, Arhgdib, Havcr2, Srebf1, Ptpn6, Phactr4, Mrc2, Ak3, Ephx2, Tead1, Myo1f, Dock8, Reep3, Vav1, Ddx58, Tst, Atf5, Trim56, Myo10, Itga6, Slc7a3, Plcg2, Mertk, Tprn, Kif23, Igdcc4, Tln1, Lrrc8a, Bcan, Zcwpw1, Arhgap18, Cxadr, Skap2, Rhou, Syngr2, Sdc3, Fubp1, Slc1a4, Phc3, Cdc42, Plcb3, Heatr5a, Tmem173, Slc1a3, Hmox1, Casp8, Acot11, Necap2, Csf2rb, Msn, Yap1, Cdk5rap2, Lrrfip1, Rhog, Lair1, Ms4a6d, Slc9a3r1, Slc7a11, Cdk2, Vasp, Arhgap25, Cd84, Arhgap30, Stom, Ssfa2, Gpsm3, Vim, Scarf2, Patl1, Aldh1a1, Rgs10, Tnfrsf1b, Glycam1, Sh3glb1, Tsc22d4, Map3k1, Pik3r5, Zfp521, Inpp5d, Gpnmb, Dcx, Selplg, Nfatc1, Rcsd1, Snx20, Ehd4, Inf2, Cebpa, Ptprc, Tmc6, Hck, Sun2, Samhd1, Samd14, Anxa5, Samsn1, Cotl1, Anxa4, Anxa3, Anxa2, Irf9, Cyba, Ifit1, Rgs20, Irf5, Dbp, Irf7, Itpripl2, Slc14a1, Igfbp5, Sh3bp2	
Inflammatory response	48	*C3ar1, Ccl3, Ccl2, Cxcl5, Aif1, C3, Csf1, Ly86, Ptgs1, Gsdmd, Tirap, Cxcl9, Tlr2, Tlr3, Nfkb2, Ccl5, Ccl4, Tlr7, Ccl6, Cxcl10, Ccrl2, Naip6, Tnfrsf1a, Slc11a1, Tnfrsf1b, Myd88, Naip5, Thbs1, Il1a, Csf1r, Spp1, Pik3cg, Havcr2, Tlr12, Gbp5, Ncf1, Hck, Rela, Tlr13, Axl, Ephx2, Ccl12, Cyba, Ccr5, Clec7a, Nfe2l2, Bmpr1b, Cd14*	4.1
Lysosome	37	*Gm2a, Lgmn, Hexa, Ifitm3, Hexb, Unc93b1, Ifi30, Il4i1, Tlr7, Tpcn1, Glb1, Slc29a3, Cd68, Laptm5, Hpse, Man2b1, Gba, Irgm1, Ctsz, Pla2g15, Hck, Gusb, H2-Dmb1, Ctss, Arrdc3, Cd63, Dnase2a, Pnpla7, Gns, Ctsl, Lamp2, Npc2, Prcp, Ctsd, Ctsb, Slc15a3, Ctsh*	5.2
Signal peptide	183	*Scpep1, A2m, Ltbp3, Osmr, Lgmn, Fgfrl1, Ptgs1, Tlr2, Tlr3, Cd52, Cspg5, Megf10, C1qc, Tlr7, Tapbp, Cxcl10, B2m, Cd48, C1ra, Olfml3, Cd44, Apod, Serpine2, Grin2c, Csf3r, Lgi4, Htra3, F11r, Ucma, Ptprf, Pdpn, F9, H2-Dmb1, Serping1, Tcn2, Sirpa, Hcst, Igsf6, C1qa, Gns, C1qb, Npc2, Serpinf1, Hepacam, Cst7, Prcp, Reln, Fxyd1, Il1r2, Il1r1, Ccl3, Ccl2, Apoc1, Lrig1, Itgb5, Loc68395, Itgb2, Fcgrt, Ccl5, Ccl4, Trf, Itgam, Timp1, Ccl6, Angptl6, Cd68, Lgals3bp, Lamb2, Itgax, Fcer1g, Fgl2, Mfap3l, Csf1r, Spp1, Tyrobp, Havcr2, Tlr12, Cfb, Slamf9, Gusb, Tgfbr2, Mrc2, Tlr13, Col16a1, Fcgr1, Fcgr3, Notch1, Lamp2, Itga6, H2-Eb1, Cd274, Mertk, Tmem119, Igdcc4, Gm2a, Mpeg1, Hexa, Ly86, Hexb, Bcan, Zcwpw1, Il4i1, Ly9, Cxadr, Sdc4, Glb1, Sdc3, Tor3a, Ednrb, Tnfrsf11a, Hpse, Ang, Scrg1, P4ha3, Csf2rb, Angpt1, Sepp1, Itih3, Man2b1, Il13ra1, Csf2ra, Lag3, Icam1, Lair1, Ctsz, Spint1, Ctss, Fcrls, Gpr37l1, Dnase2a, Cd84, Ctsl, Cd83, Cd86, Serpina3n, Bgn, Grn, Ctsd, H2-Aa, Adam17, Ctsb, Trem2, Ctsh, Pros1, Fmod, Cxcl5, C3, Csf1, Ndp, Cxcl9, Cd24a, Scarf2, Vcam1, Tnfrsf1a, Nagpa, Tnfrsf1b, Glycam1, Ly6e, Il10ra, Smoc1, Shisa5, Gpnmb, Thbs1, 2810459m11rik, Fgfbp1, Selplg, Thbs4, Gba, Ptprc, Pla2g15, H2-M3, Axl, H2-Ab1, Sparc, Il6ra, Ccl12, Fcgr2b, Gria2, Itpripl2, Liph, Bmpr1b, Cd14, Igfbp5*	1.7
Disulfide bond	156	*A2m, Adora3, Ltbp3, Atp1b2, Osmr, Ptgs1, Fgfrl1, Tlr2, Tlr3, Cspg5, Megf10, C1qc, Tapbp, Cxcl10, B2m, Cd48, C1ra, Olfml3, Cd44, Apod, St3gal4, Csf3r, F11r, Ptprf, F9, Serping1, Tcn2, Sirpa, Igsf6, C1qa, Sstr5, C1qb, Npc2, Hepacam, Ccr5, Cst7, Cx3cr1, Reln, Il1r2, C3ar1, Il1r1, Ccl3, Ccl2, Lrig1, Itgb5, Loc68395, Fcgrt, Itgb2, Abca1, Ccl5, Cd72, Ccl4, Trf, Itgam, Cd74, Ccl6, Timp1, Angptl6, Lgals3bp, P2ry6, Cd68, Lamb2, Itgax, P2ry1, Fcer1g, Fgl2, Mfap3l, Gcnt1, Csf1r, Havcr2, St6gal1, Cfb, Slamf9,*	1.9

		Tgfbr2, Mrc2, Fcgr1, Fcgr3, Notch1, Lamp2, Gpr34, Itga6, H2-Eb1, Cd274, Clec7a, Mertk, Igdcc4, Gm2a, Hexa, Hexb, Bcan, Il4i1, Ly9, Cxadr, Ccrl2, Ednrb, Tnfrsf11a, Ang, Csf2rb, Angpt1, Man2b1, Il13ra1, Lag3, Taar3, Lair1, Icam1, Ctsz, Spint1, Ctss, Clic1, Gpr37l1, Dnase2a, Cd84, Ctsl, Cd83, Cd86, Bgn, Ctsd, H2-Aa, Adam17, Ctsb, Susd3, Trem2, Ctsh, Pros1, Fmod, Cxcl5, C3, Csf1, Ndp, Cxcl9, Gpr65, Scarf2, Vcam1, Tnfrsf1a, Nagpa, Tnfrsf1b, Lect1, Ly6e, Smoc1, Il10ra, Thbs1, Selplg, Fgfbp1, Thbs4, Gba, Hpn, Axl, H2-Ab1, Sparc, Il6ra, Ccl12, P2ry13, Fcgr2b, Liph, Cd14, Igfbp5	
Defense response to virus	32	*Apobec1, Zc3hav1, Ifitm3, Cxcl9, Unc93b1, Tlr3, Oas2, Tlr7, Cxcl10, Isg20, Tmem173, Itgax, Isg15, Oasl2, Ddx60, Oasl1, Mx2, Dhx58, Ptprc, Bst2, Trim34a, Samhd1, Trim25, Stat2, Ddx58, Ifit2, Trim56, Ifit1, Cd86, Irf5, Oas1c, Eif2ak2*	5.7
Osteoclast differentiation	30	*Il1r1, Csf1, Nfkb2, Btk, Tnfrsf1a, Tnfrsf11a, Pik3r5, Il1a, Csf1r, Blnk, Nfatc1, Tyrobp, Pik3cg, Ncf1, Socs3, Ncf4, Rela, Tgfbr2, Socs1, Fcgr4, Fcgr1, Sirpa, Fcgr3, Stat2, Irf9, Cyba, Fcgr2b, Plcg2, Trem2, Map3k14*	5.6

Table 2.3 contains the top 20 DAVID functional gene ontology annotations of the OGT cKO/WT upregulated differentially-expressed genes. Redundant GO categories were removed. FE = fold-enrichment; FDR $<6.2x10^{-11}$

2.6 Synaptic genes, OGT, and OGA are not differentially-expressed in the OGT cKO mouse hippocampus at 2 months

At 2 months of age, genes that showed little alteration in the AD mouse model Tg2576/PS-$1^{P264L/P264L}$, such as the synaptic genes growth-associated protein 43 (*Gap43*), syntaxin (*Synt*), synaptophysin I (*Syp*), and synaptotagmin I (*Syt1*), were also not differentially expressed in OGT cKO hippocampi (Table 2.4) suggesting that there may not be synaptic impairments across all neurons at this point.[23] Importantly, we did not see *Ogt* or *Mgea5* (OGA) differentially expressed in the OGT cKO at 2 months despite the fact that *Ogt* is being knocked out progressively. This is likely due to the fact that our CaMKIIα promoter restricts expression of Cre recombinase to excitatory neurons in the forebrain while OGT is still present in other cell types such as inhibitory neurons or glia, which are proliferating in 2-month-old OGT cKO mice. Overall, the similarities in the transcriptional profiles between OGT cKO mice and AD mouse models suggest that they may share common underlying mechanisms of neurodegeneration.

Table 2.4 Non-differentially expressed genes in 2-month-old OGT cKO hippocampus

		OGT cKO/WT Microarray		*OGT* cKO/WT qRT-PCR		AD Mouse Model qRT-PCR[23]	
Genes	**Description**	**FC**	***P*-values**	**FC**	***P*-values**	**FC**	**SEM**
Synt	syntaxin	1.0	$5.7x10^{-1}$	-1.1	1.0	-1.1	0.07
Nr4a2	nuclear receptor subfamily 4, group A, member 2	1.2	$1.3x10^{-1}$	-1.1	0.89	-	-
Syt1	synaptotagmin I	-1.1	$8.1x10^{-3}$	-1.1	1.0	1.1	0.19
Mgea5	meningioma expressed antigen 5 (hyaluronidase) (OGA)	-1.2	$1.8x10^{-2}$	-1.1	1.0	-	-
Ogt	O-linked N-acetylglucosamine (GlcNAc) transferase[3]	-1.3	$3.7x10^{-3}$	-1.1	1.0	-	-
Syn1	synapsin I	1.1	$7.8x10^{-2}$	-1.1	1.0	1.0	0.07
Syp	synaptophysin I	-1.1	$6.5x10^{-2}$	1.0	1.0	1.0	0.05
Nr2b	glutamate receptor, ionotropic, NMDA2b (epsilon 2) (Grin2b)	1.2	$2.8x10^{-4}$	1.0	1.0	-1.2	0.05
Gap43	growth-associated protein 43	1.0	$9.7x10^{-1}$	1.4	1.0	1.0	0.01

Table 2.4 shows the genes that were not differentially expressed in 2-month-old OGT cKO hippocampi. Fold-expression changes of regulated genes in the 17-18-month old Tg2576/PS-$1^{P264L/P264L}$ mouse.[23] FC = fold-change where negative fold-change values denote decreases; SEM = standard error of the mean; microarray *P*-values are Bonferroni-corrected *P*-values; qRT-PCR *P*-values were calculated using a two-tailed Student's *t*-test.

2.7 Cholesterol and lipid biosynthesis genes are downregulated in OGT cKO hippocampi at 2 months

Based on the DAVID analysis, the downregulated genes in the OGT cKO mice at 2 months were enriched for genes involved in metabolism including cholesterol (FDR<$3.6x10^{-7}$) and lipid biosynthesis (FDR<$1.3x10^{-2}$) (Table 2.5, Appendix II). Several enzymes involved in the steroid biosynthetic pathway are downregulated in the OGT cKO mouse in addition to genes involved in glycolysis, the mevalonate pathway, and terpenoid biosynthesis (Table 2.5, Figures 2.3, 2.4). Cholesterol biosynthesis has been implicated in AD since one of the major late-onset AD mutations occurs in apolipoprotein E (*Apoe*), a critical regulator of cholesterol metabolism.[29,30] In addition, cholesterol turnover is required for proper LTM formation in the hippocampus.[31,32] Dysregulation of cholesterol has been shown to be a hallmark of several neurodegenerative diseases and psychiatric illnesses.[33-35] In addition to downregulation of

the enzymes responsible for cholesterol synthesis, we observed decreases in the expression of sterol regulatory element-binding protein 2 (SREBP2, *Srebf2,* -1.4-fold), the master TF regulator of cholesterol biosynthesis, and insulin induced gene 1 (*Insig1*, -1.5-fold), which prevents the proteolytic activation of the SREBPs.[35,36] OGT has been shown to be a critical regulator of a myriad of metabolic pathways including glycolysis, gluconeogenesis, glycogen synthesis, and lipogenesis.[37-40] In particular, OGT is known to *O*-GlcNAcylated nuclear liver X receptor (LXR), which leads to enhanced expression of SREBP-1c, the major TF regulator of lipogenesis.[37] Highlighting the interconnected nature of metabolic networks, LXR-mediated transcription of SREBP-1c requires a sterol ligand produced downstream of SREBP2 activity.[41,42] Therefore, SREBP2 downregulation will likely interfere with SREBP-1c-mediated lipogenesis. In these ways, the removal of OGT perturbs cholesterol and lipid biosynthesis by interfering with transcriptional regulators, biosynthetic enzymes, and post-transcriptional regulatory mechanisms. A previous study demonstrated that OGT knockout in *C. elegans* impaired insulin signaling, which resulted in a 3-fold reduction in lipid storage and triglyceride levels and a reduction in sterol esters accompanied by a 3-fold increase in trehalose and glycogen storage.[43] The connection between OGT and cholesterol biosynthesis contrasts a previous mammalian study that showed that inhibition of OGT failed to affect cholesterol synthesis, albeit on a significantly shorter time scale (30 min inhibitor treatment) in a different cell type (HepG2 liver carcinoma cells).[44] Overall, our study supports a critical role of OGT in cholesterol and lipid homeostasis.

Table 2.5 DAVID GO annotation of OGT cKO/WT downregulated genes at 2 months

GO term	#	Gene names	FE
Cholesterol biosynthetic process	9	*Tm7sf2, Cyp51, Mvd, Dhcr7, Insig1, Fdps, Idi1, Hsd17b7, Fdft1*	32

Steroid metabolism	11	*Tm7sf2, Cyp51, Sult4a1, Mvd, 0610007P14Rik, Dhcr7, Insig1, Fdps, Idi1, Fdft1, Srebf2*	17
Sterol biosynthesis	8	*Tm7sf2, Cyp51, Mvd, 0610007P14Rik, Dhcr7, Fdps, Idi1, Fdft1*	36
Biosynthesis of antibiotics	13	*Cyp51, Tm7sf2, Mvd, Fdps, Pfkp, Hk1, Pgam2, Acss2, Acat2, Gpi1, Fdft1, Idi1, Hsd17b7*	7.7
Lipid biosynthesis	10	*Tm7sf2, Cyp51, Mvd, 0610007P14Rik, Dhcr7, Fdps, Idi1, Hsd17b7, Fdft1, Fam57b*	7.3
Metabolic pathways	24	*Tm7sf2, Cyp51, Adss, Mvd, B3galt4, Pfkp, Fdps, Pgam2, Hk1, Acss2, Acat2, Gpi1, Acot5, Fdft1, Acot3, Tdo2, Dhcr7, Gls, B3galnt1, Inpp4b, Fuk, Idi1, Galnt13, Hsd17b7*	2.4

Table 2.5 contains the top DAVID functional gene ontology annotations of the OGT cKO/WT downregulated differentially-expressed genes at 2 months of age. Redundant and non-significant GO terms were removed from the list. Redundant GO terms were removed from the table. FE = fold-enrichment; FDR $<5.0x10^{-2}$.

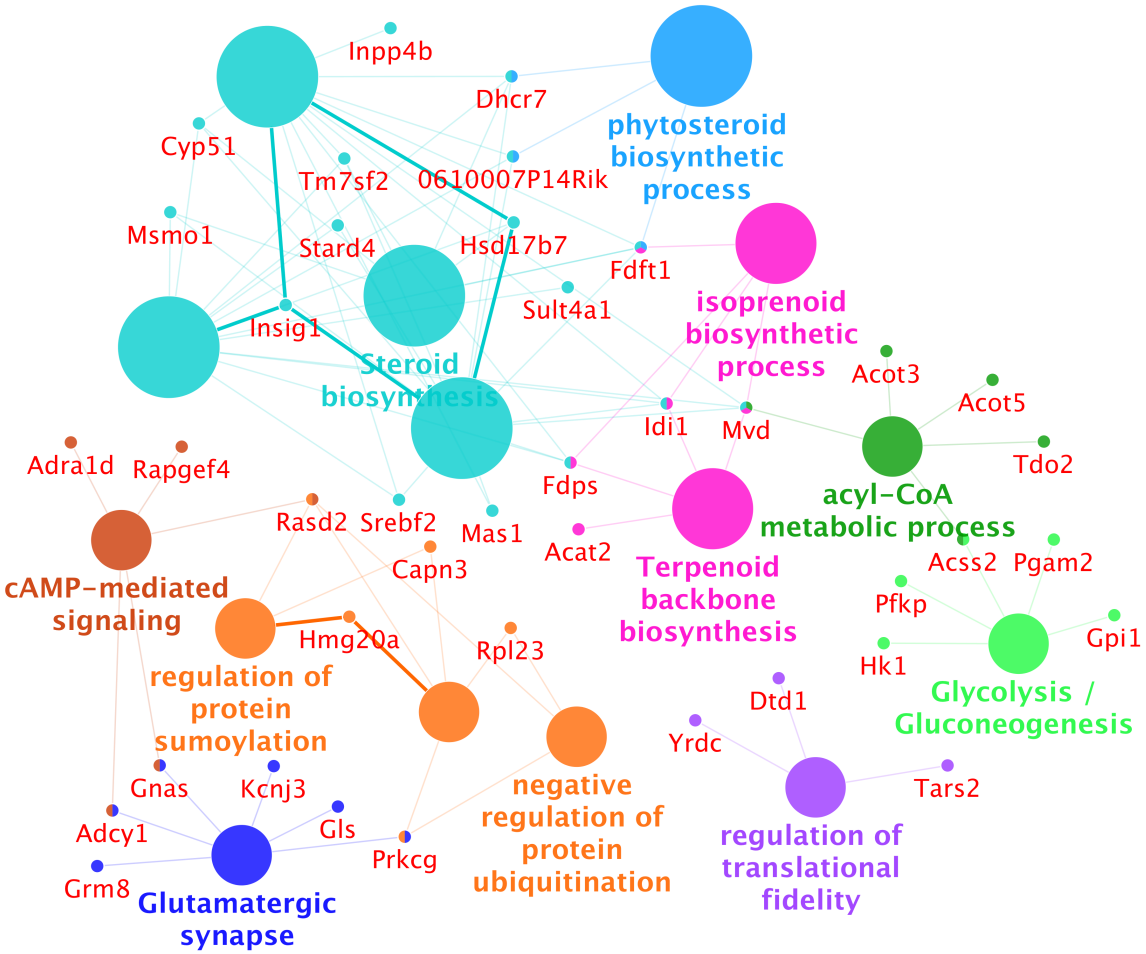

Figure 2.3 Cytoscape gene ontology annotations for OGT cKO 2 m.o. downregulated genes are enriched for metabolic genes. The categories include regulation of transcriptional fidelity, glycolysis/gluconeogenesis, glutamatergic synapse, acyl-CoA metabolic process, phytosteroid biosynthetic process, cAMP-mediated signaling, terpenoid backbone biosynthesis, isoprenoid biosynthetic process, regulation of protein sumoylation, and steroid biosynthesis. The genes that belong to and are shared by these gene ontology categories are also shown. The gene annotations were performed using the GO Biological Processes and KEGG Pathways database with the ClueGO extension in Cytoscape. The significance for all listed categories are Bonferroni step down corrected $P < 0.0042$.

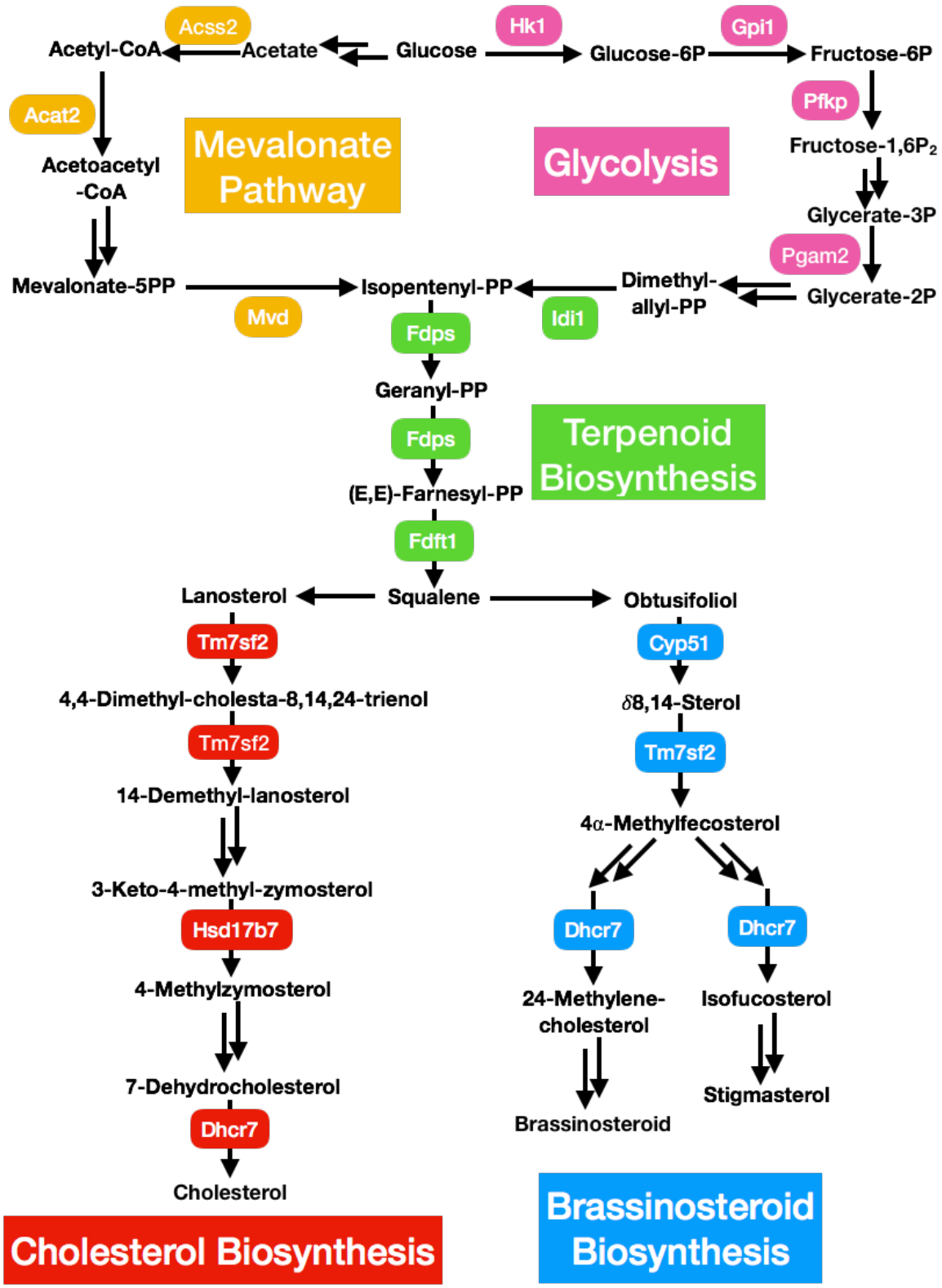

Figure 2.4 OGT cKO downregulated genes are involved in metabolism. Genes involved in glycolysis, mevalonate pathway, terpenoid biosynthesis, brassinosteroid biosynthesis, and cholesterol biosynthesis are

downregulated in the OGT cKO. All the genes listed are significantly downregulated (Bonferroni *P*-value < 0.001) and shown in the context of their substrates, products, and overall metabolic pathways.

Finally, glutamatergic synaptic genes including guanine nucleotide binding protein, α stimulating (*Gnas*, -1.5-fold); adenylate cyclase 1 (*Adcy1*, -1.3-fold); glutamate receptor, metabotropic 8 (*Grm8*, -1.5-fold); glutaminase (*Gls*, -1.5-fold); and the potassium channel (*Kcnj3*, -1.5-fold) were downregulated consistent with progressive knockout and degeneration of excitatory glutamatergic neurons. In summary, the genes downregulated in the OGT cKO at 2 months indicate impaired cholesterol and lipid biosynthesis and glutamatergic synaptic signaling.

2.8 OGT knockout is highly correlated with an immune response gene network

To determine whether entire networks of genes were deregulated in OGT cKO mice, a weighted gene coexpression network analysis (WGCNA) was performed to organize genes into biologically meaningful groups.[45,46] After performing WGCNA, we identified two gene modules that were significantly correlated with OGT deletion and not significantly correlated with age with cor = 0.71 ($P < 3.8 \times 10^{-28}$) and cor = 0.77 ($P < 1.2 \times 10^{-18}$) (Figure 2.5, Figure 2.6a). Using gene ontology analysis, we found that the first green module was enriched with genes involved in the immune response ($P < 3.4 \times 10^{-4}$) such as Bcl-2 homologous antagonist killer (*Bak1*, 1.4-fold increase) and Shc homology 2-domain containing phosphatidylinositol-3,4,5-trisphosphate 5-phosphatase 2 (*Inppl1*, 1.4-fold increase) (Figure 2.6B). Bak1, a central pro-apoptotic member of the Bcl-2 family, is required for mitochondrial permeabilization and release of cytochrome c into the cytosol in the early stages of apoptosis.[47] The inositol polyphosphate 5-phosphatase SHIP2 (*Inppl1*) regulates macrophage phagocytosis and links metabolic signaling to the immune response.[48] Interestingly, SHIP2 has recently been implicated in connecting Aβ

to tau pathology through dysregulated phosphoinositide metabolic signaling in the 3xTg AD mouse model.[49] Enhanced expression of apoptosis- and immune-related genes is consistent with the extensive apoptosis observed in OGT cKO (Figure 2.1), and the upregulation of immune response genes observed in other AD mouse models.[24]

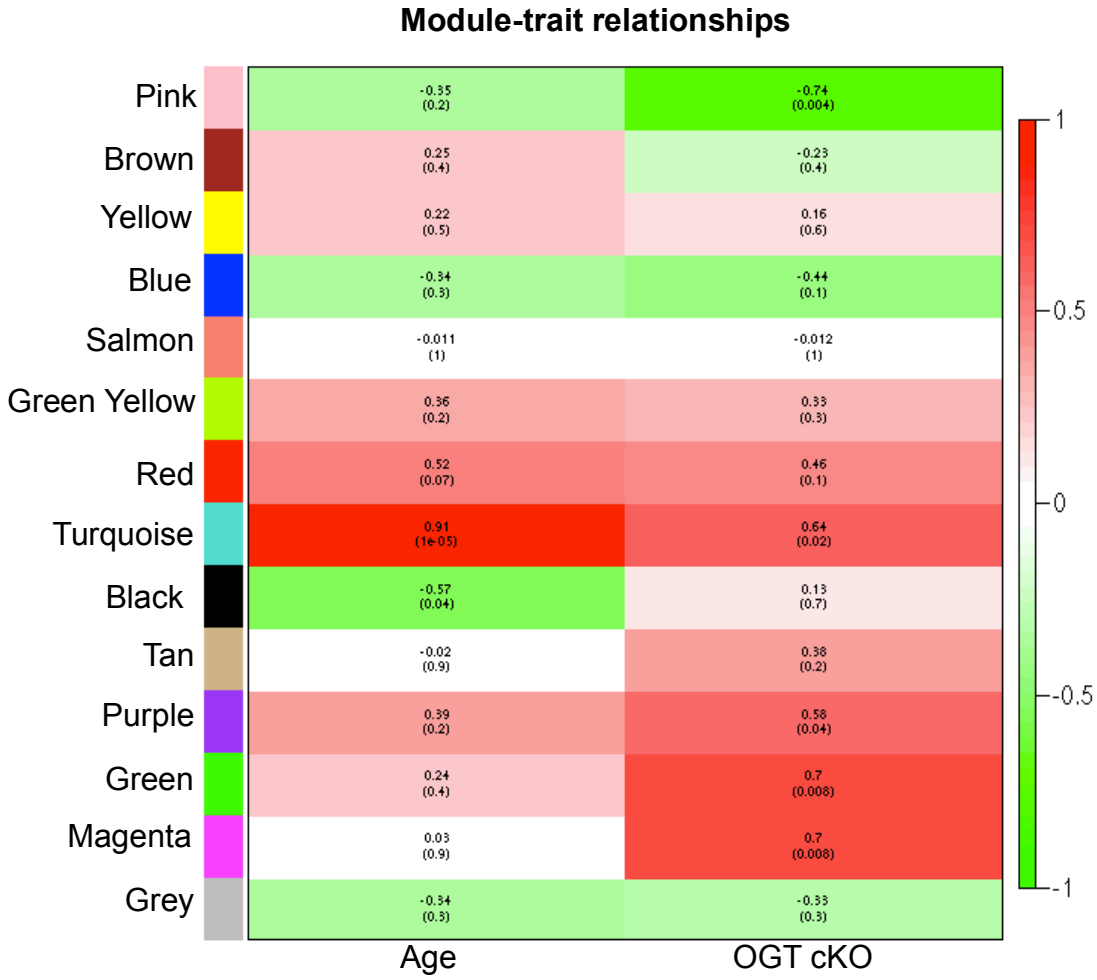

Figure 2.5 Heatmap indicating the module-trait relationships. Each of the 14 WGCNA modules can be correlated with certain traits including, in this case, mouse age and OGT cKO. Shown here is a heatmap indicating the strength of the correlation between each of the modules (given arbitrary colors) and mouse age and genotype (WT or OGT cKO).

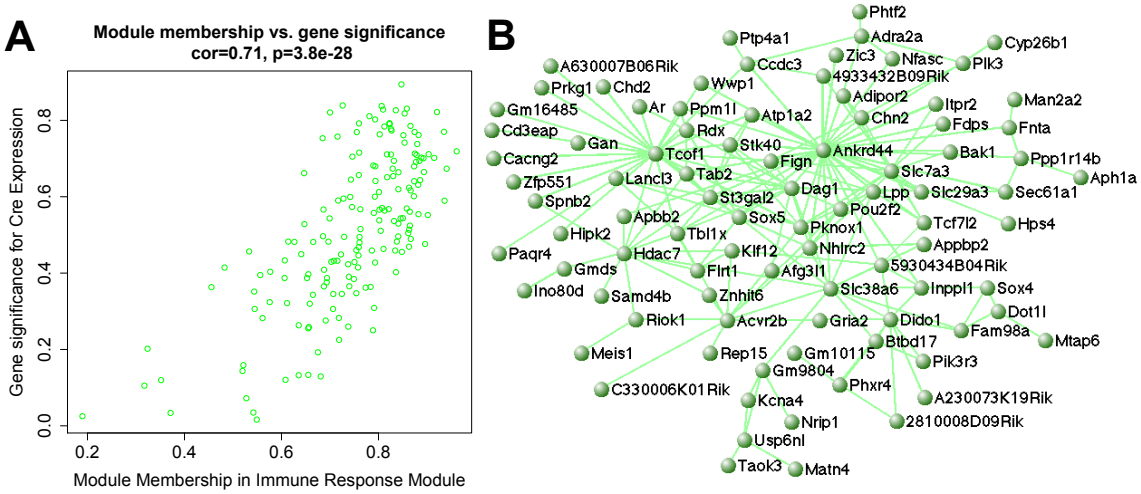

Figure 2.6 Green gene module is highly correlated with OGT cKO. (**A**) Cre expression in OGT cKO mice was significantly and highly correlated with membership in the green immune response module (cor = 0.71, $P = 3.8 \times 10^{-28}$). (**B**) The green module gene network is enriched for immune response (gene ontology enrichment $P < 3.75 \times 10^{-5}$). The gene network image was generated using VisANT (weight cutoff > 0.1).

Furthermore, the green module was enriched for genes involved in glial proliferation (Figure 2.7). Correlation of OGT cKO with a module enriched for glial differentiation and development is consistent with the extensive gliosis observed by IHC and confirmed by elevated expression of *Gfap* seen by both microarray and qPCR. Indeed, previous studies have shown that gliosis-related gene expression changes often dominate the transcriptional landscape in whole tissue global transcriptome studies.[50] Consistent with other studies looking at transcriptomic changes in AD hippocampi, we observed an upregulation of astrocytic genes such as *Gfap* and *Aqp4* and the microglial genes *Aif1* (Iba-1), *Cd68*, and *Emr1* with no changes in oligodendrocytic genes such as *Mbp, Sox10, Mog,* and *Mag* (Table 2.6).[51-53] Inconsistent with these AD human studies but consistent with AD mouse models, we did not yet observe downregulation of neuronal synaptic genes such as *Synt*, *Syn1, Syp,* and *Syt1* although there was a slight, non-significant decrease in the neuronal marker *Rbfox3* (NeuN, -1.2-fold, $P < 6.4 \times 10^{-5}$, Bonferroni-corrected P = not significant) (Table 2.4).[23,51,52] This suggests that insufficient

neuronal loss has occurred in the OGT cKO at 2 months to fully recapitulate the downregulation of neuronal marker genes and/or that the OGT cKO mice show more transcriptional similarities to the AD mouse models than to human AD patients.

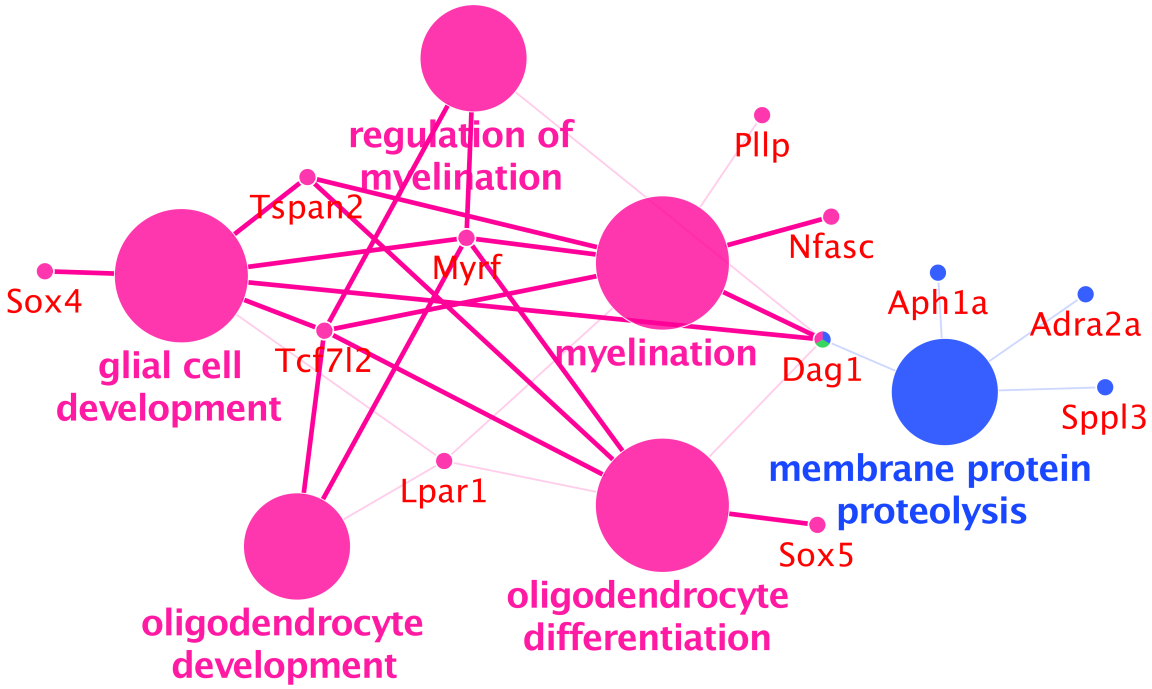

Figure 2.7 Cytoscape gene ontology annotations for the green module glial development-related genes. The categories include glial cell development and membrane protein proteolysis. The genes that belong to and are shared by these gene ontology categories are also shown. The gene annotations were created performed using the GO Biological Processes and Molecular Functions with the ClueGO extension in Cytoscape. The significance for all listed categories are Bonferroni step down corrected $P < 0.0039$.

Table 2.6 Cell type marker genes in the OGT cKO at 2 months

Genes	Description	Cell type	$\log_2$(FC)	FC	*P*-values
Gfap	glial fibrillary acidic protein	Astrocyte	2.60	6.0	0
Aqp4	aquaporin 4	Astrocyte	0.86	1.8	1.3×10^{-7}
Aif1	allograft inflammatory factor 1	Microglia	1.41	2.7	0
Cd68	CD68 antigen	Microglia	1.80	3.5	0
Emr1	EGF-like module containing, mucin-like, hormone receptor-like sequence 1	Microglia	1.17	2.2	1.5×10^{-18}
Mbp	myelin basic protein	Oligodendrocyte	0.034	1.0	N.S.
Sox10	SRY-box containing gene 10	Oligodendrocyte	0.12	1.1	N.S.
Mog	myelin oligodendrocyte glycoprotein	Oligodendrocyte	-0.20	-1.1	N.S.
Mag	myelin-associated glycoprotein	Oligodendrocyte	0.28	1.2	N.S.

Table 2.6 contains the $\log_2$(FC), FC, and *P*-values for different gene markers for astrocytes, microglia, and oligodendrocytes. OGT cKO/WT downregulated differentially-expressed genes at 2 months of age. FC = fold-change where negative fold-change values denote decreases; N.S. = not significant; *P*-values are Bonferroni corrected.

Furthermore, the green module was enriched for genes for proteins localized to the nucleus and involved in transcription ($P < 3.0\text{x}10^{-3}$ and $P < 2.6\text{x}10^{-2}$ respectively) suggesting that knocking out OGT is perturbing transcription and DNA-related processes. A few of the green module genes were DNA damage and repair genes, but these were not differentially expressed. This finding is consistent with the major role of OGT in transcriptional regulation and DNA damage response (see Chapter 4 for more on the role of *O*-GlcNAc in transcription and DNA damage response).[54] Finally, WGCNA allows one to identify "hub" genes with high connectivity within a given module (gene network). Knocking out these "hub" genes perturbs the entire gene network and affects traits that are highly correlated with its module.[55] Hub genes that have high connectivity in the green module include ankrin repeat domain 44 (*Ankrd44*, 40 interactors) and Treacher Collins Franceschetti syndrome 1, homolog (*Tcof1*, 28 interactors) (Figure 2.6B). *Ankrd44* is the gene for a regulatory component of the protein phosphatase 6 holoenzyme.[56] Protein phosphatase 6 (a.k.a. PP2a) regulates a myriad of functions, including regulating homology-directed repair of dsDNA breaks, mitotic spindle formation, E-cadherin maintenance at adherens junctions, ER to golgi transport, JNK pathway signaling, and NF-κB signaling.[57-62] *Tcof1* encodes a nucleolar protein that is important for (1) ribosomal RNA transcription, (2) maintenance of genomic integrity in response to DNA damage, (3) linking translation to DNA damage through roles (1) and (2), and (4) priming and protecting cells from oxidative stress during neuronal differentiation and development.[63-66] Overall, these hub genes could be key therapeutic targets for mediating the effects of *O*-GlcNAc loss on gliosis and neuroinflammation.

2.9 OGT knockout is highly correlated with a cell cycle arrest gene network

A second magenta module was enriched with genes involved in cell cycle arrest ($P < 3.8 \times 10^{-5}$), including antigen KI-67 (*Mki67*), protein regulator of cytokinesis 1 (*Prc1*), and kinetochore protein Spc25 (*Spc25*) (Figures 2.5 and 2.8, Table 2.7). To explore further the connection between OGT ablation and cell cycle arrest, we probed OGT cKO mice for evidence of altered neuronal cell cycle progression. Although immunostaining of hippocampal neurons for proliferating cell nuclear antigen (PCNA) and bromodeoxyuridine (BrdU) revealed no appreciable differences (Figures 2.9 and 2.10), we observed a significant increase in the levels of cyclin A2 in the OGT cKO dentate gyrus compared to WT mice (Figure 2.11B). Cyclin A2 is an initiator of DNA replication during S-phase and is a well-established marker for cell cycle progression.[67] The Cyclin A2 positive neurons were found in *O*-GlcNAc-negative neurons throughout the dentate gyrus and the hilus and CA3 regions, but not in the CA1 and CA2 regions of the hippocampus (Figure 2.11A, C). This is consistent with the distribution of CaMKIIα expression where the highest expression in the mouse hippocampus is observed in the dentate gyrus followed by the CA3 region.[68] Importantly, previous studies have observed inappropriate cell cycle advancement in neurons of AD patients and AD mouse models and specifically the presence of Cyclin A2 in neurons in the hippocampus of AD mouse.[69,70] In human AD patient hippocampi and forebrains, post-mitotic neurons undergo S phase and DNA replication prior to neuronal loss.[71]

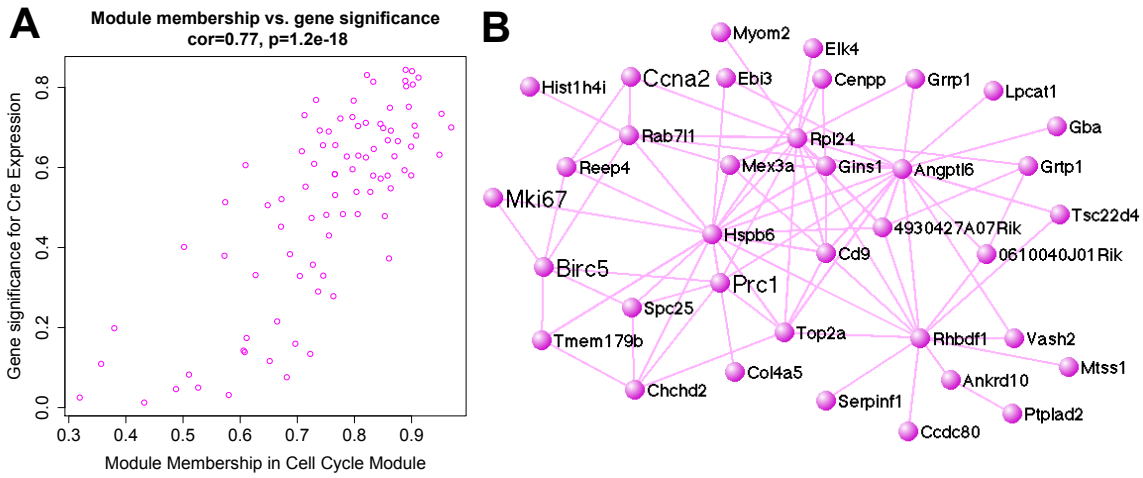

Figure 2.8 Magenta module is highly correlated with OGT cKO. (A) Cre expression in OGT cKO mice was significantly and highly correlated with membership in the magenta module (cor = 0.77, $P = 1.2 \times 10^{-18}$). (B) The magenta module was enriched for genes involved in cell cycle arrest (gene ontology enrichment $P < 3.4 \times 10^{-4}$). The magenta module gene network was generated in VisANT (weight cutoff > 0.1) and includes representative genes *Ccna2*, *Prc1*, and *Spc25*.

Table 2.7 DAVID GO annotation of magenta module genes

GO terms	#	Gene names	FE
Cell cycle	13	*Mitd1, Spc25, Mki67, Birc5, Cdca3, Ccna2, Cdkn1a, Gadd45a, Prc1, Reep3, Reep4, Ttc28, Txn14a*	6.0
Cell division	10	*Mitd1, Spc25, Birc5, Cdca3, Ccna2, Prc1, Reep3, Reep4, Ttc28, Txn14a*	7.7
Mitosis	8	*Spc25, Birc5, Cdca3, Ccna2, Reep3, Reep4, Ttc28, Txn14a*	8.9

Table 2.7 contains the top DAVID functional gene ontology annotations of the magenta module genes. Redundant and non-significant GO terms were removed from the list. FE = fold-enrichment; FDR < 5.0×10^{-2}.

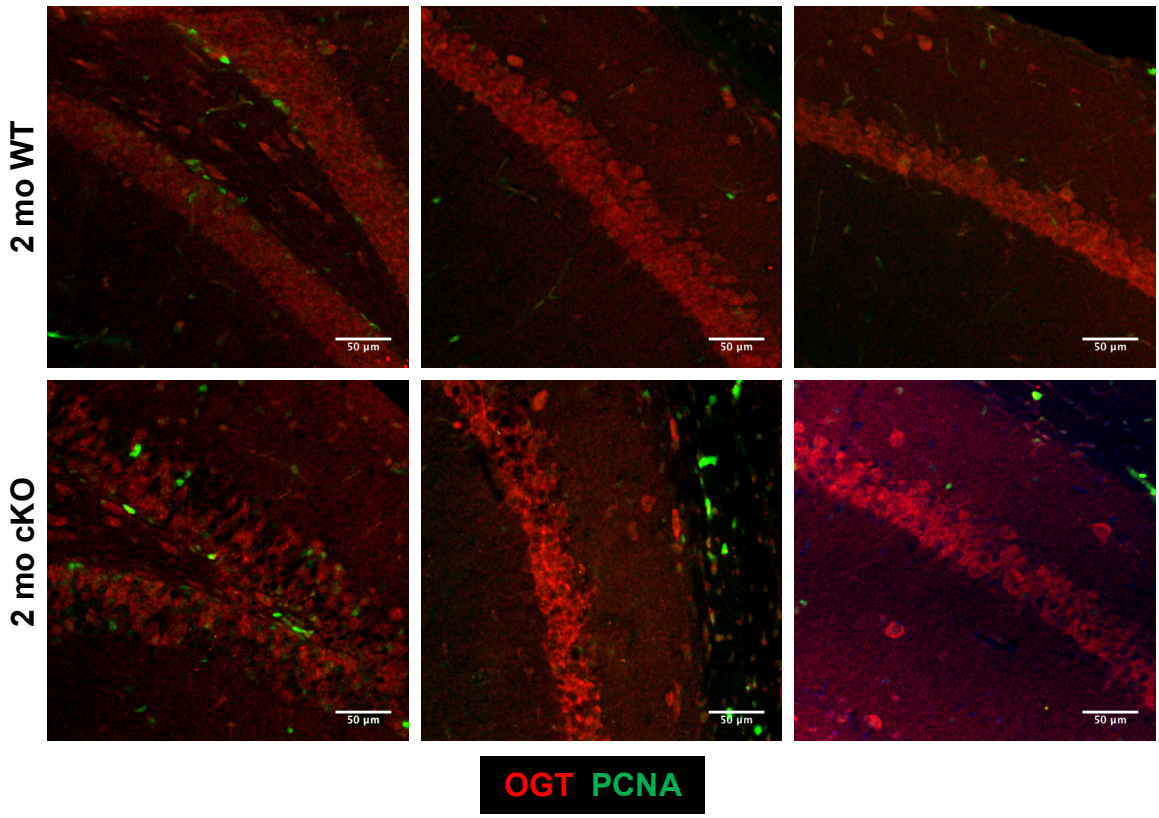

Figure 2.9 OGT cKO mice exhibit unchanged levels of PCNA-positive hippocampal neurons. No significant change in the number of PCNA-positive neurons was observed by immunostaining in the dentate gyrus or the CA1 regions of 2-month-old OGT cKO mice relative to WT mice. The few PCNA and BrdU-positive cells observed resided in the subgranular zone (SGZ) where adult neurogenesis occurs or outside of the hippocampus. Scale bar = 50 µm, n=4, each genotype.

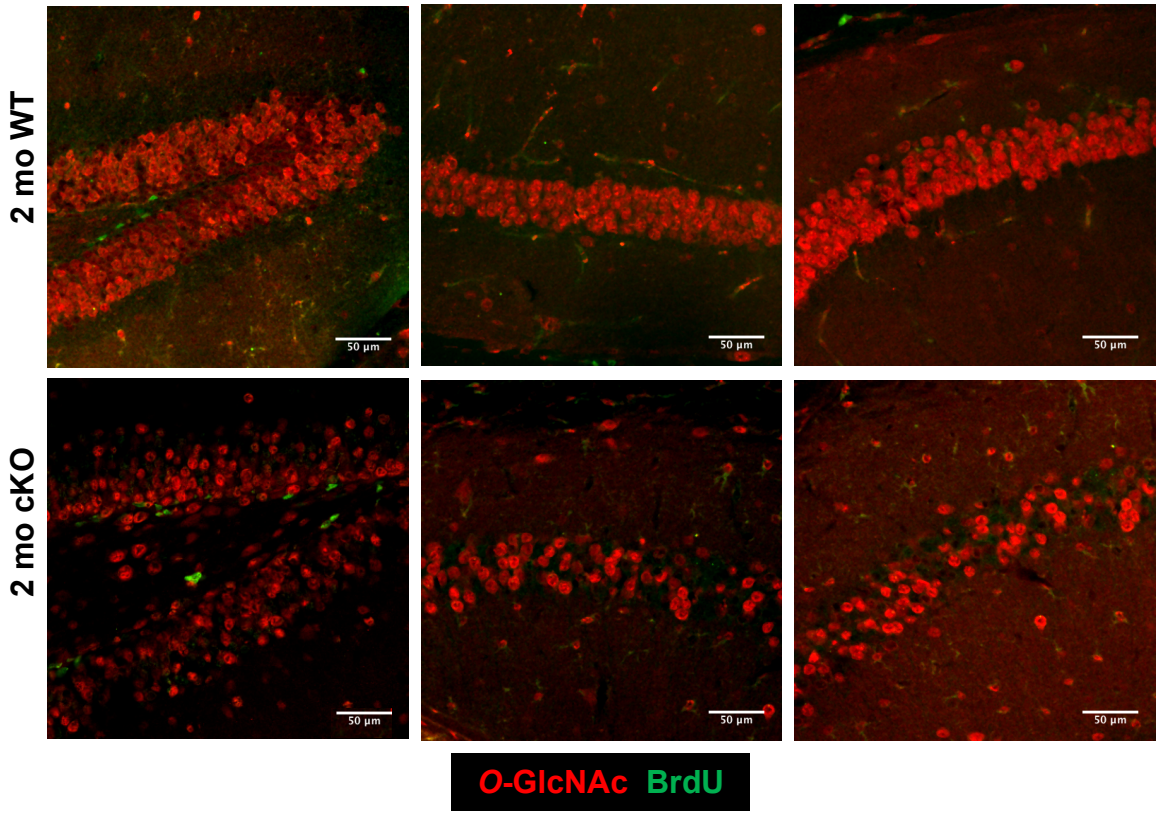

Figure 2.10 OGT cKO mice exhibit unchanged levels of BrdU-positive hippocampal neurons. No appreciable change in the number of BrdU-positive neurons was observed by immunostaining in the dentate gyrus or the CA1 regions of 2-month-old OGT cKO mice relative to WT mice. The few BrdU-positive cells observed resided in the subgranular zone (SGZ) where adult neurogenesis occurs. Scale bar = 50 µm, n=4, each genotype.

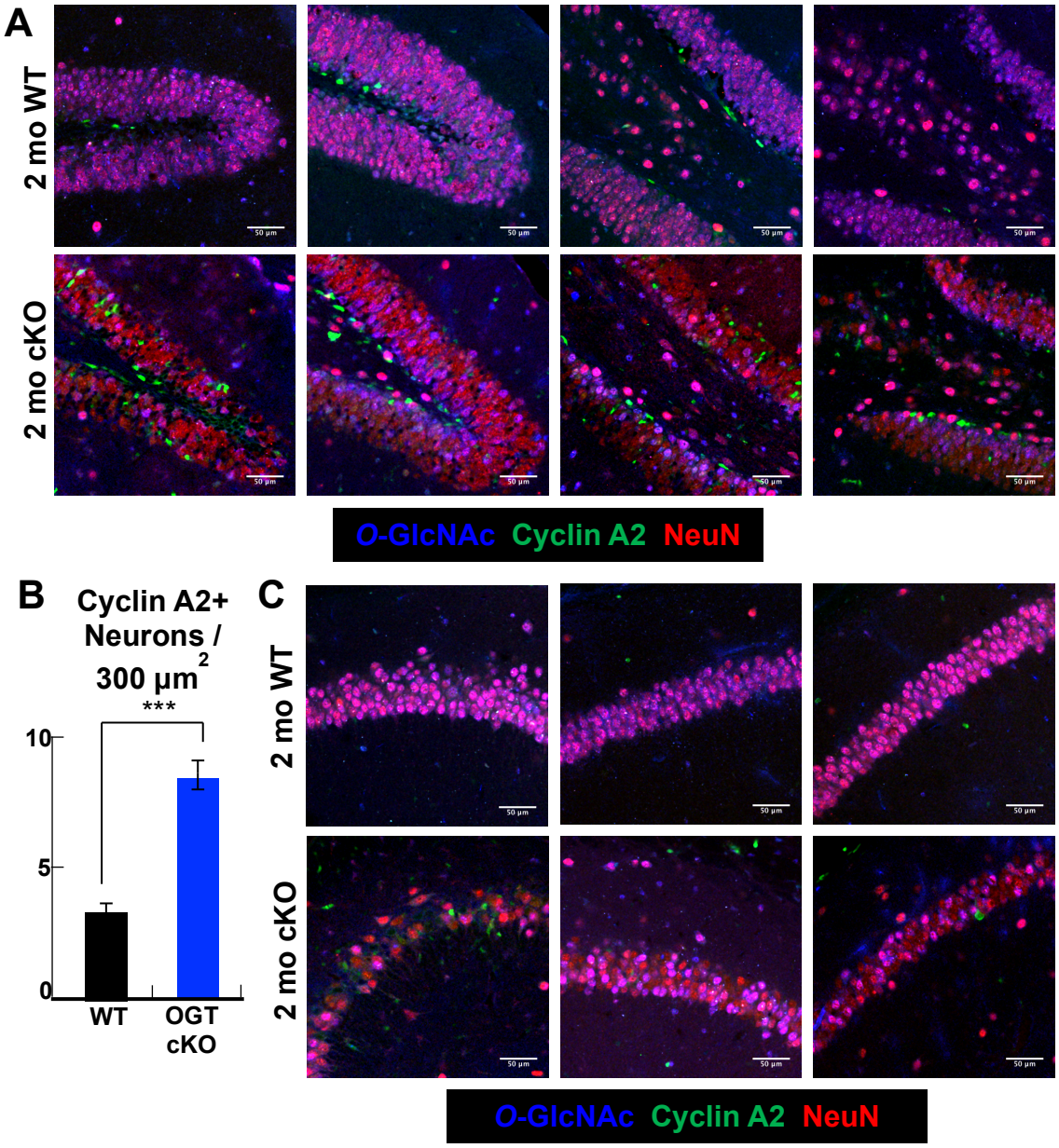

Figure 2.11 OGT cKO mice exhibit changes in levels of Cyclin A2-positive hippocampal neurons. (A) The number of Cyclin A2-positive neurons in the dentate gyrus, hilus, and CA3 regions of the hippocampus increased in the 2-month-old OGT cKO mice relative to WT mice. The Cyclin A2-positive cells observed in the WT hippocampus resided in the subgranular zone (SGZ) where adult neurogenesis occurs. (B) The number of Cyclin A2-positive neurons in the dentate gyrus significantly increased in the OGT cKO at 2 months of age. (C) The number of Cyclin A2-positive neurons was unaltered in the CA1 and CA2 regions of the OGT cKO mouse. ***$P < 0.0005$, n=4, each genotype. Scale bar = 50 µm.

We validated that several of the differentially-expressed cell cycle-related genes in the magenta gene network were significantly upregulated using qPCR (Figure 2.12). We verified that Cyclin A2 (*Ccna2*, 1.5-fold), Cyclin D3 (*Ccnd3*, 1.3-fold), and growth

arrest and DNA-damage-inducible protein α (*Gadd45a*, 1.6-fold) were upregulated in OGT cKO hippocampi at 2 months. Interestingly, several metabolic genes including *Pfkfb3* (2.2-fold) have been shown to regulate cell cycle directly. *Pfkfb3* upregulation leads to increased expression of *Ccnd3* and cell cycle progression toward G1 phase.[72,73] Importantly, increased PFKFB3 levels in neurons leads to apoptosis by shunting carbon flux through glycolysis rather than the pentose phosphate pathway (PPP), which ultimately exacerbates oxidative stress.[74] This shunting from glycolysis to PPP (a.k.a. the Warburg effect) in order to reduce oxidative stress is a strategy employed in cancer as well and is enhanced through the direct *O*-GlcNAc glycosylation of PFK1 under hypoxic conditions.[38] Increased expression of cell cycle-related genes has been observed in transgenic AD mice as well as in AD human patients.[75]

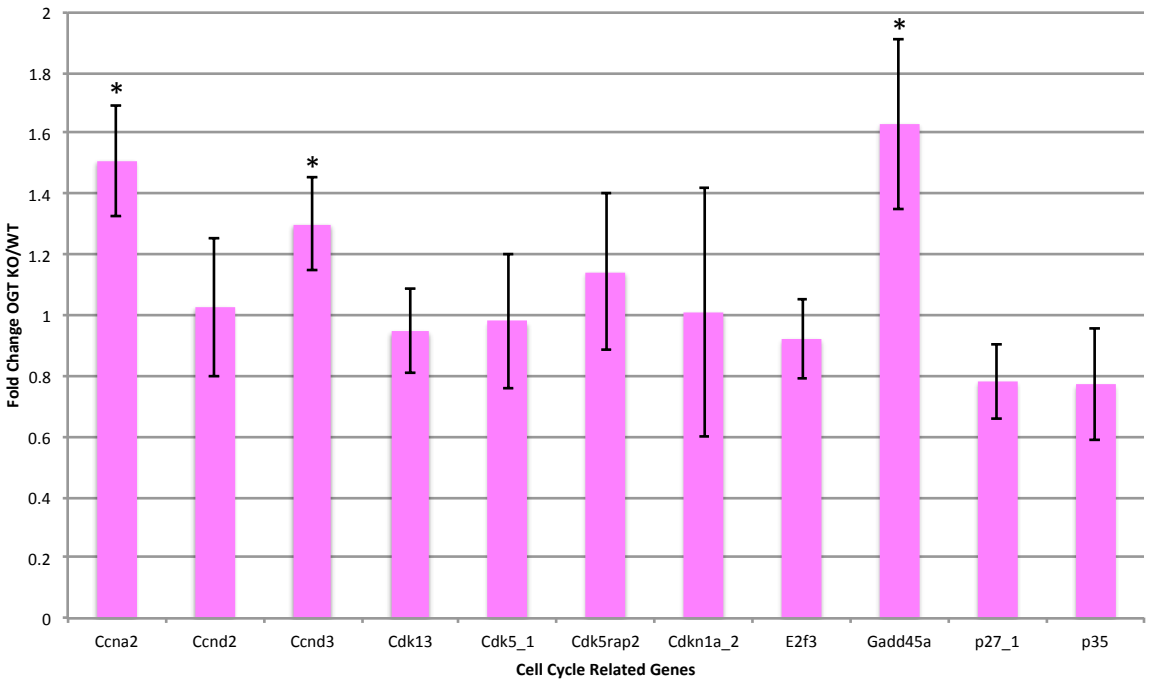

Figure 2.12 Cell cycle genes upregulated in OGT cKO mice at 2 months. We validated that cyclin A2 (*Ccna2*), cyclin D3 (*Ccnd3*), and growth arrest and DNA-damage-inducible protein (*Gadd45a*) were upregulated while other important cell cycle genes were not perturbed. *$P < 0.05$.

In addition, the magenta module's hub genes were heat shock protein family B (small) member 6 (*Hspb6*, HSPB6, 18 interactors), angiopoietin-like protein 6 (*Angptl6*, ANGPTL6, 17 interactors), and rhomboid 5 homolog 1 (*Rhbdf1*, 13 interactors), which were upregulated 2.0-fold, 1.4-fold, and 1.5-fold respectively in OGT cKO hippocampi (Figure 2.8B). A final magenta hub gene was ribosomal protein L24 (*Rpl24*, RPL24, 16 interactors), but this gene was not differentially expressed based on our microarray data. HSPB6 (a.k.a. Hsp20) has been shown to be involved in stress response, important for preventing aberrant aggregation of denatured or damaged proteins, and its association with pathological hallmarks in AD brains has been shown to be neuroprotective.[76-78] In adipose tissue, ANGPTL6 is known to be a critical mediator of energy metabolism: (1) knockout of *Angptl6* results in either embryonic lethality or morbid obesity and insulin resistance in mice and (2) inhibition of mitochondrial oxidative phosphorylation leads to enhanced *Angptl6* expression, which then increases the expression of fibroblast growth factor 21 (*Fgf21*).[79-81] Several studies have implicated *Rhbdf1*, which encodes a regulator of EGF/TGF-α signaling, in Alzheimer's patients.[82,83] The final hub gene, RPL24, is a critical component of the ribosome that mediates protein synthesis and plays a key role in cell cycle, growth, and survival.[84] Together, the hub genes, *Hspb6, Angptl6, Rhbdf1,* and *Rpl24*, are central mediators of cell cycle arrest gene expression in the OGT cKO mouse.

Finally, the protein levels of cyclin-dependent kinase 5 (Cdk5), a negative regulator of cell cycle progression, were significantly decreased in OGT cKO hippocampi when compared to WT.[85] Despite no change in *Cdk5* mRNA levels (Figure 2.12), IHC analysis also indicated a specific reduction in Cdk5 protein levels in *O*-GlcNAc-null hippocampal neurons (Figure 2.13), suggesting the potential for post-transcriptional

regulation of Cdk5 by *O*-GlcNAc. Cdk5 has been implicated as a critical regulator of synaptic plasticity, phosphorylation of tau, cell cycle progression, and DNA damage response in AD and other neurodegenerative diseases.[86-88] Taken together, these WGCNA, qPCR, microarray, IHC, and Western blot analyses provide evidence that there is enhanced cell cycle progression in the hippocampus of OGT cKO mice.

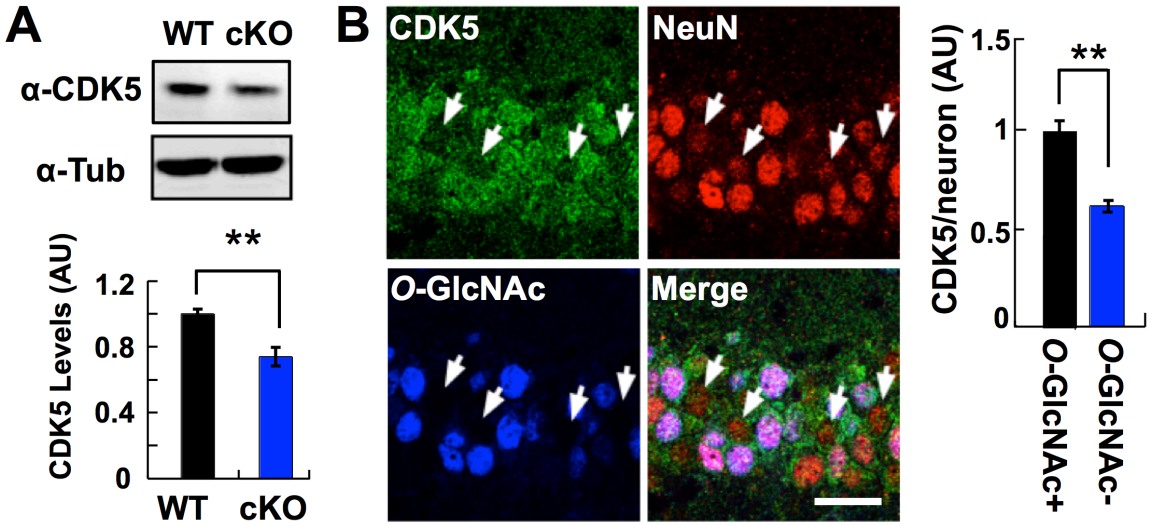

Figure 2.13 Cdk5 levels are depleted in OGT cKO neurons in the hippocampus. (*A*) A significant decrease in Cdk5 expression levels was detected by Western blotting in the hippocampus of 2-month-old OGT cKO mice. $n = 8$. $^*P < 0.005$. (*B*) *O*-GlcNAc-negative neurons have decreased Cdk5 immunostaining (arrowheads) in the hippocampus at 2 months. Scale bar = 10 µm. Figure from Andrew Wang.

2.10 OGT cKO, amyloid-forming, and plaque-forming mice are highly correlated with a immune response gene network

We next wanted to compare our OGT cKO with other AD and neurodegenerative mouse models in a more global fashion to see if the OGT cKO fully recapitulates the transcriptional changes observed in these mouse models. In a recent study from Dr. Frances Edwards and colleagues, tangle-forming and amyloid-forming AD and FTDP17 (frontotemporal dementia with parkinsonism) mouse models were compared based on their disease pathology and gene expression changes (Figure 2.14).[89] The tangle-forming mice ($MAPT^{P301L}$) demonstrated increased hyperphosphorylated tau, leading to the

formation of neurofibrillary tangles (NFTs) in addition to increased immune response and decreased synaptic gene expression. On the other hand, the amyloid-forming mice had a variety of different genotypes: TAS10 ($APP^{K670N,M671L}$), TPM ($PSEN1^{M146V}$), HET-TASTPM ($APP^{Swe/+}/PSEN1^{M146V/+}$), HO-TASTPM ($APP^{Swe/Swe}/PSEN1^{M146V/M146V}$). Depending on the genotype and age, the amyloid-forming mice exhibited increased levels of Aβ peptides, accumulation of Aβ to form Aβ plaques, and elevated immune response gene expression.[89] We obtained the hippocampal samples from this data set, 113 samples altogether, and compared the gene expression traits to our OGT cKO mice using WGCNA (Figures 2.14, 2.15).

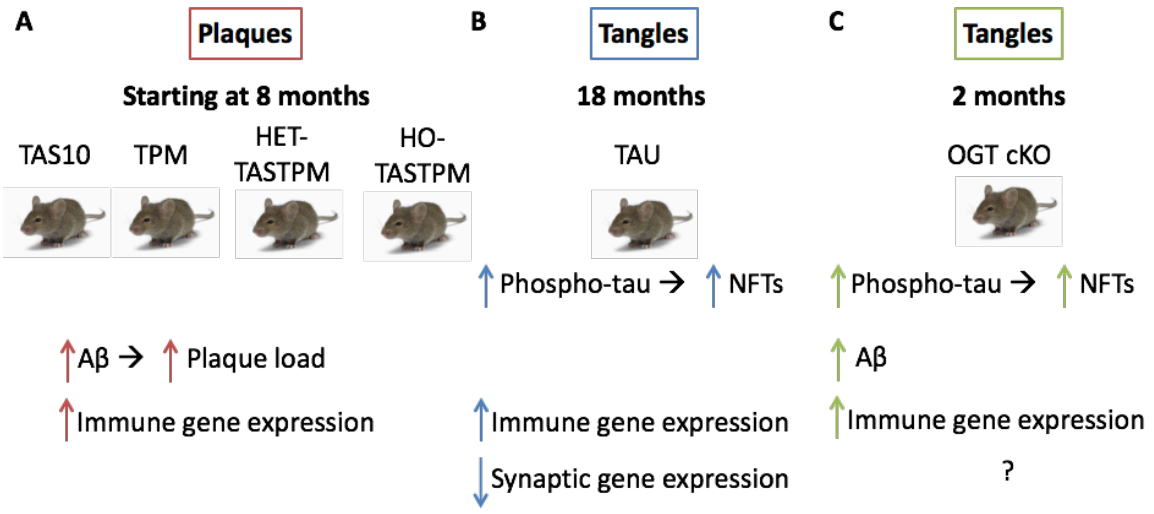

Figure 2.14 Comparison of the characteristics of the mice from the AD/FTDP mouse study and the OGT cKO mouse. (*A*) The plaque-forming mice are one of four different genotypes TAS10, TPM, HET-TASTPM, and HO-TASTPM. Depending on the genotype, these mice increase their Aβ peptide load, which leads to a 1:1 increase in plaque load (starting at 8 months) and an increase in immune gene expression. (*B*) The tangle-forming mice have the $MAPT^{M301L}$ mutation, leading to increased hyperphosphorylated tau, NFTs (18 months), and immune gene expression and decreased synaptic gene expression. (C) The OGT cKO at 2 months of age displays increased hyperphosphorylated tau, NFTs, amyloidogenic Aβ peptides (not yet plaques), and immune gene expression.

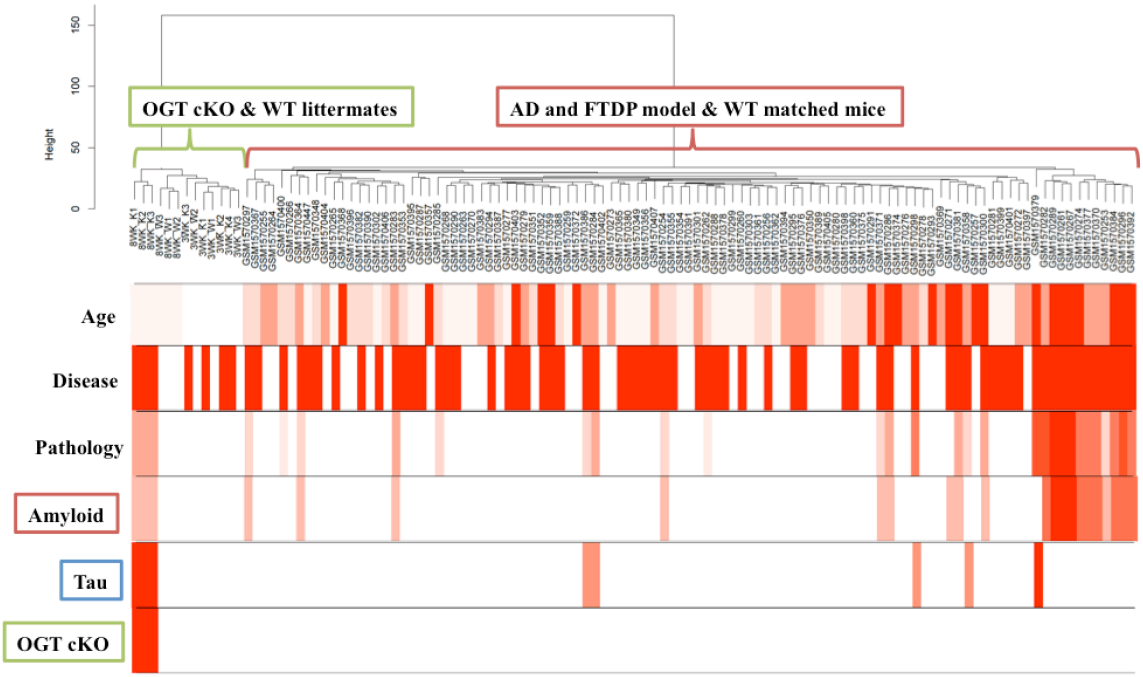

Figure 2.15 WGCNA dendrogram of hippocampal samples and traits. Shown here is the WGCNA sample dendrogram clustering similar samples and their annotation with the following traits: age (range was 3 weeks to 18 months), disease (presence or absence of disease), pathology (level of pathology associated with the presence of NFTs and plaques), amyloid (level of Aβ peptides and plaque formation), tau (level of hyperphosphorylated tau and NFT formation), OGT cKO (presence or absence of OGT knockout).

In a heatmap of the overall trait-module relationships, we observed that across most traits, OGT cKO and tau NFT-forming mice exhibit transcriptional similarities while the amyloid-plaque forming mice diverge from these two mice (Figure 2.16). The green module, enriched for immunity (FDR < 6.2×10^{-9}), was positively correlated with all traits: age (cor = 0.41, $P < 2 \times 10^{-6}$), disease (cor = 0.29, $P < 9 \times 10^{-4}$), pathology (cor = 0.77, $P < 2 \times 10^{-25}$), OGT cKO (cor = 0.45, $P < 2 \times 10^{-7}$), tau tangle-forming (cor = 0.54, $P < 7 \times 10^{-11}$), amyloid plaque-forming (cor = 0.64, $P < 1 \times 10^{-15}$) (Figure 2.16). The green module was enriched for immunity (FDR < 6.2×10^{-9}), both innate (FDR < 1.0×10^{-6}) and adaptive (FDR < 2.0×10^{-4}), NF-κB signaling pathway (FDR < 1.0×10^{-2}), and lysosome (FDR < 2.3×10^{-2}) (Table 2.8, Figure 2.17). This green module contains many of the upregulated immune-response and gliosis related genes in the OGT cKO mouse,

including *Gfap, Cd14, C3, Gusb, Tyrobp,* and *Man2b1*, which we validated with microarray and qPCR (Figure 2.18, Table 2.2).

The highest correlation with this module is with pathology supporting the idea that the more amyloid plaques and NFTs, the more immune response the mice exhibit. The next highest correlation is with the plaque formation followed by tangle formation, suggesting that amyloid plaque deposition is more highly correlated with immune response than tau NFTs. This is consistent with AD literature, which suggests that increasing levels of Aβ peptide lead directly to immune response, which in turn leads to hyperphosphorylation of tau and NFTs.[86] That being said, the causality vs. correlation relationship between immune response, Aβ pathology, and tau pathology in AD is still being adjudicated in the scientific courtroom. The OGT cKO had the next highest correlation with the green module suggesting that the immune response in the OGT cKO mice at 2 months was less pronounced than the amyloid plaque- and tau tangle-forming mice, which are generally older and have higher tangle and especially plaque formation than our 2-month-old OGT cKO mice. The high correlation of this immune response green module with pathology, amyloid plaque formation, NFT formation, and OGT cKO support previous findings showing extensive gliosis and immune response in these different mutant mice and show that amyloid plaque formation appears to correlate most highly with immune activation.

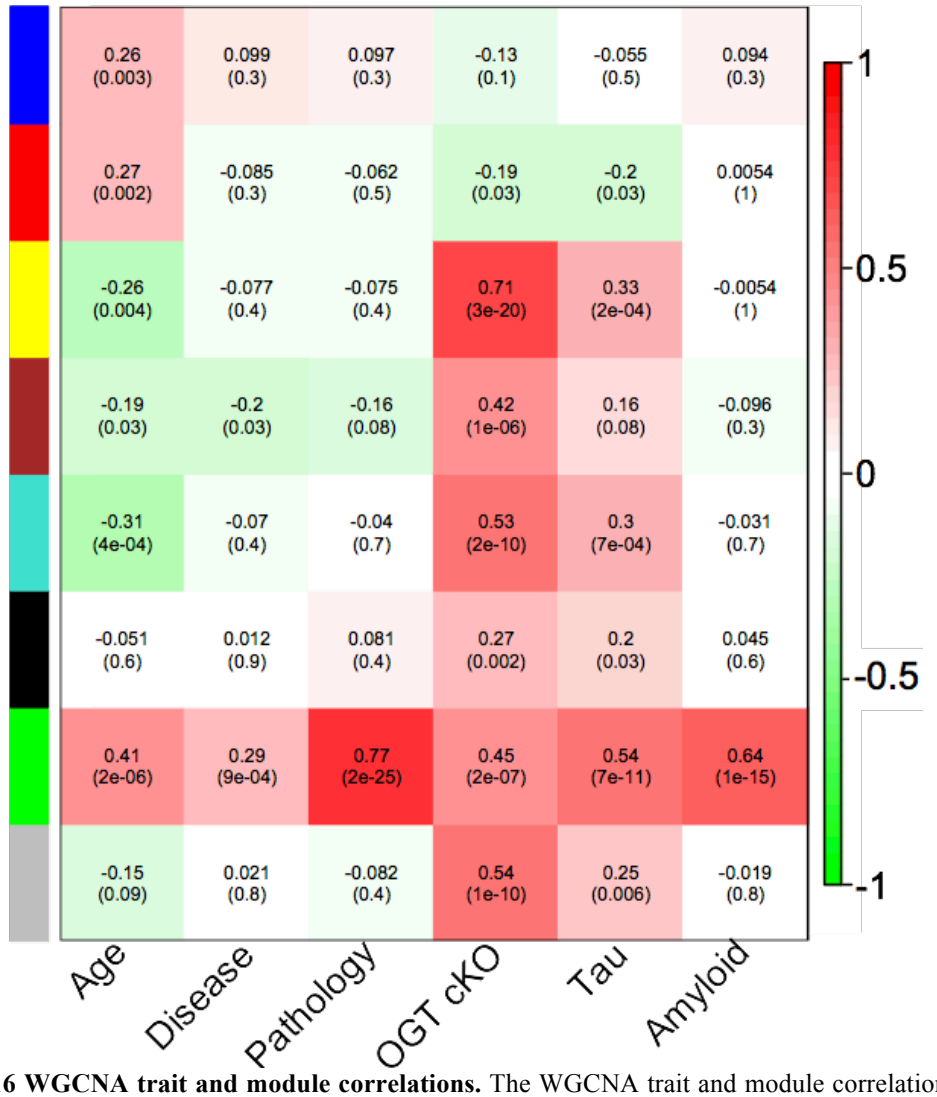

Figure 2.16 WGCNA trait and module correlations. The WGCNA trait and module correlations and *P*-values are shown here. Overall, there were 8 different modules that were generated from our WGCNA. Please note that the different modules are given arbitrary colors that have no correlation with the previous WGCNA analysis colors/modules.

Table 2.8 DAVID GO annotation of green module genes

GO term	#	Genes	FE
Immunity	23	*Havcr2, Tnfaip8l2, Itk, Ifitm2, C3, Ifitm3, Tlr13, Unc93b1, Tnfrsf17, Serping1, Oas2, Tlr7, Lgals9, Btk, Cd84, Ddx58, Prkd2, Cd86, Tap2, Inpp5d, Csk, Mx2, Cd14*	6.7
Immune system process	23	*Havcr2, Tnfaip8l2, Itk, Ifitm2, C3, Ifitm3, Tlr13, Unc93b1, Tnfrsf17, Serping1, Oas2, Tlr7, Lgals9, Btk, Cd84, Ddx58, Prkd2, Cd86, Tap2, Inpp5d, Csk, Mx2, Cd14*	6.0
Innate immune response	22	*Havcr2, Tnfaip8l2, Itk, Ifitm2, C3, Ifitm3, Tlr13, Unc93b1, Serping1, Oas2, Fes, Tlr7, Trim21, Btk, Cd84, Ddx58, Cyba, Fcer1g, Csk, Mx2, Cd14, Tyrobp*	5.5

Glycoprotein	66	*Kcne1l, Aebp1, Adora3, Osmr, Il4i1, Aqp4, Cd52, Ggt1, Kcnk13, Tlr7, Mmp2, Ednrb, Tor3a, Olfml3, Ch25h, Slc2a1, Lgi4, Asph, Man2b1, Ltb, Icam1, Cln3, Pnpla2, Serping1, Mcm3, Hcst, Cd84, Cd83, Ctsl, Cd37, Cd86, Serpina3n, Npc2, Bgn, Tnfsf13b, Adam17, Emp3, Pros1, Xdh, Abca9, C3, Slc39a12, Cd109, Unc93b1, Itgb5, Lrig1, Oas2, Sorcs3, Slc11a1, P2ry6, Lgals3bp, Smoc1, Pltp, Havcr2, Tmc6, Slamf9, Efemp2, Gusb, Rhbdf1, Tlr13, Frrs1, Tst, Fcgr2b, Liph, Slc15a3, Cd14*	2.0
Membrane	103	*Kcne1l, Tspo, Osmr, Aqp4, Ggt1, Cd52, Mmp2, Tlr7, Vcl, Btk, Ch25h, Slc2a1, Gng3, Asph, Dnajc3, Sgpl1, Scamp2, Tnfrsf17, Ifi47, Pnpla2, Sspn, Hcst, Igsf6, Cd37, Parp14, Emp3, Fgd2, Abca9, Ifitm2, Ifitm3, Unc93b1, Itgb5, Lrig1, Oas2, Llgl1, Sorcs3, Slc11a1, Lgals3bp, P2ry6, Laptm5, Vrk2, Fcer1g, Tyrobp, Havcr2, Slamf9, Acy3, Gusb, Rhbdf1, Fbxo2, Tlr13, Ephx1, Ddx58, Gngt2, Uaca, Slc25a10, Plcg2, Plau, Gfap, Ai467606, Kcnk13, Fes, Hvcn1, Ednrb, Ptges, Csk, Ltb, Rhog, Agpat2, Icam1, Cln3, Fmnl3, Ms4a6d, Mcm3, Cd84, Prkd2, Cd83, Cd86, Tnfsf13b, Prdx6, Adam17, Fhod1, Map3k11, Slc39a12, Hk2, Cd109, Atp5g3, Glipr2, Lpxn, Igtp, Tap2, Tgm2, Inpp5d, Ehd4, Tmc6, Slc10a3, Anxa3, Frrs1, Cyba, Rab32, Fcgr2b, Liph, Slc15a3, Cd14*	1.5
Extracellular exosome	54	*Gna14, Aebp1, Tspo, Mlph, Ggt1, Aldh1l2, Vcl, Tor3a, Slc2a1, Cdk5rap2, Csk, Man2b1, Dnajc3, Rhog, Idua, Icam1, Scamp2, Serping1, Arrdc1, Cd84, Ctsl, Renbp, Cd37, Cd86, Serpina3n, Npc2, Bgn, Prdx6, Pros1, C3, Ifitm3, Itgb5, Glipr2, Lgals3bp, Tgm2, Gsto2, Glo1, Ehd4, Havcr2, Tmc6, Acy3, Efemp2, Gusb, Fbxo2, Dbi, Anxa3, Akr1b8, Tst, Uaca, Capg, Plcg2, Hpgd, Cd14, Plau*	2.1
Adaptive immunity	10	*Cd84, Havcr2, Prkd2, Itk, Cd86, Tap2, Unc93b1, Tnfrsf17, Csk, Btk*	12
SH2 domain	10	*Itk, Socs3, Plcg2, Shc1, Inpp5d, Fes, Csk, Vav1, Sh3bp2, Btk*	9.4
Lysosome	13	*Cln3, Ifitm3, Gusb, Unc93b1, Il4i1, Tlr7, Ctsl, Npc2, Laptm5, Prdx6, Man2b1, Slc15a3, Idua*	6.1
Phosphoprotein	96	*Mocos, Gfap, Adora3, Ai467606, Pdlim4, Aqp4, Fes, Aldh1l2, Skap2, Hvcn1, Mmp2, Btk, Vcl, Ednrb, Plcb3, Oplah, Slc2a1, Casp8, Shc1, Cdk5rap2, Asph, Gng3, Csk, Dnajc3, Rhog, Sgpl1, Cln3, Fmnl3, Scamp2, Socs3, Ms4a6d, Anks1, Acads, Mlxipl, Pnpla2, Mcm3, Card10, Hcst, Cd84, Prkd2, Eml3, Renbp, Hspb6, Prdx6, Parp14, Adam17, Map3k14, Mcts1, Fhod1, Map3k11, Fgd2, Triobp, C3, Ifitm3, Mapkapk3, Unc93b1, Itgb5, Llgl1, Lpxn, Vrk2, Laptm5, Lyl1, Fcer1g, Glo1, Inpp5d, Tyrobp, Ehd4, Nr1h3, Havcr2, Fyb, Tmc6, Itk, Acy3, Rhbdf1, Fbxo2, Aff1, Samsn1, Vav1, Dbi, Anxa3, Tst, Ddx58, Ikbke, Cyba, Rab32, Rassf4, Uaca, Rps6ka1, Fcgr2b, Helb, Plcg2, Capg, Slc15a3, Plau, Sh3bp2, Igfbp5*	1.5
NF-κB signaling pathway	10	*Ddx58, Icam1, Tnfsf13b, Plcg2, Map3k14, Ltb, Ccl4, Plau, Cd14, Btk*	7.1
Disulfide bond	50	*Adora3, Osmr, Il4i1, Ggt1, Mmp2, Ednrb, Olfml3, Asph, Dnajc3, Man2b1, Idua, Icam1, Tnfrsf17, Serping1, Hcst, Igsf6, Cd84, Ctsl, Cd83, Cd86, Bgn, Npc2, Tnfsf13b, Prdx6, Adam17, Pros1, Xdh, Ccl3, C3, Cd109, Itgb5, Lrig1, Ccl4, P2ry6, Lgals3bp, Smoc1, Fcer1g, Glo1, Pltp, Tyrobp, Havcr2, Klk6, Slamf9, Efemp2, Igf1, Fcgr2b, Liph, Cd14, Plau, Igfbp5*	1.9
Lysosome	14	*Cln3, Gusb, Ifitm3, Unc93b1, Il4i1, Tlr7, Ctsl, Slc11a1, Npc2, Laptm5, Prdx6, Man2b1, Slc15a3, Idua*	4.4

Table 2.8 contains the significant DAVID functional gene ontology annotations of the green immune response module. Redundant and non-significant GO terms were removed from the list. FE = fold-enrichment; FDR $<5.0\text{x}10^{-2}$.

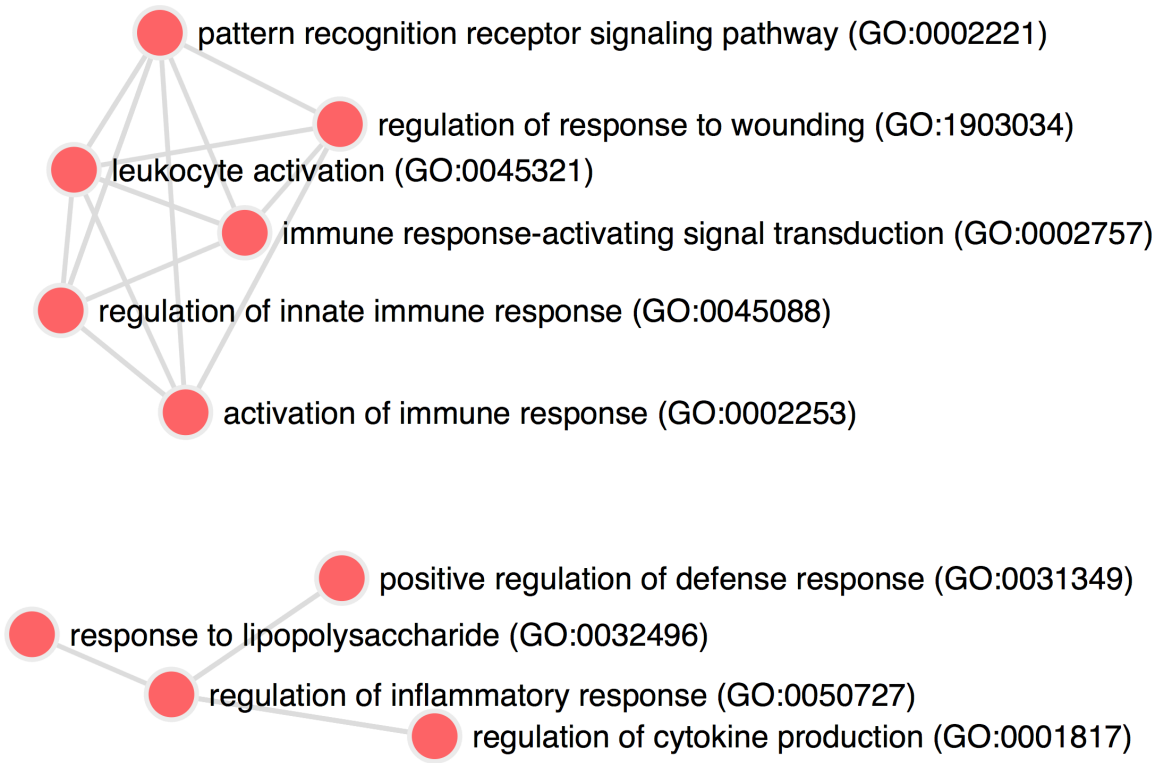

Figure 2.17 Top 10 gene ontology annotations for green immune response module. Shown above are the top 10 gene ontology annotations for the green module from the Enrichr database GO processes (adjusted $P < 6.4 \times 10^{-5}$).

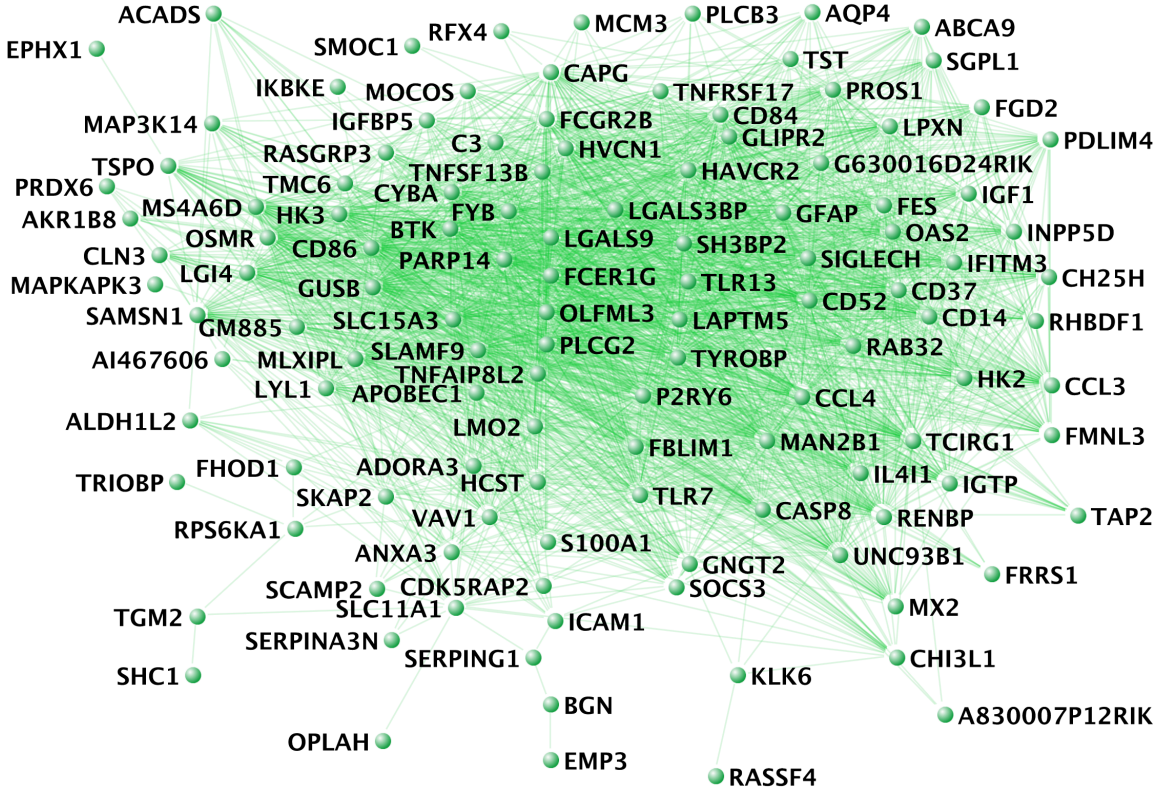

Figure 2.18 Green module is enriched for immune response genes. The green module was enriched for genes involved in immunity (DAVID GO enrichment FDR < $6.2x10^{-9}$). The immune response gene network was generated in VisANT (weight cutoff > 0.1).

2.11 OGT cKO and plaque-forming mice but not amyloid forming mice are anti-correlated with a synaptic gene network

The red module was enriched for genes associated with the postsynaptic density (FDR < $6.4x10^{-9}$) and the synapse (FDR < 0.029) was anti-correlated with the tau tangle-formation (cor = -0.19, $P < 0.03$) and OGT cKO (cor = -0.2, $P < 0.03$), but not correlated with pathology, disease, and amyloid plaque-forming mice (Figures 2.16 and 2.19, Table 2.9). In addition, the red module was enriched for genes associated with neuronal cell body (FDR < $2.8x10^{-4}$), dendrite (FDR < 0.024), calcium transport (FDR < 0.038), growth cone (FDR < 0.040), and glutamatergic synaptic transmission (FDR < 0.043), suggesting that this module could be a more general neuronal and synaptic growth, activity, and plasticity module (Table 2.9). The anti-correlation with synaptic genes is consistent with (1) the Matarin and colleagues study that found that the tau tangle-forming mice are anti-correlated with a synaptic module and (2) our differential expression results in Section 2.6 revealing that the OGT cKO mouse displays downregulation of glutamatergic synaptic genes.[89] Both OGT cKO and tau are disrupting synaptic gene transcription while amyloid plaque-formation does not appear to disrupt it directly. This finding is consistent with previous studies demonstrating that synaptic loss is directly correlated with the presence of tau tangles in AD and removal of tau inoculates the hippocampus from stress-induced synaptic degeneration that occurs in AD.[90,91] Furthermore, a recent study showed that knockout of OGT in hippocampal neurons

results in fewer synapses and a higher proportion of immature synaptic spines, suggesting that *O*-GlcNAc cycling is critical for the maintenance of synapses.[92]

Table 2.9 DAVID GO annotation of red synapse-related module

GO terms	#	Genes	FE
Phosphoprotein	81	*Gprin1, Als2, Hmgn3, Pip5k1b, Sart3, Prkg1, Rgl1, Bzw2, Trim2, Diras2, Dab1, Trim9, Aak1, Trp63, Tlk1, Bcl7a, Kcnq2, Jph1, Brd9, Islr2, Tomm34, Nol6, Arhgef3, Cacng8, Baiap2, Actn1, Mbd4, Tle1, Cacng3, Rb1, Gal, Tmem74, Gtf2h2, Gtf2h1, Prkcb, Uhrf2, Rab11fip3, Ryr1, Zfpm1, Doc2b, Cpsf2, Dbn1, Unc13b, Ywhaz, Napa, Abi1, Ensa, Srf, Mlf2, Ephb2, Cdh8, Snn, Tnrc6c, Gp1bb, Syn2, Bcl11a, Pafah1b3, Rnf10, Camk2b, Nedd4l, Tcf4, Camk2a, Dtna, Trhde, Klf13, Grin1, Mapk10, Gas7, Zfp608, Atm, Itpr1, E130012a19Rik, Gria2, Rpl22, Bbc3, Hebp2, Trps1, Tsc2, Zfp532, Ube2e2, Plekha2*	2.0
Postsynaptic density	16	*Als2, Ywhaz, Cacng8, Baiap2, Grin1, Abi1, Mapk10, Itpr1, Dab1, Gria2, Syn2, Bcl11a, Camk2b, Camk2a, Dbn1, Lrp4*	12
Alternative splicing	56	*Als2, Fgf5, Hmgn3, Pip5k1b, Prkg1, Sart3, Pmvk, Dab1, Trim9, Aak1, Trp63, Rapgef4, Bcl7a, Kcnq2, Tomm34, Nol6, Nfkbiz, Arhgef3, Baiap2, Tle1, Mbnl2, Sez6l, Zcchc14, Prkcb, Rab11fip3, Uhrf2, Tlcd1, Dbn1, Unc13b, Camta2, Abi1, Ensa, Slco2a1, Ephb2, Mettl2, Dusp15, Bcl11a, Syn2, Rnf10, Nedd4l, Tcf4, Camk2a, Olfm1, Dtna, Grin1, Mapk10, Gas7, Zfp608, Itpr1, Rasl11b, Gria2, Tsc2, Parp6, Zfp532, Lrp4, Dusp7*	2.2
Neuronal cell body	16	*Als2, Baiap2, Grin1, Sez6l, Gal, Itpr1, Ephb2, Slc17a8, Dab1, Gria2, Tsc2, Rapgef4, Camk2a, Dbn1, Olfm1, Lrp4*	5.3
Circadian entrainment	8	*Gria2, Grin1, Ryr1, Camk2b, Prkg1, Camk2a, Itpr1, Prkcb*	11
Dendrite	13	*Als2, Slc17a8, Gria2, Trim9, Tsc2, Grin1, Trp63, Rapgef4, Camk2b, Camk2a, Lrp4, Itpr1, Ephb2*	4.7
Synapse	11	*Slc17a8, Gria2, Trim9, Cacng8, Syn2, Grin1, Abi1, Unc13b, Camk2a, Olfm1, Dtna*	5.7
Calcium ion transport	8	*Cacng8, Grin1, Ryr1, Cacng3, Camk2b, Camk2a, Itpr1, Prkcb*	9.2
Growth cone	8	*Gprin1, Als2, Gria2, Tsc2, Grin1, Abi1, Rapgef4, Dbn1*	8.9
Synaptic transmission, glutamatergic	5	*Cdh8, Als2, Grin1, Napa, Unc13b*	28

Table 2.9 contains the significant DAVID functional gene ontology annotations of the red synapse-related module. Redundant and non-significant GO terms were removed from the list. FE = fold-enrichment. FDR $<5.0x10^{-2}$.

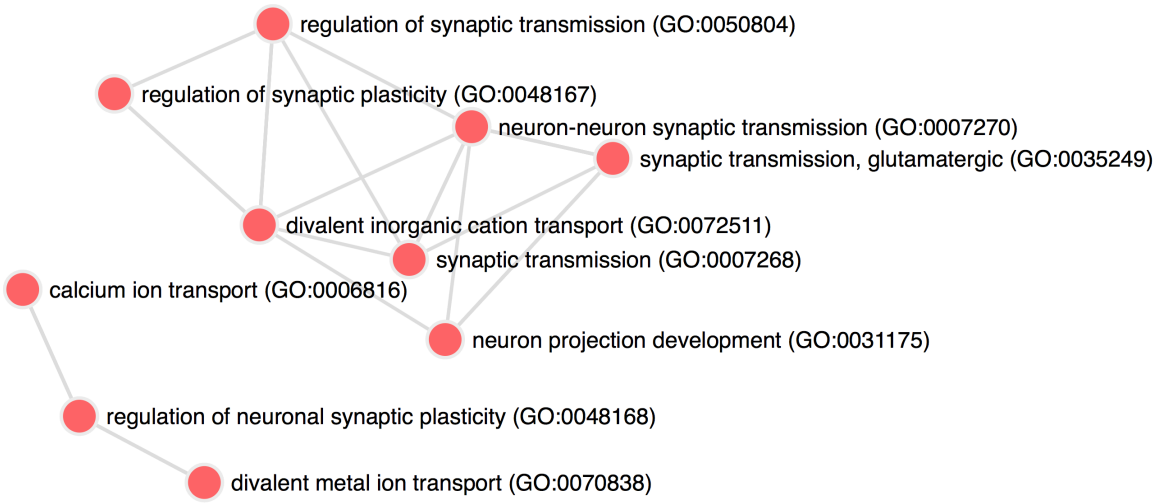

Figure 2.19 Top 10 gene ontology annotations for red synapse-related module. Shown above are the top 10 gene ontology annotations for the red module from the Enrichr database GO processes (adjusted $P < 5.5\text{x}10^{-3}$).

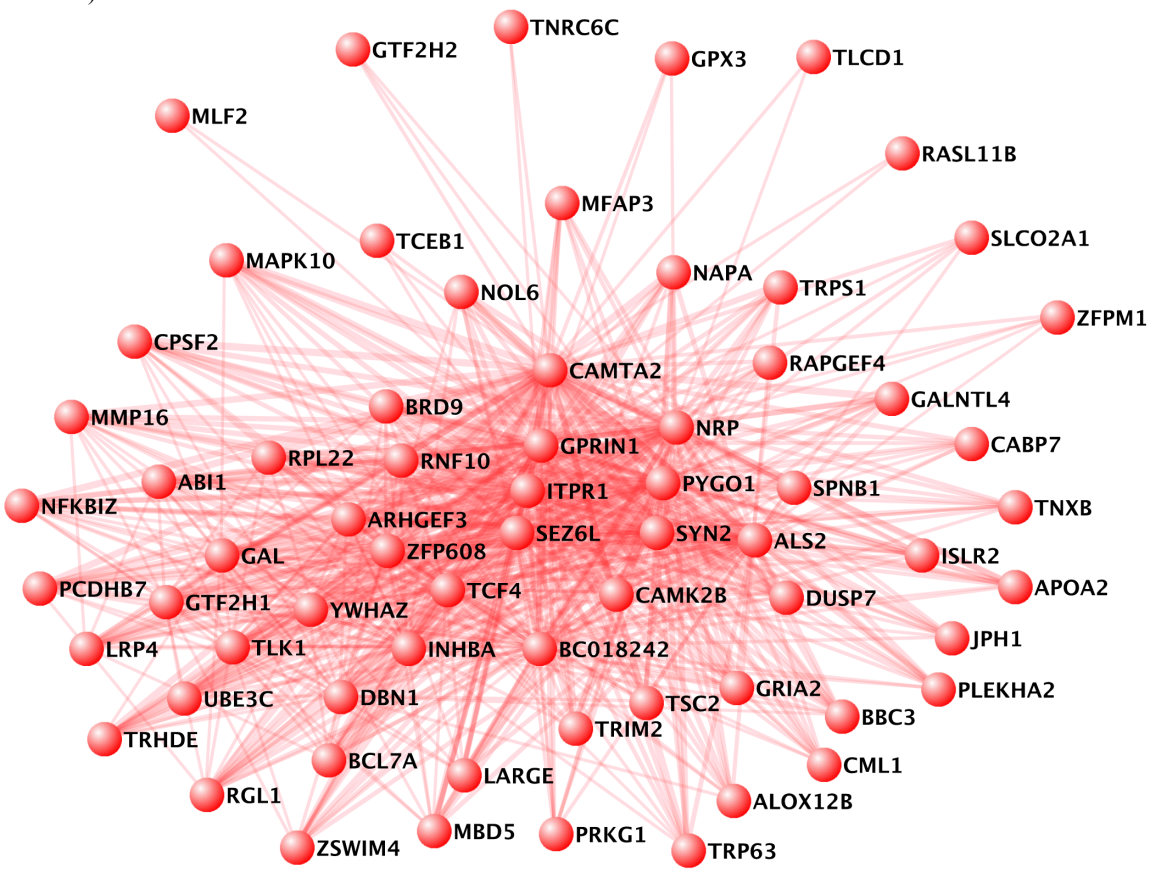

Figure 2.20 Red module is enriched for synaptic and neuronal activity genes. The red module was enriched for genes involved in postsynaptic density (FDR < $6.4\text{x}10^{-9}$), synapse (FDR < 0.029), neuronal cell body (FDR < $2.8\text{x}10^{-4}$), dendrite (FDR < 0.024), calcium transport (FDR < 0.038), growth cone (FDR < 0.040), and glutamatergic synapses (FDR < 0.043). The gene network was generated in VisANT (weight cutoff > 0.1).

2.12 OGT cKO mice are highly correlated with a nuclear gene network

The yellow module was enriched for genes associated with the nucleus (FDR < $3.5x10^{-9}$), chromatin regulators (FDR < $6.0x10^{-4}$), and transcription (FDR < $1.0x10^{-3}$) was anti-correlated with the tau tangle-formation (cor = 0.33, $P < 3.0x10^{-20}$) and OGT cKO (cor = 0.71, $P < 2.0x10^{-4}$), but not correlated with pathology, disease, and amyloid plaque-forming mice (Figure 2.15, Table 2.10). OGT is known to plays a singular role in the nucleus through its interaction with several chromatin modifying complexes and modification of chromatin, nuclear pore proteins, and transcription factors (see Chapter 4). In particular, the yellow module is enriched for various post-translational modifications including phosphoprotein (FDR < $3.4x10^{-15}$), acetylation (FDR < $3.3x10^{-6}$), Ubl conjugation (FDR < $3.3x10^{-6}$), and methylation (FDR < $1.8x10^{-3}$), which, transcription by influencing transcription factor stability and the transcriptional accessibility of the chromatin state.[93] OGT and OGA mediate chromatin stability, nuclear pore stability, and DNA repair mechanisms through substantial crosstalk with these other PTMs (see Chapter 4).[54,94-96]

Finally, the yellow module is associated with alternative splicing (FDR < $2.6x10^{-6}$) and splice variant (FDR < $7.1x10^{-3}$). This module includes the neuron-specific RNA-binding protein (RNABP)-encoding genes, *Elavl3* and *Elavl4* ((embryonic lethal, abnormal vision, *Drosophila*)-like 3 and 4 (Hu antigens C and D)), which are responsible for mediating mRNA levels and splicing in order to control neuronal excitability and glutamate availability.[97] These neuronal alternative splicers are responsible for splicing APP itself, which leads to increased levels of Aβ peptides in AD.[98] OGT and OGA themselves are subject to alternative splicing, which is closely regulated by the *O*-GlcNAc levels and metabolic environment.[99] In particular, OGA (*Mgea5*) is associated

with late-onset AD and is alternatively spliced in AD.[100,101] While the role of *O*-GlcNAc in regulating alternative splicing has not yet been fully explored, *O*-GlcNAc has been found to modify at least 10 different splicing factors so far, but the roles of these modifications on splicing remains to be determined.[102,103] In addition to *Elavl3* and *Elavl4*, several other yellow module genes are members of and regulate the spliceosome including *Ddx41* (DEAD (Asp-Glu-Ala-Asp) box polypeptide 41), *Khsrp* (KH-type splicing regulatory protein), and *Aqr* (aquarius).[104-106]

Table 2.10 DAVID GO annotation of yellow nucleus-related module

GO terms	#	Genes	FE
Phosphoprotein	154	*Atp1b1, Xpo6, Plekhm1, Xpo4, Morf4l2, Bbx, Tssc4, Trim46, Cul2, Epc1, Top1, Cul5, Pacsin1, App, Sin3b, Ank2, Nt5c3, H2afy, Dnajc5, Frs2, Stag2, Rnf31, Scamp1, Slc12a6, Aldh6a1, Ptprk, Ctrb1, Mecp2, Spag1, Stim1, Dll1, Ythdf1, Stk4, Gcc2, Jup, Eif2ak1, Hif1a, Siah1a, Mapk4, Vamp2, Nek4, Glg1, Dcbld2, Palm, Hdlbp, Slc38a2, Napg, Pfkfb2, Azi2, Zfp451, Nipbl, Fbxo42, Ddx41, Bcor, Stk38l, Asf1a, Sdf4, Zc3h14, Ehmt1, Osbpl8, Syt11, Eef1a2, Smad2, Ubp1, E130308a19Rik, Pold3, Dnajb9, Hdac2, Atp2a2, Smarcc1, Prkar1a, Tmpo, Klf4, Gpbp1, Hp1bp3, Ctcf, Rsrc2, Pcbp2, Parg, Nckipsd, Twistnb, Nsf, Wdr33, Nfx1, Psmd9, Usp13, Golga2, Kcnma1, Lair1, Ssbp2, Sgk3, Nup88, Ralbp1, Snapc3, Adnp, Pfkp, Ldb3, Mpp5, Topors, Rad50, Jmy, Pja2, Kif1c, Eif4g2, Senp3, Myrip, Nab2, Khsrp, Carm1, Mdm1, Clock, Rev3l, Usp7, B230219D22rik, Pard3, Nup160, Tpm1, Aldh3a2, Hic1, Stk32c, Cdyl, Dgkb, Nr1d2, Rasgrp2, Kif4, Per1, Chd1, Tbc1d4, Gtf3c2, Kif21a, Nfatc2, Fen1, Rasa2, Cnnm3, Msh6, Pdk2, Foxl2, Dnm1l, Immt, Kif18a, Raf1, Nlgn2, Nlgn3, Elavl4, Ppp1r13l, Pwp2, Rps6ka4, Tfrc, Pecam1, Apbb2, Hist1h2ao, Tob1, Fez1, Cbs*	1.8
Nucleus	100	*Xpo6, Xpo4, Morf4l2, Bbx, Cbx7, Zfp92, Top1, Epc1, Sin3b, Aspa, Zfp90, Smarcd1, H2afy, Pdgfc, Scrt1, Stag2, Polk, Polh, Socs1, Hdac10, Mecp2, Dll1, Stk4, Aqr, Hif1a, Siah1a, Mapk4, Hdlbp, Zfp451, Nipbl, Ddx41, Bcor, Asf1a, Zc3h14, Klf7, Ehmt1, Osbpl8, Eef1a2, Smad2, Ubp1, Pold3, Hdac2, Smarcc1, Tmpo, Scmh1, Klf4, Hp1bp3, Gpbp1, Ctcf, Dph3, Pcbp2, Hey2, Parg, Nckipsd, Twistnb, Wdr33, Nfx1, Tbl1xr1, Ssbp2, Nup88, Snapc3, Adnp, Topors, Rad50, Jmy, Mxd4, Senp3, Smu1, Gnaq, Nab2, Khsrp, Carm1, Clock, Mdm1, Rev3l, Usp7, Zfp64, Nup160, Spo11, Hic1, Cdyl, Nr1d2, Kif4, Chd1, Per1, Nfatc2, Gtf3c2, Fen1, Msh6, Foxl2, L3mbtl3, Kif18a, Raf1, Ppp1r13l, Pwp2, Rps6ka4, Dusp8, Hist1h2ao, Cbs, Tob1*	2.0

Alternative splicing	96	*Slc8a3, Prr16, Xpo6, Gpbp1, Hp1bp3, Bbx, Tssc4, Trim46, Cul2, Epc1, Sin3b, App, Aasdhppt, Ank2, Chst10, Nt5c3, Pcbp2, Smarcd1, H2afy, Parg, Nfx1, Golga2, Rnf31, Kcnma1, Polk, Lair1, Ssbp2, Nrxn3, Nup88, Spag1, Mecp2, Pfkp, Ldb3, Rad50, Jmy, Man2a2, Pja2, Smu1, Eif4g2, Hif1a, Nab2, Lrp12, Nptn, Nek4, Eda, Carm1, Mdm1, C87436, Clock, Usp7, Palm, Pard3, Zfp64, Cabp2, Nup160, Spo11, Angel2, Tpm1, Azi2, Hic1, Nphp3, Nipbl, Cdyl, Dgkb, Pde1c, Rasgrp2, Tbc1d4, Slco3a1, Strbp, Bcor, Nfatc2, Kif21a, B4galt7, Sdf4, Stk38l, Zc3h14, Cnnm3, Dnm1l, Ehmt1, L3mbtl3, Immt, Raf1, Smad2, Elavl3, Elavl4, Ubp1, E130308a19Rik, Peo1, Atp2a2, Smarcc1, Pecam1, Mep1b, Tmpo, Scmh1, Apbb2, Cbs*	1.8
Acetylation	72	*Xpo6, Hp1bp3, Ube2g1, Tssc4, Ctcf, Cul2, Top1, Smarcd1, H2afy, Abcb10, Parg, Dnajc5, Nsf, Stag2, Wdr33, Scamp1, Aldh6a1, Tbl1xr1, Ssbp2, Ralbp1, Nup88, Mecp2, Adnp, Pfkp, Ythdf1, Stk4, Pkia, Gcc2, Rad50, Jup, Pja2, Smu1, Eif4g2, Hif1a, Aqr, Khsrp, Rab14, Vamp2, Usp7, Palm, Hdlbp, Pard3, Pfkfb2, Tpm1, Hic1, Nipbl, Pde1c, Nr1d2, Slc30a5, Tbc1d4, Mtmr9, Bcor, Kif21a, Stk38l, Fen1, Rasa2, Zc3h14, Msh6, Dnm1l, Osbpl8, Immt, Eef1a2, Smad2, Ppp1r13l, Pwp2, Pold3, Fem1c, Hdac2, Smarcc1, Prkar1a, Tmpo, Hist1h2ao*	2.0
Ubl conjugation	45	*Usp7, B230219D22rik, Slc38a2, Ctcf, Rsrc2, Hic1, Cul2, Top1, Zfp451, Cul5, App, Sin3b, H2afy, Per1, Pdgfc, Nfatc2, Frs2, Wdr33, Rnf31, Zc3h14, Foxl2, Ehmt1, Dnm1l, Polh, Syt11, Fzd1, Kif18a, Adnp, Dll1, Smad2, Fzd2, Topors, Drg2, Jmy, Pold3, Hdac2, Hif1a, Nab2, Smarcc1, Khsrp, Clock, Klf4, Hist1h2ao, Fez1, Cbs*	2.6
Isopeptide bond	32	*Usp7, B230219D22rik, Ctcf, Tpm1, Rsrc2, Hic1, Cul2, Top1, Zfp451, App, Cul5, H2afy, Wdr33, Zc3h14, Foxl2, Dnm1l, Ehmt1, Polh, Kif18a, Adnp, Dll1, Topors, Pold3, Hdac2, Hif1a, Atp2a2, Smarcc1, Khsrp, Clock, Klf4, Hist1h2ao, Cbs*	3.0
Cytoplasm	121	*Slc8a3, Xpo6, Plekhm1, Xpo4, Bbx, Cbx7, Top1, Cul5, Aspa, App, Sin3b, Pacsin1, Ank2, Nt5c3, Pdgfc, Frs2, Rnf31, Polh, Ctrb1, Socs1, Mecp2, Spag1, Hdac10, Stim1, Ythdf1, Pkia, Stk4, Gcc2, Jup, Pcf11, Eif2ak1, Hif1a, Mapk4, Siah1a, Nek4, Palm, Hdlbp, Pfkfb2, Wars2, Angel2, Azi2, Strbp, Stk38l, Zc3h14, Eef1a2, Syt11, Smad2, Ubp1, E130308a19Rik, Hdac2, Dnajb9, Atp2a2, Prkar1a, Klf4, Ube2g1, Dph3, Aasdhppt, Pigh, Ankrd12, Pcbp2, Hey2, Parg, Nsf, Nfx1, Psmd9, Golga2, Kcnma1, Ssbp2, Ldb3, Pfkp, Mpp5, Adnp, Jmy, Kif1c, Pja2, Eif4g2, Senp3, Smu1, Myrip, Pank2, Gzmn, Rab5a, Khsrp, Carm1, Mdm1, Clock, Usp7, Pard3, Cabp2, Upp2, Tpm1, Hic1, Numa1, Dgkb, Rasgrp2, Kif4, Per1, Tbc1d4, Chd1, Mtmr9, Kif21a, Nfatc2, Rasa2, Pdk2, Msh6, Dnm1l, Kif18a, Raf1, Nlgn2, Fzd2, Drg2, Elavl4, Ppp1r13l, Fem1c, Rps6ka4, Tfrc, Apbb2, Dusp8, Tob1, Fez1, Cbs*	1.5
Chromatin regulator	16	*Tbl1xr1, Ehmt1, L3mbtl3, Morf4l2, Hdac10, Ctcf, Cbx7, Epc1, Hdac2, Smarcc1, Smarcd1, Chd1, H2afy, Bcor, Carm1, Asf1a*	5.3
Protein binding	89	*Atp1b1, Gpbp1, Plekhm1, Ctcf, Cul2, Cul5, Aspa, Sin3b, App, Pacsin1, Ank2, Zfp90, Pcbp2, Hey2, Smarcd1, Abcb10, Dnajc5, Scrt1, Frs2, Nsf, Nfx1, Rnf31, Golga2, Scamp1, Slc12a6, Kcnma1, Polk, Tbl1xr1, Ssbp2, Ralbp1, Polg, Socs1, Mecp2, Ldb3, Adnp, Mpp5, Secisbp2, Stim1, Dll1, Topors, Gcc2, Mxd4, Jmy, Jup, Pja2, Senp3, Eif4g2, Myrip, Hif1a, Gnaq, Siah1a, Rab5a, Rab14, Vamp2, Carm1, Clock, Usp7, Pard3, Nr1d2, Per1, Mtmr9, Bcor, Ddx41, Nfatc2, Foxl2, Ehmt1, Osbpl8, L3mbtl3, Immt, Syt11, Raf1, Smad2, Fzd2, Ppp1r13l, Ppp1r9a, Dnajb9, Hdac2, Tfrc, Atp2a2, Smarcc1,*	1.6

		Pecam1, Prkar1a, Tmpo, Scmh1, Apbb2, Klf4, Tob1, Fez1, Bmpr1a	
Transcription	46	*Zfp64, Gpbp1, Morf4l2, Bbx, Ctcf, Cbx7, Hic1, Zfp92, Epc1, Zfp451, Sin3b, Cdyl, Nr1d2, Zfp90, Hey2, Chd1, Per1, Bcor, Gtf3c2, Twistnb, Nfatc2, Scrt1, Asf1a, Nfx1, Tbl1xr1, Foxl2, Klf7, Ssbp2, L3mbtl3, Snapc3, Hdac10, Adnp, Mecp2, Smad2, Ubp1, Ppp1r13l, Mxd4, Hif1a, Hdac2, Nab2, Smarcc1, Khsrp, Carm1, Scmh1, Clock, Klf4*	2.2
Methylation	30	*Palm, Gpbp1, Hic1, Zfp451, Cdyl, Smarcd1, Tbc1d4, H2afy, Strbp, Fen1, Wdr33, Mto1, Golga2, Ssbp2, Eef1a2, Mecp2, Adnp, Ldb3, Raf1, Elavl4, Ppp1r13l, Kif1c, Eif4g2, Smarcc1, Rab14, Khsrp, Tmpo, Carm1, Nek4, Hist1h2ao*	2.8
DNA-binding	41	*Zfp64, Gpbp1, Hp1bp3, Bbx, Ctcf, Spo11, Hic1, Zfp92, Top1, Zfp451, Nr1d2, Zfp90, Kif4, Hey2, Pcbp2, Chd1, H2afy, Strbp, Nfatc2, Scrt1, Nfx1, Polk, Msh6, Foxl2, Klf7, Ssbp2, Polh, Polg, Snapc3, Adnp, Mecp2, Smad2, Ubp1, Mxd4, Hif1a, Khsrp, Tmpo, Clock, Klf4, Hist1h2ao, Rev3l*	2.3
Covalent chromatin modification	16	*Tbl1xr1, Ehmt1, L3mbtl3, Morf4l2, Hdac10, Ctcf, Cbx7, Epc1, Hdac2, Smarcc1, Smarcd1, Chd1, H2afy, Bcor, Carm1, Asf1a*	4.6
Metal-binding	67	*Slc8a3, Slc6a2, Plekhm1, Ctcf, Dph3, Zfp92, Trim46, App, Aspa, Aasdhppt, Zfp90, Nt5c3, Yod1, Scrt1, Nsf, Nfx1, Usp13, Rnf31, Kcnma1, Polk, Polh, Nrxn3, Ldb3, Adnp, Pfkp, Stim1, Topors, Stk4, Rad50, Man2a2, Pja2, Myrip, Gnaq, Siah1a, Nek4, Aoc2, Rev3l, Zfp64, Cabp2, Spo11, Ppat, Zfp111, Hic1, Stk32c, Zfp451, Dgkb, Pde1c, Nr1d2, Rasgrp2, Ddx41, Sdf4, Stk38l, B4galt7, Fen1, Rasa2, Zc3h14, Klf7, Ehmt1, Syt11, Raf1, Smad2, Zfp709, Atp2a2, Mep1b, Klf4, Cbs, Bmpr1a*	1.7
Splice variant	91	*Prr16, Xpo6, Gpbp1, Hp1bp3, Bbx, Tssc4, Trim46, Cul2, Epc1, Sin3b, App, Aasdhppt, Ank2, Chst10, Nt5c3, Pcbp2, Smarcd1, H2afy, Parg, Nfx1, Rnf31, Slc12a6, Kcnma1, Polk, Lair1, Ssbp2, Nup88, Spag1, Mecp2, Pfkp, Ldb3, Rad50, Jmy, Pja2, Smu1, Eif4g2, Hif1a, Nab2, Lrp12, Nptn, Nek4, Eda, Carm1, Mdm1, C87436, Clock, Usp7, Palm, Pard3, Zfp64, Cabp2, Nup160, Spo11, Angel2, Tpm1, Azi2, Nphp3, Nipbl, Cdyl, Dgkb, Pde1c, Rasgrp2, Tbc1d4, Slco3a1, Strbp, Bcor, Nfatc2, Kif21a, B4galt7, Sdf4, Stk38l, Zc3h14, Cnnm3, Dnm1l, L3mbtl3, Immt, Raf1, Smad2, Elavl3, Elavl4, Ubp1, E130308a19Rik, Peo1, Atp2a2, Smarcc1, Pecam1, Mep1b, Tmpo, Scmh1, Apbb2, Cbs*	1.5
Repressor	20	*Tbl1xr1, Mecp2, Hdac10, Ctcf, Ppp1r13l, Cbx7, Hic1, Mxd4, Eif4g2, Sin3b, Cdyl, Hdac2, Nr1d2, Nab2, Zfp90, Hey2, Scrt1, Scmh1, Bcor, Nfx1*	3.3
Chromatin binding	20	*Msh6, Polg, Hp1bp3, Mecp2, Adnp, Ctcf, Smad2, Cbx7, Top1, Sin3b, Nipbl, Hdac2, Smarcc1, Smarcd1, Chd1, H2afy, Parg, Nfatc2, Asf1a, Stag2*	3.2
Ubiquitin protein ligase binding	15	*Usp7, Dnm1l, Syt11, Ube2g1, Smad2, Cul2, Cul5, Hif1a, Pcbp2, Prkar1a, Per1, Yod1, Cbs, Usp13, Rnf31*	3.9

Table 2.10 contains the significant DAVID functional gene ontology annotations of the yellow nuclear-related module. Redundant and non-significant GO terms were removed from the list. FE = fold-enrichment. FDR <$5.0x10^{-2}$.

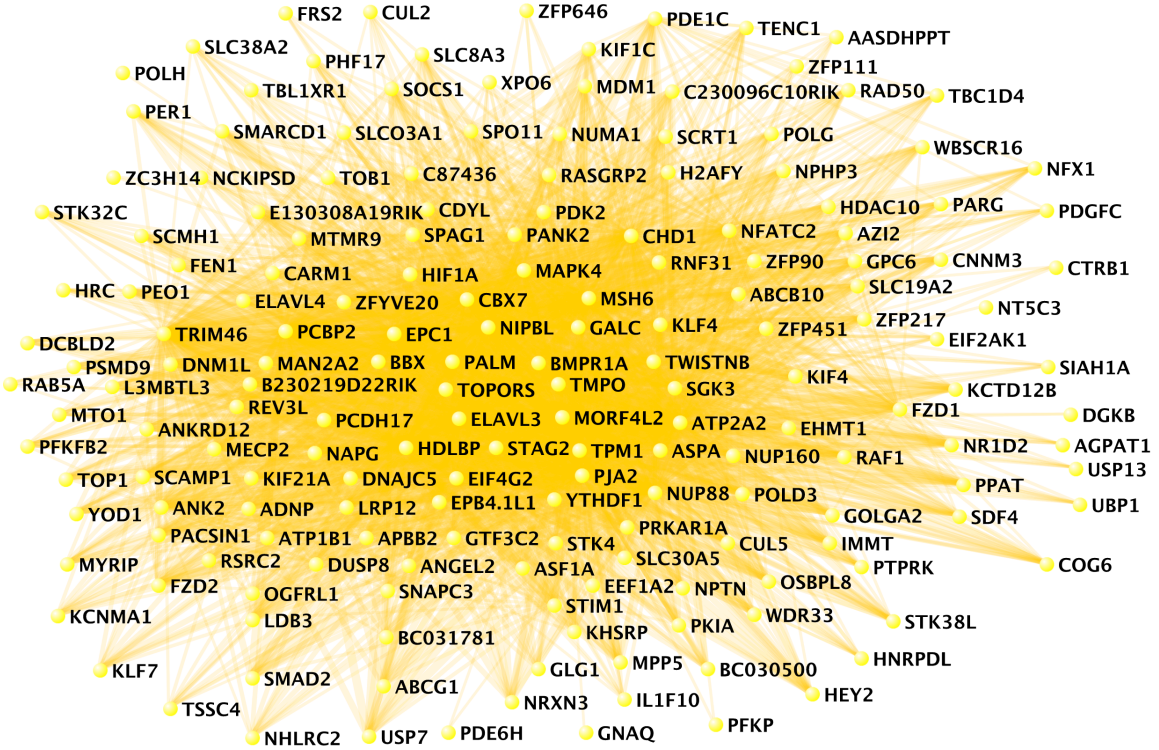

Figure 2.21 Yellow module is enriched for nuclear genes. The yellow module was enriched for genes involved in nucleus (FDR < $3.5x10^{-9}$), chromatin regulators (FDR < $6.0x10^{-4}$), transcription (FDR < $1.0x10^{-3}$), and alternative splicing (FDR < $2.6x10^{-6}$). In addition, the module is enriched for genes that are involved in PTMs including phosphorylation (FDR < $3.4x10^{-15}$), acetylation (FDR < $3.3x10^{-6}$), Ubl conjugation (FDR < $3.3x10^{-6}$), and methylation (FDR < $1.8x10^{-3}$). The gene network was generated in VisANT (weight cutoff > 0.1).

2.13 Discussion

In this study, we generated a forebrain-specific conditional *Ogt* knockout mouse to study the roles of *O*-GlcNAcylation in adult neurons. As the mice survived to adulthood, the effects of *Ogt* deletion on learning, memory, and adult neuronal function could be directly evaluated. Loss of OGT led to progressive neuronal death and other phenotypes associated with neurodegenerative diseases, including gliosis, activation of immune response and cell cycle genes, aberrant phosphorylation of tau, and amyloidogenic Aβ-42 peptides. OGT cKO mice also displayed behavioral deficits such as abnormal nesting behavior, and memory impairments, which are characteristics observed

in neurodegenerative mouse models of AD.[108] Notably, we found that human AD patients showed a significant decrease in OGT protein expression levels in the frontal cerebral cortex compared to control individuals, and this decrease correlated with progressive cognitive decline. Together, our studies reveal important neuroprotective roles for *O*-GlcNAcylation and suggest that alterations in *O*-GlcNAc signaling may contribute to neuronal pathology.

Both tau phosphorylation and APP processing were significantly altered in OGT cKO mice. Upon *Ogt* deletion, we observed enhanced tau aggregation and hyperphosphorylation at sites associated with neurofibrillary tangles. These findings further support previous studies suggesting a reciprocal relationship between *O*-GlcNAc and phosphorylation on tau. For example, increasing global *O*-GlcNAc levels reduced tau phosphorylation at Ser-199, Thr-212, Thr-217, Ser-262, Ser-396, and Ser-422 in mouse brain slices.[109] Moreover, inhibition of OGA elevated *O*-GlcNAc levels and decreased tau hyperphosphorylation in an AD mouse model.[110] Although we observed no significant change in the levels of tau *O*-GlcNAcylated at Ser-400, it is possible that *O*-GlcNAcylation of tau is differentially regulated at specific sites or that a small amount of residual OGT may be sufficient to maintain *O*-GlcNAc levels at this site.

With regard to APP, previous studies have suggested that higher *O*-GlcNAcylation levels can enhance non-amyloidogenic processing of APP by raising α-secretase activity in vitro and lowering γ-secretase activity.[111,112] In accordance with these observations, we found that loss of OGT enhanced the pathological processing of APP in vivo, increasing the ratio of the amyloidogenic 42-mer Aβ-peptide to the 40-mer. Notably, accumulation of hyperphosphorylated tau and Aβ-peptides is not observed in

many neurodegenerative mouse models, and both phenotypes are rarely observed together. For example, 5XFAD mice that express 5 different familial AD mutations in APP and presenilin 1 showed no accumulation of hyperphosphorylated tau, and mutant P301L tau transgenic mice displayed no increases of amyloid beta load, despite the presence of extensive neuronal death.[113,114] Thus, the defects in tau phosphorylation and APP processing observed in OGT cKO mice are not likely indirect effects caused by a global requirement for OGT in proper neuronal function and survival. Together, the findings suggest that the *O*-GlcNAc modification plays a central role in regulating both APP and tau, and dysfunctional *O*-GlcNAc signaling may contribute to improper APP processing and tau pathology.

We performed gene microarray analyses to obtain insights into the global, systems-level changes induced by loss of OGT. Our studies revealed that several cell cycle genes were upregulated in OGT cKO mice, including *Mki67*, *Prc1*, and *Spc25*. Consistent with an important role for OGT in cell cycle regulation, *O*-GlcNAcylation has previously been shown to modulate cell cycle progression by prolonging cyclin A and B expression and catalyzing proteolytic maturation of the critical cell cycle regulator, host cell factor-1 (HCF-1).[115,116] Interestingly, several genes involved in controlling oxidative stress were also significantly upregulated in OGT cKO mice, including heme oxygenase 1 (*Hmox1*), cyclooxygenase 1 (*Ptgs1*), and activity-dependent neuroprotective protein homeobox 2 (*ADNP2*). *O*-GlcNAcylation has previously been shown to be required for stress granule assembly in response to oxidative stress and to decrease oxidative stress in cardiomyocytes by reducing reactive oxygen species.[117,118] Thus, one important mechanism by which OGT may exert its neuroprotective effects is through the regulation

of critical cell cycle regulators and modulators of oxidative stress. The 'two-hit' hypothesis of AD postulates that both oxidative stress and mitotic dysregulation are necessary and sufficient to cause the neurodegeneration associated with AD.[119] Further supporting the gene expression analyses, we found that cyclin A2, a marker of cell cycle progression, was increased in OGT cKO mice, providing strong evidence for enhanced cell cycle progression in the hippocampi of these mice. Moreover, Cdk5 protein expression levels were significantly decreased upon loss of OGT. Cdk5 represses neuronal cell cycle advancement and is an important upstream regulator of oxidative stress through phosphorylation of peroxiredoxin I/II and p53.[119,120] Interestingly, a recent paper suggests that blocking *O*-GlcNAcylation of Cdk5 can lead to neuronal apoptosis by enhancing its association with the p53 pathway.[121] Several other studies have implicated aberrant cell cycle advancement in AD-associated neurodegeneration through deregulation of Cdk5 levels and activity.[120,122] Indeed, cyclin inhibitors that halt cell cycle progression have been shown to reduce the toxicity of Aβ peptides suggesting that they could be effective AD therapeutics.[87,123] Altogether, these results suggest that a major mode by which OGT ablation leads to neurodegeneration is through cell-cycle dysfunction. Future studies will focus on understanding the detailed mechanisms by which OGT affects Cdk5 function, the cell cycle and oxidative stress in neurons.

Lagerlof *et al.* reported that the tamoxifen-induced deletion of *Ogt* from CaMKIIα-positive neurons in adult mice leads to obesity from overeating.[124] This phenotype was due to reduced satiety caused by OGT ablation in the paraventricular nucleus (PVN) of the hypothalamus. Interestingly, no change in neuronal number in the hippocampus or PVN was noted upon quantification of DAPI+ cells, although the age of

the mice analyzed was not reported. The phenotypic differences between this and our model could be due to several explanations. First, there are likely differences in the timing of the OGT KO in the CaMKIIα-Cre versus the CaMKIIα-CreER^{T2} tamoxifen-inducible systems. In our study, loss of OGT and *O*-GlcNAcylation began at 4 weeks of age, and the neuronal loss and degenerative phenotypes were not significant until 8 weeks of age. In the Lagerlof study, tamoxifen injections were initiated at 6 weeks of age, and phenotypic responses were monitored up to 4 weeks later. Second, it is possible that the neurodegenerative phenotypes were not yet apparent during the window of their study as tamoxifen-induced CRE recombination can take several days. Furthermore, variability in the location and timing of CaMKIIα promoter-driven Cre recombination has been previously described and attributed to differences in the location of CaMKIIα-Cre transgene insertion within the genome.[125] Alternatively, excitatory forebrain neurons may be more vulnerable to OGT deletion at specific stages of maturation. Lastly, any effects on satiety in our model were likely obscured by the strong neurodegenerative phenotype. The phenotypic differences between the two OGT cKO models suggest that OGT plays specific roles in neuronal health and homeostasis during various stages, and they highlight the importance of the precise spatiotemporal coordination of *O*-GlcNAcylation.

The *O*-GlcNAc modification appears to play multiple, complex roles in neurodegeneration and, paradoxically, previous studies have suggested both neuroprotective and neurodegenerative effects upon decreasing *O*-GlcNAcylation.[110,126] We show that loss of *O*-GlcNAcylation in healthy neurons leads to progressive neurodegeneration *in vivo*, providing strong evidence that *O*-GlcNAc has neuroprotective functions in adult mammalian neurons. The OGT cKO and AD mouse models share

many of the same neurodegenerative, transcriptional, and behavioral phenotypes, suggesting common mechanisms of neurodegeneration. It is noteworthy that loss of OGT alone is sufficient to induce neurodegenerative pathologies and that this neurodegeneration occurs relatively rapidly. Induction of such phenotypes in other mouse models generally requires mutation or overexpression of multiple familial AD-related proteins such as tau, APP, and presenilin, and the pathological phenotypes take 9 to 12 months to progress.[108,127] The rapid course of neurodegeneration in OGT cKO mice underscores the critical importance of OGT in the maintenance of adult neuronal health and suggests that dysfunctional *O*-GlcNAc signaling may be an important contributor to neuronal pathology. Collectively, our studies provide a direct link between the ablation of *O*-GlcNAcylation and the induction of neurodegenerative phenotypes, suggesting that strategies to control *O*-GlcNAcylation and its neuroprotective effects may represent a novel approach for the treatment of neurodegenerative conditions.

2.14 Methods

2.14.1 Maintenance and breeding of OGT cKO mice

Mice were housed in groups whenever possible, and all animal procedures were performed in accordance with Institutional Animal Care and Use Committee guidelines of the California Institute of Technology. Only male mice were considered in this study due to random X inactivation of the *Ogt* gene in females, which would complicate phenotype analysis. OGT cKO mice were produced at the expected frequencies and were indistinguishable from WT littermates at birth.

As OGT cKO mice did not breed well, OGTfl and CaMKIIα-Cre mouse lines were maintained separately. By breeding homozygous OGTfl females (OGTfl-/-) with

heterozygous CaMKIIα-Cre males (CaMKIIα-Cre +/-), OGT cKO (OGTfl -/Y;CaMKIIα-Cre-/+) mice were produced, along with wild-type littermates (OGTfl -/Y; CaMKIIα-Cre+/+). The ROSA26L-eYFP mice were kindly provided by Dr. Ellen Rothenberg and bred with the CaMKIIα-Cre+/+ mice in order to determine the spatiotemporal expression and recombination of Cre recombinase.[128] As OGT cKO mice had an excessive grooming phenotype that resulted in skin lesions, the mice were culled at 6-7 months for humane reasons.

2.14.2 Behavioral studies

Fear conditioning was performed as described previously.[129] Briefly, mice were placed in a chamber (Med Associates) for the first time and allowed to explore for 120 s, after which an audible tone was played for 30 s. During the last 2 s of tone, a 0.7-mA foot shock was applied. This 150-s sequence was repeated, after which mice were returned to their home cages. After 24 h, mice were placed in the same chamber and monitored for 5 min to evaluate context-dependent memory. Mice were returned to their home cages for 1 h, and then placed into an altered context chamber (altered scent, shape, and lighting) for 5 min, with a tone playing for the last 180 s. All freezing quantification was done by Med Associates software, and freezing was normalized to pre-tone freezing % for cued tests. No significant difference in pre-tone freezing was observed between the two groups using an unpaired, two-tailed Student's *t*-test.

2.14.3 Antibodies

The following primary antibodies were used for immunohistochemistry (1:250 dilution) or Western (1:1000): OGT antibodies: TI-14 (Sigma, O6014), AL-25 and AL-28 (G.W. Hart, Johns Hopkins); Tubulin (Sigma, T9026); *O*-GlcNAc (RL2) (Pierce,

MA1-072); Tau antibodies: pThr231-AT180 (Pierce, MN1040), pSer202/Thr205-AT8 (Pierce, MN1020), pThr205 (Life Technologies, 44738G), pThr231 (Millipore, AB9668), tau-5 (Millipore, MAB361), pSer396 (Abcam, 32057); *O*-GlcNAc Ser400 (Anaspec, AS-55945, Western: 1:200); NeuN (Millipore, MAB377); NeuN (Abcam, ab134014, IHC: 1:100); GFP (Life Technologies, G10362); Iba-1 (WakoUSA, 019-19741); GFAP (Cell Signaling Technologies, 3670P); Cdk5 (Santa Cruz Biotechnology, SC-173); Cyclin A2 (Abcam, ab32386, IHC: 1:50); PCNA (Abcam, ab18197, IHC: 1:100); BrdU (Abcam, ab6326, IHC: 1:100). The following secondary antibodies were used for IHC (1:400 dilution): goat anti-mouse Alexa Fluor-405 (Life Technologies, A-31553), goat anti-mouse Alexa Fluor-488 (Life Technologies, A-11001), goat anti-mouse Alexa Fluor-546 (Life Technologies, A-11003), goat anti-rabbit Alexa Fluor-488 (Life Technologies, A-11008); goat anti-rabbit Alexa Fluor-405 (Life Technologies, A-31556); goat anti-rabbit Alexa Fluor-546 (Life Technologies, A-11035); goat anti-chicken Alexa Fluor-546 (Life Technologies, A-11040); goat anti-rat Alexa Fluor-488 (Life Technologies, A-11006). The following secondary antibodies for Western (1:10,000 dilution): goat anti-mouse Alexa Fluor-680, highly cross-adsorbed (Life Technologies, A21058); goat anti-mouse Alexa-Fluor-790 (Life Technologies, A11357); goat anti-rabbit Alexa Fluor-680 (Life Technologies, A21109); goat anti-rabbit Alexa Fluor-790 (Life Technologies, A11369).

2.14.4 Western blotting

Mouse cortical, hippocampal, and cerebellar samples extracted and then dounced in 2% sodium dodecyl sulfate (SDS) solution in water augmented with Roche cOmplete™, EDTA Protease Inhibitor Cocktail (Millipore Sigma, SKU 5056489001) and phosphatase inhibitors. Then, the protein amount was calculated using the Pierce

BCA (bicinchoninic acid) Protein Assay (Pierce, 23222 and 23224) as described by the manufacturer's instructions. Equal amounts of protein were diluted in water and 4X SDS-polyacrylamide gel electrophoresis (SDS-PAGE) loading buffer (200 mM Tris pH 6.8, 400 mM DTT, 8% SDS, 40% glycerol, 0.4% bromophenol blue) and heated to 95 °C for 10 min. The samples and ladder (Precision Plus Protein Dual Color Standards (Bio-Rad)) were separated using NuPAGE 4-12% Bis-Tris protein gels (NP0355BOX, ThermoFisher Scientific) at 180V at room temperature (RT) for 1 hour. Following resolution, the proteins were then transferred onto Immobilion-FL PVDF membrane (IPFL00010, EMD Millipore) at 250 mA at 4 °C for 1.5 hours. The membranes were blocked for 1 hour at RT in blocking buffer (either 5% BSA (bovine serum albumin) in TBST (50 mM Tris pH 7.4, 150 mM NaCl, 0.1% Tween) or with 5% nonfat milk in TBST according to the antibody manufacturer's specifications). Following the blocking step, the blots were incubated overnight at 4°C in the diluted primary antibody in the blocking buffer with gentle rocking. Blots were rinsed three times for 5 minutes with TBST, incubated with secondary antibodies at RT for 1.5 hours with gentle rocking, rinsed three times with TBST again, and then imaged using the Li-COR Odyssey® CLx Infrared Imaging System. The western blot intensities were quantified using Image Studio™ Lite Software (Li-COR) and significance in a pairwise comparison was determined using an unpaired, two-tailed Student's *t*-test.

2.14.5 Immunohistochemistry

For Nissl staining, slices were incubated in 100% EtOH followed by Histoclear (Electron Microscopy Sciences, 641101-01) for 2 min each. Slices were then sequentially rehydrated in 100%, 70%, and 50% aqueous EtOH for 2 min each. Slices were stained

with a 0.1% cresyl violet solution for 10 min, rinsed in distilled water, and differentiated in 90% EtOH with 1% acetic acid for 10 s. After a final wash in 100% EtOH, slices were cleared for 2 min in Histoclear and mounted with Vectashield.

For Fluoro-Jade C (Millipore, AG325) and Thioflavine S (Sigma, T1892) IHC staining, slices were incubated in 0.06% potassium permanganate solution for 10 min, washed in double-distilled H_2O, and transferred to a 0.0001% solution of Fluoro-Jade C in 0.1% acetic acid, or a 0.05% Thioflavine S solution in 50% EtOH for 10 min. Following a 5 min wash in H_2O, (or 50% EtOH for Thioflavine S), slices were mounted with Vectashield. For Cyclin A2 and PCNA staining, slices underwent antigen retrieval for one hour at 37 degrees in citrate buffer (0.01 M sodium citrate in 0.1% Triton X-100 in H_2O, pH 6.0) prior to blocking. For BrdU staining, slices were incubated in 2 N HCl for 20 minutes at 37 degrees followed by 10 min of neutralization in 0.1 M sodium borate buffer, pH 8.5 (two 5 min incubations). Next, the slices were rinsed three times with PBS and then blocked as normal.

Brain samples of frontal cortex from control (n = 6), Braak VI (n = 8), and Braak IV-V (n = 4) patients were obtained from the Alzheimer's Disease Research Center at the University of California, Los Angeles. Samples were from patients with a similar age, gender, and postmortem interval (PMI). Slices were pre-treated with 0.01 M citrate buffer (37 °C, pH 3.5) followed by treatment with Sudan black (0.1% w/v in 70% EtOH, Sigma, 199664)) and stained as described above. Four representative regions were imaged in each slice, and at least four slices were imaged per individual. Images were coded and discrete quantitative scoring of OGT protein signal (scale from 1-4) was carried out with researchers blind to sample ID.

2.14.6 BrdU Assay for Neurogenesis

The BrdU assay for neurogenesis was performed as previously described. Briefly, 2-month old male mice were injected with 100-200 μL of sterile 10 mg/ml BrdU (5-Bromo-2'-deoxyuridine, Sigma Aldrich, B5002-1g) in PBS buffer intraperitoneally in order to achieve a final concentration of 200 mg/kg BrdU. Twenty-four hours following the injection, the mice were transcardially perfused followed by dissection, fixation, and immunohistochemical staining as described previously.[130]

2.14.7 Aβ-Peptide ELISA

The Amyloid-beta ELISA Kits 1-40 and 1-42 (Covance, SIG-38954, 38956) were used to quantify Aβ-peptide levels following the manufacturer's protocol. Whole cortices were lysed in TBS (50 mM Tris-HCl, pH 7.5, 150 mM NaCl) containing 1% Triton-X100 and protease inhibitor cocktail (Roche, 11697498001), centrifuged at 100,000*g*, and the supernatant was assayed following the ELISA kit protocol.

2.14.8 RNA extraction, qRT-PCR, and Microarray Analysis

Hippocampal tissue was isolated from 3-week-old or 2-month-old mice, flash frozen, and stored at -80 °C in nuclease-free tubes until extraction. Total RNA was extracted using an RNeasy kit with RNase-free DNase treatment per the manufacturer's instructions (Qiagen, 79254). Following RNA extraction, the samples were sent to Phalanx Biotech Group (Belmont, CA) for microarray analysis. Briefly, a library was generated from the mRNA using the Ambion Amino Allyl MessageAmp II aRNA Amplification Kit (Life Technologies, AM1753) and applied to Mouse OneArrays v2 containing probes for over 23,000 genes (Phalanx Biotech). The microarray intensities were normalized using over 800 control probes throughout the array. In addition to

microarray analysis, the extracted mRNA was reverse transcribed using the iScript cDNA Synthesis Kit (Bio-rad, 1708891) for qRT-PCR. Following reverse transcription, the cDNA was used for qPCR analysis using Perfecta SYBR Green Fastmix with ROX (VWR, 101414-280) on an AB7300 Real Time System (Applied Biosystems). The qRT-PCR expression values were calculated using the comparative C_T method, and expression values were normalized to the geometric mean of 5 different reference genes as previously described.[131] The efficiencies of the qPCR primers were calculated using Python version 2.7.13 and were utilized in the calculation of the expression values as previously described.[131] A list of primers used in this study can be found in Appendix III. Statistical significance of qRT-PCR results was determined using an unpaired t-test. Reported *P* values for the microarray results from this study were calculated using a Bonferroni correction (all differentially-expressed genes have Bonferroni *P*-value < 0.001 unless otherwise noted).[132] All programs are available upon request.

2.14.9 WGCNA and Gene Ontology Analysis

Prior to performing the first WGCNA, the microarray data was pre-processed using limma in R version 3.3.2 and Python version 2.7.13. The AD and FTDP mouse model comparative analysis utilized hippocampal data from Matarin and colleagues downloaded from http://www.mouseac.org/ (GEO number GSE64398).[89] Then, the Matarin microarray data were aligned with our microarray data from the OGT cKO and the WT littermates using Python version 2.7.13. Following alignment, the Partek® Genomics Suite®, version 6.6 Copyright ©2017 was used to perform a quantile normalization across all of the microarray data sets.[133] Using the pre-processed microarray data, we performed WGCNA in R package version 3.0.0 on all microarray-

detected genes using the protocols previously described.[45,46] Following hierarchical clustering and module assignment, gene ontology enrichment analysis was performed using Bioconductor packages GO and the Database for Annotation, Visualization and Integrated Discovery (DAVID) as previously described.[134] The package VisANT version 5.0 (correlation cutoff of 0.1 (cor > 0.1)), Cytoscape version 3.5.1, ClueGO version 2.3.3, and CluePedia version 1.3.3 was used to visualize the WGCNA gene networks.[135-138] All programs are available upon request.

2.14.10 Statistical Analyses

Unless otherwise stated, all results are expressed as the mean ± standard error of the mean (SEM) and are representative of at least four experimental replicates. Statistical tests for significant deviation between samples were performed using an unpaired, two-tailed Student's *t*-test.

2.15 References

1 Shafi, R. *et al.* The O-GlcNAc transferase gene resides on the X chromosome and is essential for embryonic stem cell viability and mouse ontogeny. *Proceedings of the National Academy of Sciences* (2000) **97**, 11:5735-5739.

2 O'Donnell, N., Zachara, N.E., Hart, G.W. & Marth, J.D. Ogt-Dependent X-Chromosome-Linked Protein Glycosylation Is a Requisite Modification in Somatic Cell Function and Embryo Viability. *Molecular and Cellular Biology* (2004) **24**, 4:1680-1690.

3 Liu, K. *et al.* Accumulation of protein O-GlcNAc modification inhibits proteasomes in the brain and coincides with neuronal apoptosis in brain areas with high O-GlcNAc metabolism. *J Neurochem* (2004) **89**, 4:1044-1055.

4 Zhou, Y. *et al.* Interactions between the NR2B receptor and CaMKII modulate synaptic plasticity and spatial learning. *J Neurosci* (2007) **27**, 50:13843-13853.

5 Hayashi, S. & McMahon, A.P. Efficient recombination in diverse tissues by a tamoxifen-inducible form of Cre: a tool for temporally regulated gene activation/inactivation in the mouse. *Dev Biol* (2002) **244**, 2:305-318.

6 Dragatsis, I. & Zeitlin, S. CaMKIIalpha-Cre transgene expression and recombination patterns in the mouse brain. *Genesis* (2000) **26**, 2:133-135.

7 Kennedy, J.L., Farrer, L.A., Andreasen, N.C., Mayeux, R. & St George-Hyslop, P. The genetics of adult-onset neuropsychiatric disease: complexities and conundra? *Science* (2003) **302**, 5646:822-826.

8 Schweizer C, B.S., Bluethmann H, Mansuy IM, Fritschy JM, Mohler H, Lüscher B. The gamma 2 subunit of GABA(A) receptors is required for maintenance of receptors at mature synapses. *Mol Cell Neurosci.* (2003) **24**, 2:442-450.

9 Fekairi, S. *et al.* Human SLX4 is a Holliday junction resolvase subunit that binds multiple DNA repair/recombination endonucleases. *Cell* (2009) **138**, 1:78-89.

10 Garner, E., Kim, Y., Lach, F.P., Kottemann, M.C. & Smogorzewska, A. Human GEN1 and the SLX4-associated nucleases MUS81 and SLX1 are essential for the resolution of replication-induced Holliday junctions. *Cell Rep* (2013) **5**, 1:207-215.
11 Wilson, J.S. *et al.* Localization-dependent and -independent roles of SLX4 in regulating telomeres. *Cell Rep* (2013) **4**, 5:853-860.
12 Navia-Paldanius, D. *et al.* Chemoproteomic, biochemical and pharmacological approaches in the discovery of inhibitors targeting human alpha/beta-hydrolase domain containing 11 (ABHD11). *Eur J Pharm Sci* (2016) **93**, 253-263.
13 Arya, M., Srinivasan, M. & Rajasekharan, R. Human alpha beta hydrolase domain containing protein 11 and its yeast homolog are lipid hydrolases. *Biochem Biophys Res Commun* (2017) **487**, 4:875-880.
14 Barresi, M.J. *et al.* Essential genes for astroglial development and axon pathfinding during zebrafish embryogenesis. *Dev Dyn* (2010) **239**, 10:2603-2618.
15 Francelle, L. *et al.* Striatal long noncoding RNA Abhd11os is neuroprotective against an N-terminal fragment of mutant huntingtin in vivo. *Neurobiol Aging* (2015) **36**, 3:1601 e1607-1616.
16 Osterhout, J.A. *et al.* Cadherin-6 mediates axon-target matching in a non-image-forming visual circuit. *Neuron* (2011) **71**, 4:632-639.
17 Kirk, L.M. *et al.* Distribution of the SynDIG4/proline-rich transmembrane protein 1 in rat brain. *J Comp Neurol* (2016) **524**, 11:2266-2280.
18 Chen, N. *et al.* Interaction proteomics reveals brain region-specific AMPA receptor complexes. *J Proteome Res* (2014) **13**, 12:5695-5706.
19 Rodriguez-Rodriguez, P., Fernandez, E., Almeida, A. & Bolanos, J.P. Excitotoxic stimulus stabilizes PFKFB3 causing pentose-phosphate pathway to glycolysis switch and neurodegeneration. *Cell Death Differ* (2012) **19**, 10:1582-1589.
20 Rodriguez-Rodriguez, P., Almeida, A. & Bolanos, J.P. Brain energy metabolism in glutamate-receptor activation and excitotoxicity: role for APC/C-Cdh1 in the balance glycolysis/pentose phosphate pathway. *Neurochem Int* (2013) **62**, 5:750-756.
21 Schoenberg, D.R. & Maquat, L.E. Regulation of cytoplasmic mRNA decay. *Nat Rev Genet* (2012) **13**, 4:246-259.
22 Katayama, S. *et al.* Antisense transcription in the mammalian transcriptome. *Science* (2005) **309**, 5740:1564-1566.
23 Dickey, C.A. *et al.* Selectively reduced expression of synaptic plasticity-related genes in amyloid precursor protein + presenilin-1 transgenic mice. *J Neurosci* (2003) **23**, 12:5219-5226.
24 Wu, Z.L. *et al.* Comparative analysis of cortical gene expression in mouse models of Alzheimer's disease. *Neurobiol Aging* (2006) **27**, 3:377-386.
25 Ulrich, J.D., Ulland, T.K., Colonna, M. & Holtzman, D.M. Elucidating the Role of TREM2 in Alzheimer's Disease. *Neuron* (2017) **94**, 2:237-248.
26 Van Cauwenberghe, C., Van Broeckhoven, C. & Sleegers, K. The genetic landscape of Alzheimer disease: clinical implications and perspectives. *Genet Med* (2016) **18**, 5:421-430.
27 Sims, R. *et al.* Rare coding variants in PLCG2, ABI3, and TREM2 implicate microglial-mediated innate immunity in Alzheimer's disease. *Nat Genet* (2017) **49**, 9:1373-1384.
28 Ulland, T.K. *et al.* TREM2 Maintains Microglial Metabolic Fitness in Alzheimer's Disease. *Cell* (2017) **170**, 4:649-663 e613.
29 Mahley, R.W. Apolipoprotein E: cholesterol transport protein with expanding role in cell biology. *Science* (1988) **240**, 4852:622-630.
30 Puglielli, L., Tanzi, R.E. & Kovacs, D.M. Alzheimer's disease: the cholesterol connection. *Nat Neurosci* (2003) **6**, 4:345-351.
31 Kotti, T.J., Ramirez, D.M., Pfeiffer, B.E., Huber, K.M. & Russell, D.W. Brain cholesterol turnover required for geranylgeraniol production and learning in mice. *Proc Natl Acad Sci U S A* (2006) **103**, 10:3869-3874.
32 Kotti, T., Head, D.D., McKenna, C.E. & Russell, D.W. Biphasic requirement for geranylgeraniol in hippocampal long-term potentiation. *Proc Natl Acad Sci U S A* (2008) **105**, 32:11394-11399.
33 Luthi-Carter, R. *et al.* SIRT2 inhibition achieves neuroprotection by decreasing sterol biosynthesis. *Proc Natl Acad Sci U S A* (2010) **107**, 17:7927-7932.

34 Bryleva, E.Y. *et al.* ACAT1 gene ablation increases 24(S)-hydroxycholesterol content in the brain and ameliorates amyloid pathology in mice with AD. *Proc Natl Acad Sci U S A* (2010) **107**, 7:3081-3086.
35 Shimano, H. & Sato, R. SREBP-regulated lipid metabolism: convergent physiology - divergent pathophysiology. *Nat Rev Endocrinol* (2017) **advance online publication**.
36 Yang, T. *et al.* Crucial step in cholesterol homeostasis: sterols promote binding of SCAP to INSIG-1, a membrane protein that facilitates retention of SREBPs in ER. *Cell* (2002) **110**, 4:489-500.
37 Anthonisen, E.H. *et al.* Nuclear receptor liver X receptor is O-GlcNAc-modified in response to glucose. *J Biol Chem* (2010) **285**, 3:1607-1615.
38 Yi, W. *et al.* Phosphofructokinase 1 glycosylation regulates cell growth and metabolism. *Science* (2012) **337**, 6097:975-980.
39 Dentin, R., Hedrick, S., Xie, J., Yates, J., 3rd & Montminy, M. Hepatic glucose sensing via the CREB coactivator CRTC2. *Science* (2008) **319**, 5868:1402-1405.
40 Ruan, H.B., Singh, J.P., Li, M.D., Wu, J. & Yang, X. Cracking the O-GlcNAc code in metabolism. *Trends Endocrinol Metab* (2013) **24**, 6:301-309.
41 Rong, S. *et al.* Expression of SREBP-1c Requires SREBP-2-mediated Generation of a Sterol Ligand for LXR in Livers of Mice. *Elife* (2017) **6**, e25015.
42 Wong, J., Quinn, C.M. & Brown, A.J. SREBP-2 positively regulates transcription of the cholesterol efflux gene, ABCA1, by generating oxysterol ligands for LXR. *Biochem J* (2006) **400**, 3:485-491.
43 Hanover, J.A. *et al.* A Caenorhabditis elegans model of insulin resistance: altered macronutrient storage and dauer formation in an OGT-1 knockout. *Proc Natl Acad Sci U S A* (2005) **102**, 32:11266-11271.
44 Perez-Cervera, Y. *et al.* Insulin signaling controls the expression of O-GlcNAc transferase and its interaction with lipid microdomains. *FASEB J* (2013) **27**, 9:3478-3486.
45 Langfelder, P. & Horvath, S. WGCNA: an R package for weighted correlation network analysis. *BMC Bioinformatics* (2008) **9**, 559.
46 Langfelder, P. & Horvath, S. Fast R Functions for Robust Correlations and Hierarchical Clustering. *J Stat Softw* (2012) **46**, 11:17.
47 Tait, S.W. & Green, D.R. Mitochondria and cell death: outer membrane permeabilization and beyond. *Nat Rev Mol Cell Biol* (2010) **11**, 9:621-632.
48 Ooms, L.M. *et al.* The role of the inositol polyphosphate 5-phosphatases in cellular function and human disease. *Biochem J* (2009) **419**, 1:29-49.
49 Kam, T.I. *et al.* FcgammaRIIb-SHIP2 axis links Abeta to tau pathology by disrupting phosphoinositide metabolism in Alzheimer's disease model. *Elife* (2016) **5**, e18691.
50 Srinivasan, K. *et al.* Untangling the brain's neuroinflammatory and neurodegenerative transcriptional responses. *Nat Commun* (2016) **7**, 11295.
51 Hokama, M. *et al.* Altered expression of diabetes-related genes in Alzheimer's disease brains: the Hisayama study. *Cereb Cortex* (2014) **24**, 9:2476-2488.
52 Miller, J.A., Woltjer, R.L., Goodenbour, J.M., Horvath, S. & Geschwind, D.H. Genes and pathways underlying regional and cell type changes in Alzheimer's disease. *Genome Med* (2013) **5**, 5:48.
53 Wirz, K.T. *et al.* Cortical beta amyloid protein triggers an immune response, but no synaptic changes in the APPswe/PS1dE9 Alzheimer's disease mouse model. *Neurobiol Aging* (2013) **34**, 5:1328-1342.
54 Hart, G.W., Slawson, C., Ramirez-Correa, G. & Lagerlof, O. Cross talk between O-GlcNAcylation and phosphorylation: roles in signaling, transcription, and chronic disease. *Annu Rev Biochem* (2011) **80**, 1:825-858.
55 Langfelder, P., Mischel, P.S. & Horvath, S. When is hub gene selection better than standard meta-analysis? *PLoS One* (2013) **8**, 4:e61505.
56 Stefansson, B., Ohama, T., Daugherty, A.E. & Brautigan, D.L. Protein phosphatase 6 regulatory subunits composed of ankyrin repeat domains. *Biochemistry* (2008) **47**, 5:1442-1451.
57 Zhong, J. *et al.* Protein phosphatase PP6 is required for homology-directed repair of DNA double-strand breaks. *Cell Cycle* (2011) **10**, 9:1411-1419.
58 Stefansson, B. & Brautigan, D.L. Protein phosphatase 6 subunit with conserved Sit4-associated protein domain targets IkappaBepsilon. *J Biol Chem* (2006) **281**, 32:22624-22634.

59 Zeng, K., Bastos, R.N., Barr, F.A. & Gruneberg, U. Protein phosphatase 6 regulates mitotic spindle formation by controlling the T-loop phosphorylation state of Aurora A bound to its activator TPX2. *J Cell Biol* (2010) **191**, 7:1315-1332.
60 Ma, X. *et al.* PP6 Disruption Synergizes with Oncogenic Ras to Promote JNK-Dependent Tumor Growth and Invasion. *Cell Rep* (2017) **19**, 13:2657-2664.
61 Bhandari, D. *et al.* Sit4p/PP6 regulates ER-to-Golgi traffic by controlling the dephosphorylation of COPII coat subunits. *Mol Biol Cell* (2013) **24**, 17:2727-2738.
62 Ohama, T., Wang, L., Griner, E.M. & Brautigan, D.L. Protein Ser/Thr phosphatase-6 is required for maintenance of E-cadherin at adherens junctions. *BMC Cell Biol* (2013) **14**, 1:42.
63 Valdez, B.C., Henning, D., So, R.B., Dixon, J. & Dixon, M.J. The Treacher Collins syndrome (TCOF1) gene product is involved in ribosomal DNA gene transcription by interacting with upstream binding factor. *Proc Natl Acad Sci U S A* (2004) **101**, 29:10709-10714.
64 Ciccia, A. *et al.* Treacher Collins syndrome TCOF1 protein cooperates with NBS1 in the DNA damage response. *Proc Natl Acad Sci U S A* (2014) **111**, 52:18631-18636.
65 Larsen, D.H. *et al.* The NBS1-Treacle complex controls ribosomal RNA transcription in response to DNA damage. *Nat Cell Biol* (2014) **16**, 8:792-803.
66 Werner, A. *et al.* Cell-fate determination by ubiquitin-dependent regulation of translation. *Nature* (2015) **525**, 7570:523-527.
67 Gong, D. & Ferrell, J.E., Jr. The roles of cyclin A2, B1, and B2 in early and late mitotic events. *Mol Biol Cell* (2010) **21**, 18:3149-3161.
68 Wang, X., Zhang, C., Szabo, G. & Sun, Q.Q. Distribution of CaMKIIalpha expression in the brain in vivo, studied by CaMKIIalpha-GFP mice. *Brain Res* (2013) **1518**, 9-25.
69 Yang, Y., Mufson, E.J. & Herrup, K. Neuronal cell death is preceded by cell cycle events at all stages of Alzheimer's disease. *Journal of Neuroscience* (2003) **23**, 7:2557-2563.
70 Yang, Y., Varvel, N.H., Lamb, B.T. & Herrup, K. Ectopic cell cycle events link human Alzheimer's disease and amyloid precursor protein transgenic mouse models. *J Neurosci* (2006) **26**, 3:775-784.
71 Yang, Y., Geldmacher, D.S. & Herrup, K. DNA replication precedes neuronal cell death in Alzheimer's disease. *J Neurosci* (2001) **21**, 8:2661-2668.
72 Buchakjian, M.R. & Kornbluth, S. The engine driving the ship: metabolic steering of cell proliferation and death. *Nat Rev Mol Cell Biol* (2010) **11**, 10:715-727.
73 Yalcin, A. *et al.* Nuclear targeting of 6-phosphofructo-2-kinase (PFKFB3) increases proliferation via cyclin-dependent kinases. *J Biol Chem* (2009) **284**, 36:24223-24232.
74 Herrero-Mendez, A. *et al.* The bioenergetic and antioxidant status of neurons is controlled by continuous degradation of a key glycolytic enzyme by APC/C-Cdh1. *Nat Cell Biol* (2009) **11**, 6:747-752.
75 Esteras, N. *et al.* Altered cell cycle-related gene expression in brain and lymphocytes from a transgenic mouse model of Alzheimer's disease [amyloid precursor protein/presenilin 1 (PS1)]. *Eur J Neurosci* (2012) **36**, 5:2609-2618.
76 Weeks, S.D. *et al.* Molecular structure and dynamics of the dimeric human small heat shock protein HSPB6. *J Struct Biol* (2014) **185**, 3:342-354.
77 Wilhelmus, M.M. *et al.* Specific association of small heat shock proteins with the pathological hallmarks of Alzheimer's disease brains. *Neuropathol Appl Neurobiol* (2006) **32**, 2:119-130.
78 Cameron, R.T. *et al.* The phosphorylation of Hsp20 enhances its association with amyloid-beta to increase protection against neuronal cell death. *Mol Cell Neurosci* (2014) **61**, Supplement C:46-55.
79 Hato, T., Tabata, M. & Oike, Y. The role of angiopoietin-like proteins in angiogenesis and metabolism. *Trends Cardiovasc Med* (2008) **18**, 1:6-14.
80 Oike, Y. *et al.* Angiopoietin-related growth factor antagonizes obesity and insulin resistance. *Nat Med* (2005) **11**, 4:400-408.
81 Kang, S.G. *et al.* ANGPTL6 expression is coupled with mitochondrial OXPHOS function to regulate adipose FGF21. *J Endocrinol* (2017) **233**, 1:105-118.
82 Mukherjee, S. *et al.* Genome-Wide Analysis of Amyloid Beta (Ab) Peptide Obtained from Histelide Identifies Suggestive Hits in Rhbdf1, Grid1, and Ptprd Regions in the Adult Changes in Thought (Act) Study. *Alzheimer's & Dementia* (2014) **10**, 4:P317.
83 Raj, T. *et al.* Integrative analyses of splicing in the aging brain: role in susceptibility to Alzheimer's Disease. *bioRxiv* (2017).

84 Wilson-Edell, K.A. *et al.* RPL24: a potential therapeutic target whose depletion or acetylation inhibits polysome assembly and cancer cell growth. *Oncotarget* (2014) **5**, 13:5165-5176.
85 Zhang, J. *et al.* Cdk5 suppresses the neuronal cell cycle by disrupting the E2F1-DP1 complex. *J Neurosci* (2010) **30**, 15:5219-5228.
86 Heneka, M.T., Golenbock, D.T. & Latz, E. Innate immunity in Alzheimer's disease. *Nat Immunol* (2015) **16**, 3:229-236.
87 Folch, J. *et al.* Role of cell cycle re-entry in neurons: a common apoptotic mechanism of neuronal cell death. *Neurotox Res* (2012) **22**, 3:195-207.
88 Odajima, J. *et al.* Cyclin E constrains Cdk5 activity to regulate synaptic plasticity and memory formation. *Dev Cell* (2011) **21**, 4:655-668.
89 Matarin, M. *et al.* A genome-wide gene-expression analysis and database in transgenic mice during development of amyloid or tau pathology. *Cell Rep* (2015) **10**, 4:633-644.
90 Merino-Serrais, P. *et al.* The influence of phospho-tau on dendritic spines of cortical pyramidal neurons in patients with Alzheimer's disease. *Brain* (2013) **136**, Pt 6:1913-1928.
91 Lopes, S. *et al.* Tau protein is essential for stress-induced brain pathology. *Proc Natl Acad Sci U S A* (2016) **113**, 26:E3755-3763.
92 Lagerlof, O., Hart, G.W. & Huganir, R.L. O-GlcNAc transferase regulates excitatory synapse maturity. *Proc Natl Acad Sci U S A* (2017) **114**, 7:1684-1689.
93 Kouzarides, T. Chromatin modifications and their function. *Cell* (2007) **128**, 4:693-705.
94 Chen, Q. & Yu, X. OGT restrains the expansion of DNA damage signaling. *Nucleic Acids Res* (2016) **44**, 19:9266-9278.
95 Akan, I., Love, D.C., Harwood, K.R., Bond, M.R. & Hanover, J.A. Drosophila O-GlcNAcase Deletion Globally Perturbs Chromatin O-GlcNAcylation. *J Biol Chem* (2016) **291**, 19:9906-9919.
96 Lee, J.S. & Zhang, Z. *O*-linked N-acetylglucosamine transferase (OGT) interacts with the histone chaperone HIRA complex and regulates nucleosome assembly and cellular senescence. *Proc Natl Acad Sci U S A* (2016) **113**, 23:E3213-3220.
97 Ince-Dunn, G. *et al.* Neuronal Elav-like (Hu) proteins regulate RNA splicing and abundance to control glutamate levels and neuronal excitability. *Neuron* (2012) **75**, 6:1067-1080.
98 Fragkouli, A. *et al.* Neuronal ELAVL proteins utilize AUF-1 as a co-partner to induce neuron-specific alternative splicing of APP. (2017) **7**, 44507.
99 Park, S.K. *et al.* A conserved splicing silencer dynamically regulates *O*-GlcNAc transferase intron retention and *O*-GlcNAc homeostasis. *Cell Rep* (2017) **20**, 5:1088-1099.
100 Bertram, L. *et al.* Evidence for genetic linkage of Alzheimer's disease to chromosome 10q. *Science* (2000) **290**, 5500:2302-2303.
101 Twine, N.A., Janitz, K., Wilkins, M.R. & Janitz, M. Whole transcriptome sequencing reveals gene expression and splicing differences in brain regions affected by Alzheimer's disease. *PLoS One* (2011) **6**, 1:e16266.
102 McKay, S.L. & Johnson, T.L. A bird's-eye view of post-translational modifications in the spliceosome and their roles in spliceosome dynamics. *Mol Biosyst* (2010) **6**, 11:2093-2102.
103 Shan, X.Y. *O-linked N-acetylglucosamine protein modification in mouse models of neurodegenerative diseases* Ph.D. thesis, Simon Fraser University, (2011).
104 De, I. *et al.* The RNA helicase Aquarius exhibits structural adaptations mediating its recruitment to spliceosomes. *Nat Struct Mol Biol* (2015) **22**, 2:138-144.
105 Zhu, X. *et al.* Spatiotemporal expression of KHSRP modulates Schwann cells and neuronal differentiation after sciatic nerve injury. *Int J Biochem Cell Biol* (2014) **48**, Supplement C:1-10.
106 Zhang, Z. *et al.* The helicase DDX41 senses intracellular DNA mediated by the adaptor STING in dendritic cells. *Nat Immunol* (2011) **12**, 10:959-965.
107 Su, C. & Schwarz, T.L. O-GlcNAc Transferase Is Essential for Sensory Neuron Survival and Maintenance. *J Neurosci* (2017) **37**, 8:2125-2136.
108 Oddo, S. *et al.* Triple-transgenic model of Alzheimer's disease with plaques and tangles: intracellular Aβ and synaptic dysfunction. *Neuron* (2003) **39**, 3:409-421.
109 Liu, F., Iqbal, K., Grundke-Iqbal, I., Hart, G.W. & Gong, C.X. O-GlcNAcylation regulates phosphorylation of tau: a mechanism involved in Alzheimer's disease. *Proc Natl Acad Sci U S A* (2004) **101**, 29:10804-10809.

110 Yuzwa, S.A. *et al.* Increasing O-GlcNAc slows neurodegeneration and stabilizes tau against aggregation. *Nat Chem Biol* (2012) **8**, 4:393-399.
111 Jacobsen, K.T. & Iverfeldt, K. O-GlcNAcylation increases non-amyloidogenic processing of the amyloid-beta precursor protein (APP). *Biochem Biophys Res Commun* (2011) **404**, 3:882-886.
112 Kim, C. *et al.* O-linked beta-N-acetylglucosaminidase inhibitor attenuates beta-amyloid plaque and rescues memory impairment. *Neurobiol Aging* (2013) **34**, 1:275-285.
113 Oakley, H. *et al.* Intraneuronal β-amyloid aggregates, neurodegeneration, and neuron loss in transgenic mice with five familial Alzheimer's disease mutations: potential factors in amyloid plaque formation. *Journal of Neuroscience* (2006) **26**, 40:10129-10140.
114 Götz, J., Chen, F., Van Dorpe, J. & Nitsch, R. Formation of neurofibrillary tangles in P301L tau transgenic mice induced by Aβ42 fibrils. *Science* (2001) **293**, 5534:1491-1495.
115 Slawson, C. *et al.* Perturbations in O-linked β-N-acetylglucosamine protein modification cause severe defects in mitotic progression and cytokinesis. *Journal of Biological Chemistry* (2005) **280**, 38:32944-32956.
116 Capotosti, F. *et al.* O-GlcNAc transferase catalyzes site-specific proteolysis of HCF-1. *Cell* (2011) **144**, 3:376-388.
117 Ngoh, G.A., Watson, L.J., Facundo, H.T. & Jones, S.P. Augmented O-GlcNAc signaling attenuates oxidative stress and calcium overload in cardiomyocytes. *Amino Acids* (2011) **40**, 3:895-911.
118 Ohn, T., Kedersha, N., Hickman, T., Tisdale, S. & Anderson, P. A functional RNAi screen links O-GlcNAc modification of ribosomal proteins to stress granule and processing body assembly. *Nature cell biology* (2008) **10**, 10:1224-1231.
119 Herrup, K. & Yang, Y. Cell cycle regulation in the postmitotic neuron: oxymoron or new biology? *Nat Rev Neurosci* (2007) **8**, 5:368-378.
120 Zhang, J. *et al.* Nuclear localization of Cdk5 is a key determinant in the postmitotic state of neurons. *Proceedings of the National Academy of Sciences* (2008) **105**, 25:8772-8777.
121 Ning, X. *et al.* The O-GlcNAc Modification of Cdk5 Involved in Neuronal Apoptosis Following In Vitro Intracerebral Hemorrhage. *Cellular and Molecular Neurobiology* (2016) 1-10.
122 Zhang, J., Li, H., Zhou, T., Zhou, J. & Herrup, K. Cdk5 levels oscillate during the neuronal cell cycle: Cdh1 ubiquitination triggers proteosome-dependent degradation during S-phase *Journal of Biological Chemistry* (2012) **287**, 31:25985-25994.
123 Xu, X. *et al.* Prevention of beta-amyloid induced toxicity in human iPS cell-derived neurons by inhibition of Cyclin-dependent kinases and associated cell cycle events. *Stem Cell Res* (2013) **10**, 2:213-227.
124 Lagerlöf, O. *et al.* The nutrient sensor OGT in PVN neurons regulates feeding. *Science* (2016) **351**, 6279:1293-1296.
125 Tsien, J.Z. *et al.* Subregion- and Cell Type-Restricted Gene Knockout in Mouse Brain. *Cell* (1996) **87**, 7:1317-1326.
126 Wang, P. *et al.* O-GlcNAc cycling mutants modulate proteotoxicity in Caenorhabditis elegans models of human neurodegenerative diseases. *Proc Natl Acad Sci U S A* (2012) **109**, 43:17669-17674.
127 Dickey, C.A. *et al.* Selectively reduced expression of synaptic plasticity-related genes in amyloid precursor protein+ presenilin-1 transgenic mice. *Journal of Neuroscience* (2003) **23**, 12:5219-5226.
128 Scripture-Adams, D.D. *et al.* GATA-3 dose-dependent checkpoints in early T cell commitment. *J Immunol* (2014) **193**, 7:3470-3491.
129 Haubensak, W. *et al.* Genetic dissection of an amygdala microcircuit that gates conditioned fear. *Nature* (2010) **468**, 7321:270-276.
130 Wojtowicz, J.M. & Kee, N. BrdU assay for neurogenesis in rodents. *Nat Protoc* (2006) **1**, 3:1399-1405.
131 Hellemans, J., Mortier, G., De Paepe, A., Speleman, F. & Vandesompele, J. qBase relative quantification framework and software for management and automated analysis of real-time quantitative PCR data. *Genome Biol* (2007) **8**, 2:R19.
132 Dudoit, S., Yang, Y., Callow, M. & Speed, T. Statistical methods for identifying differentially expressed genes in replicated cDNA microarray experiments. *Statistica Sinica* (2002) 111-139.
133 Smyth, G.K. in *Bioinformatics and Computational Biology Solutions Using R and Bioconductor* (eds Robert Gentleman *et al.*) 397-420 (Springer New York, 2005).
134 GO.db: A set of annotation maps describing the entire Gene Ontology v. Version 3.4.1 (2017).

135 Hu, Z. *et al.* VisANT 4.0: Integrative network platform to connect genes, drugs, diseases and therapies. *Nucleic Acids Res* (2013) **41**, Web Server issue:W225-231.
136 Shannon, P. *et al.* Cytoscape: a software environment for integrated models of biomolecular interaction networks. *Genome research* (2003) **13**, 11:2498-2504.
137 Bindea, G. *et al.* ClueGO: a Cytoscape plug-in to decipher functionally grouped gene ontology and pathway annotation networks. *Bioinformatics* (2009) **25**, 8:1091-1093.
138 Bindea, G., Galon, J. & Mlecnik, B. CluePedia Cytoscape plugin: pathway insights using integrated experimental and in silico data. *Bioinformatics* (2013) **29**, 5:661-663.